Interaction between two calcite surfaces in aqueous solutions

Study of nano-scale interfacial forces using AFM and SFA

by

Shaghayegh Javadi

Thesis submitted in fulfillment of
the requirments for the degree of
PHILOSOPHIAE DOCTOR
(PhD)

Faculty of Science and Technology
Department of Energy Resources

2019

University of Stavanger
NO-4036 Stavanger
NORWAY
www.uis.no

ISBN: 978-82-7644-881-8
ISSN: 1890-1387
PhD Thesis UiS No. 483

I, SHAGHAYEGH JAVADI, declare that this thesis titled, 'INTERACTION BETWEEN TWO CALCITE SURFACES IN AQUEOUS SOLUTIONS: Study of nano-scale interfacial forces using AFM and SFA' and the work presented in it are my own. I confirm that:

1. This work was done wholly or mainly while in candidature for a research degree at this University.

2. Where any part of this thesis has previously been submitted for a degree or any other qualification at this University or any other institution, this has been clearly stated.

3. Where I have consulted the published work of others, this is always clearly attributed.

4. Where I have quoted from the work of others, the source is always given. With the exception of such quotations, this thesis is entirely my own work.

5. I have acknowledged all main sources of help.

6. Where the thesis is based on work done by myself jointly with others, I have made clear exactly what was done by others and what I have contributed myself.

Signed: 

Date: October 2019

"The Sun atoms shake; my eye electron shakes eight minutes later, because of a direct interaction across."

Richard Feynman's Nobel Prize lecture, Dec. 1965

Preface

Carbonate-bearing rocks in the upper Earth's crust are prone to continuous changes under influences of various physical and chemical processes. The macroscopic mechanical strength of carbonates is generally controlled by the cohesion between contacting grains at a molecular scale. These grains deform in contact regions due to the chemistry of pore fluid. The repulsive and attractive forces that operate at the grain contacts may be affected by the dissolution and recrystallization kinetics at the mineral-liquid interfaces. The processes by which the nano-scale interfacial forces are influenced by changing properties of the confined fluid are largely unknown. In this thesis, I investigate these processes and their possible contribution to the strength of calcite-bearing rocks and materials.

The Atomic Force Microscope (AFM) and Surface Force Apparatus (SFA) are two powerful tools that provide an opportunity of direct observation of mineral reactions to the contacting fluid and measuring the surface forces at nano-scale in air and liquid environments. In this project, we perform an extended number of experiments using the AFM and SFA to improve our understanding of variation in interfacial forces linked to the strength of calcite and calcite-bearing rocks.

In the AFM experiments, we bring an *in situ* fabricated calcite probe into contact with an opposing freshly cleaved calcite surface in a fluid cell containing aqueous solutions with varying chemical compositions. We also combine the AFM force measurements with a technique called inverse imaging, for *in situ* simultaneous characterization of the calcite probes. Based on these experiments, we discuss that the possible variation in local topography of contacts, together with a strong dependence on ionic strength of the solution, can explain the variation in strength of calcite rocks in aqueous solutions.

With the SFA, we can perform *in situ* observations of the possible changes in the surfaces via light interferometry technique while measuring the interfacial interactions at nano-scale. At this scale, interactions between contacting surface asperities define the nature

of interfacial forces, repulsive or attractive. We discuss how the crystal growth, dissolution and changes in surface roughness affect these interaction forces and their implications on the strength of calcite-bearing rocks.

Acknowledgments

Every PhD is different and accomplished with a lot of ups and downs that, usually, comes with significant personality deformations, mostly plastic kinds. This is at least how I can describe my PhD. When I started this journey, it was pretty much like diving down into a deep ocean, where I could explore the unknowns. As I swam deeper and longer, the perpetual darkness of that ocean scared me, small creatures distracted me and large ones caught me. There were a lot of barriers to overcome. Passing every single one of them strengthened me and shaped me to the person I am today. Now, I'm at the end of that journey. When I look back, all I remember is the great memories and experiences I have gained from the very first moment until now. I have received help from many people for which I will be forever grateful.

First, I would like to express my deepest gratitude to my supervisor, Anja Røyne, for her abundant help. She spent countless hours at the computer with me, trying to make sense of the extremely complicated data. The door to her office was always open to my endless questions and discussions. She patiently helped me to get through the whole project. I deeply appreciate her time and insightful comments. I would also like to thank Aksel Hiorth, for all the discussions and help with the Phreeqc simulations every time I was in Stavanger.

To Merete Madland, the inspiring leader of the IOR centre, whose encouragement and support are appreciated in a great deal. The Research Council of Norway and the industry partners of The National IOR Centre of Norway, ConocoPhillips Skandinavia AS, Aker BP ASA, Vår Energi AS, Equinor ASA, Neptune Energy Norge AS, Lundin Norway AS, Halliburton AS, Schlumberger Norge AS, Wintershall Norge AS, and DEA Norge AS, are greatly acknowledged. To the wonderful and amazing members of the IOR centre, Bente Dale and Iren Lobekk, thank you for always being so genuinely kind and helpful to me.

To Tue Hassenkam and Susan Stipp for their support during my short stay in the University of Copenhagen. To all my smart col-

leagues and friends at the PGP (Njord centre). You are a group of amazing and talented people, whom I am very lucky to get to know and work with. I would like to thank Luiza Angheluta for helping me with data analysis, and Knut Jørgen Måløy for welcoming me to his group, where I got to know of this PhD project. To Francois Renard for his invaluable advice and suggestions. To Joanna Dziadkowiec, my countless long days in the lab could not turn to be so amazing without you. Those days that we both tried to deal with calcite, me with AFM and you with SFA and our discussions not only scientifically but also about our lives and experiences, they all have been engraved in my mind and will forever be cherished. Anne P., Anne B., Marcel, Frank, again Joanna and Aylin, your friendship means a world to me. I cannot thank you enough for being always there for me, not only during the fun times but also the time of my frustrations and anxiety especially in the last months of my PhD. You are the best friends I could ever ask for.

Many people have, positively, affected my professional life. Among those, I would like to express my gratitude to my former supervisors in the Max Planck Institute for Dynamic and Self Organization in Germany, Lucas Goehring and Stephan Herminghaus. To Lucas, the fact that I became an experimentalist today is because of you. I shall always thank you for your patience and abundant knowledge that guided me in the lab while I was working in your group. To Stephan, although my time in your group was too short I would like you to know that I learned a lot in the regular discussions and seminars led by you. You truly are an amazing teacher.

To my friends outside the university campus and my beloved siblings, thank you for all your emotional support and fun times that made me forget about all my problems.

To my beautiful nieces and nephew, Melina, Matilda and John Yar, you are still too young to understand the massive positive impact of your existence on your auntie's life. When you are old enough to read this (assuming your generation still read theses in the future), I want you to know that even though I was not living close to you, the photos and videos of yours, documenting every single motion you made and words you talked, made many cloudy days of my life shiny and bright. For that, I must be super thankful to your

parents for not only being supportive brothers and sisters to me but also updating me with your growth process. The most exciting and adorable growth process I observed for the last 3 and half years of my life.

To my parents, words cannot describe my feelings for you. The person I am today who could overcome many obstacles in her life to reach to this point is shaped by you. Thank you for your endless support and encouragements.

And finally, last but by no means least, Shahin Jafarzadeh, my brilliant and supportive husband. Having a partner like you by my side is the best thing I have in life. Your love and infinite support have been a powerful encouragement to me all the way through.

Shaghayegh Javadi
Oslo, October 2018

Contents

Chapter 1

Introduction

1.1 Motivation

Sedimentary rocks are formed by the deposition of weathered remains of other rocks, cementation of mineral or organic particles, and/or by precipitation from solutions. Carbonate rocks, such as chalk, are example of porous media. They may contain significant amount of fluid within the space between their grains. This has made them important groundwater aquifers (Croizé et al., 2013), and also reservoirs of about 60 and 40% of the world's oil and gas, respectively (Croizé, 2010). They are, as well, potential reservoirs for CO_2 sequestration purposes (Lackner et al., 1995). Although the importance of the chalk has been well recognized, our understanding of the mechanisms that control the properties of the material, in particular in contact with fluid, is still far from complete.

During production or extraction of fluid from chalk reservoirs, the pore pressure may decline and result a higher effective stress on the solid structure. This may lead to compaction, i.e. decreasing the volume of reservoir and compressing the underlying sediments. As a result, a subsidence of the surface above the reservoir will take place. Subsidence due to natural causes (fluid expulsion) is fairly common, such as sinking of the Venice, Italy into its surrounding lagoon at the rate of a few centimeters per century. Over-pumping

the ground water basins, however, may increase the subsidence rate substantially. This is the case in, e.g. San Joaquin Valley, California, where a subsidence of 9 meters has been observed, as reported by (Waal, 1986); as well as Venice, Italy (between years 1940-1970) that measured to 1.7 cm/yr and 1.4 cm/yr in industrial area and city center respectively (see e.g., (Doornhof et al., 2006) for discussion in detail). During the oil production the chalk fields in the North Sea have experienced reservoir compaction. The Ekofisk field, one of the main oil reservoirs in the North Sea, is an overpressured highly porous, low permeable chalk reservoir, with a production of about 36 million barrels/day oil production, reported by NPD (2019), as of 2018. The production of oil from the Ekofisk field comes from two chalk formations, Ekofisk and Tor (that are from the early Paleocene and late Cretaceous ages, respectively (Sylte et al., 1999)). Seabed subsidence, in the North Sea, was first observed in 1984 (13 years after the start of oil production in 1971), a possible indication for compaction.

To compensate the decrease in pore pressure (that result into compaction) and also displace the hydrocarbon, water flooding started in 1987 in the North Sea (Doornhof et al., 2006). Despite of this, the subsidence rate remained almost constant until 1998. Although the subsidence rate was reduced by water flooding, from 42 cm/yr in 1998 to 15 cm/yr in 2006, the magnitude of subsidence was still remained a considerable issue. So, why did the compaction continue even after the pore pressure was restored? The answer to this, is generally believed to lie in the chalk-water interaction. It has often been observed that water-saturated chalk can have a drastically reduced mechanical strength. This is the phenomenon that commonly referred to as *water weakening* of chalk.

High porosity chalks fail not only in shear mode but also under compression, which can be caused by, for example, a hydrostatic load. This mode of compressive failure is known as pore-collapse (Blanton, 1981), and is the result of the chalk grains collapsing into pore spaces. At the microscopic scale, compressive failure is thought to be the distribution of shear failure [1] within the material.

[1] Mathematically, the relation between shear failure with shear stress and

Therefore, a rock matrix with strong grain-bonding cements can be resistant to shear failure, and eventually to pore collapse at the macroscopic scale.

The strength of chalk is mainly controlled by three parameters, 1) cohesion, a measure of the bond strength between the grains or contacting surfaces, 2) friction coefficient μ (or the internal friction angle, ϕ, where $\mu = \tan(\phi)$), and 3) the hydrostatic yield value. All of these parameters are affected by pore fluid properties, as shown by Risnes (2001), with chalk being the weakest in water and strongest when dry. Figure 1.1 shows that, by moving from dry to water saturated chalk, the cohesion and friction angle (ϕ) decreases. This is also the case for the hydrostatic yield value.

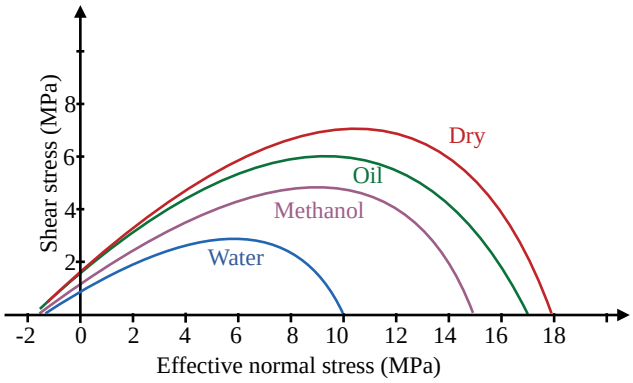

Figure 1.1: Yield curves for high porosity outcrop chalk, mainly the Liége chalk data, with different pore fluids. This plot reflects the dramatic effect of water on strength of chalk and is adapted from (Risnes, 2001, Figure 5) with permission. Effective stress (x-axis) is the applied stress minus the pore-collapse stress. In this plot, each curve meets the x-axis at the pore collapse stress of the hydrostatic yield value; and y-axis at the intrinsic shear resistance of the material or the cohesion. These values are the lowest for the water-saturated chalk.

Various mechanical and chemical mechanisms have been linked

normal stress is described by the Mohr-Coulomb failure criterion (Ottosen and Ristinmaa, 2005) with an end-cap, taking the intrinsic shear resistance (also referred to as cohesion) of material into account (see (Risnes, 2001) for a detailed discussion).

to the water weakening effect. In general the reduction of mechanical strength of chalk takes place through mechanisms led by 1) physical effects, e.g. pore collapse, capillary forces (Delage et al., 2008) and wettability alteration (Andersson et al., 2016) , 2) chemical effects, e.g. dissolution which is accompanied by ion migration (Ca^{+2} , CO_3^{-2}) (Gutierrez et al., 2000); and 3) physio-chemical effects, e.g. pressure solution (Hellmann et al., 1996), and adsorption pressure by attraction of water molecules to the chalk grains, reported by Risnes et al. (2005) to be the reason for the decreased cohesion of the chalk. Subcritical crack growth at the grain boundaries due to fluid diffusion into grain contacts (Bergsaker et al., 2016; Røyne et al., 2011) have been, also, suggested to describe this phenomenon.

A number of studies have suggested that the weakening effect of water and pore fluid salinity on chalk is attributed to the interaction between chalk grains (Megawati et al., 2012; Nermoen et al., 2018; Risnes and Flaageng, 1999; Risnes et al., 2003). They suggest that the salinity of fluid influences the electrostatic repulsive forces between the grains, because of the change in surface charge and concentration of adsorbed ions (see next section). Similarly, Hiorth et al. (2010), Nermoen et al. (2015), Madland et al. (2011), Hellmann et al. (2002b), Gutierrez et al. (2000), Heggheim et al. (2005), Ciantia et al. (2015), and Nielsen et al. (2016) propose that chalk deformation in water or/and saline solutions is influenced by surface charge variation, due to ionic exchange at contacting grains. They also show that mineral dissolution and precipitation affected by chemical and/or physio-chemical effects are additional mechanisms to describe the chalk deformation in contact with water molecules.

Despite the progress that has been made, there is no solid agreement on how much the variation in ion distribution near surfaces in solutions can explain the deformation in carbonate rocks. Additionally, the effect of fluid composition on the cohesion of chalk grains, and a potential link between surface forces and reactivity of confined mineral surfaces, yet remain to be not fully understood.

Cohesion between two initially separated surfaces is also known as adhesion, the term that is mostly used in this work. In this thesis, the main focus lies on the interfacial forces between calcite surfaces in aqueous solutions and their implications for the behaviour of

calcite in contact with brines of various ionic strength. We study this by measuring the adhesion between two calcite surfaces at nanoscale.

Chalk is actually made of skeletal debris of pelagic algae with a spherical calcareous exoskeleton (coccosphere) which itself is made of wheel-shaped coccolith platelets. Each of these tablet-shaped crystals is of many individual calcite crystals (D'Heur, 1984; Hassenkam et al., 2011) (see Figure 1.2). Given that calcite is the main component of chalk (>99% for most types), the effect of fluid composition on surface forces acting at calcite-calcite interfaces is likely to influence the mechanical properties of chalk (Risnes et al., 2003).

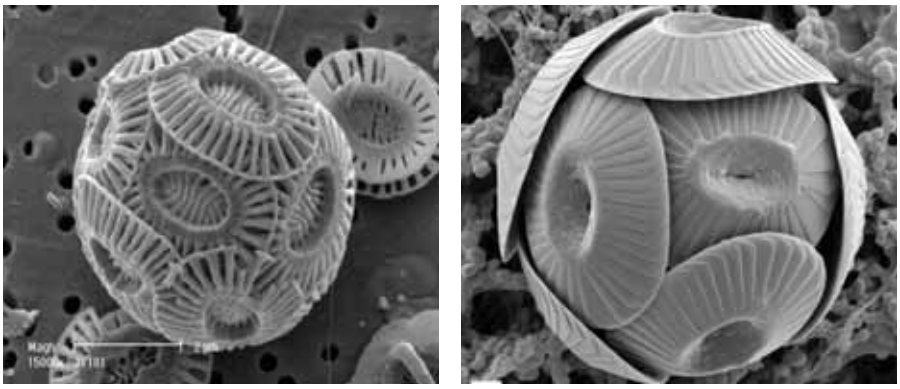

Figure 1.2: Examples of coccolithophores. **left:** A complete coccosphere of an Emiliania huxleyi, that are made of coccolith platelets; **right:** Heterococcolith, made of micrometer-scaled shields of calcite crystals. This image is originally from (Young et al., 2017) with permission.

1.1.1 Water weakening of chalk

Mechanical properties of cohesive granular or polycrystalline materials are controlled by the strength of the constituent grains and the cohesion between individual grains (Shchukin, 2002). The cohesion between grains may be influenced, significantly, by variation in the pore fluid composition. Water weakening may be described by the cohesion reduction of chalk that has been observed in aqueous solutions (Risnes and Flaageng, 1999). It has been shown that the

strength of saturated chalk is correlated with the activity of water in the pore fluid, and attributed to the grain cohesion influenced by the water activity (see Figure 1.3) (Risnes et al., 2005).

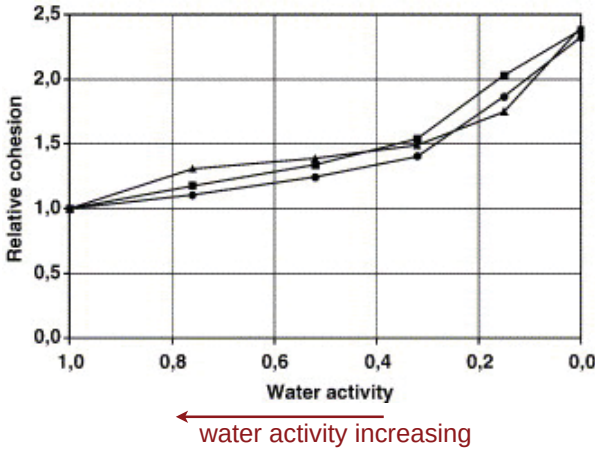

Figure 1.3: Relative cohesion of chalk samples, in contact with water, decreases with water activity. This figure is slightly modified from (Risnes et al., 2005) with permission.

As Risnes (2001) and Hellmann et al. (2002b) suggested, water weakening may be related to repulsive forces due to adsorbed water molecules on adjacent highly hydrophilic calcite surfaces. In line with their work, Risnes et al. (2005) showed that the chalk strength decreases with increasing water activity in water and ethylene glycol mixtures, and hypothesized that this could be explained by repulsive forces acting at the grain contacts. Following this reasoning, Røyne et al. (2015), who used atomic force microscopy (AFM) to measure forces between two calcite surfaces in water-glycol mixtures, measured a strong repulsion between two calcite surfaces in pure water. In addition, the measured adhesion between the surfaces, in ethylene glycol mixtures, was found to be inversely proportional to the water activity. Water activity, however, is also influenced by the salinity of the pore fluid (Blandamer et al., 2005; Kohns et al., 2016) because water molecules become more involved with ion-dipole interactions in the bulk fluid. Even though the water activity has

been a successful mechanism to describe the water weakening, it is not sufficient to explain the behaviour of saturated chalk in salt solutions.

The interaction forces between two neighbouring surfaces depends on the ionic strength and the chemical composition of the contacting fluid because these parameters determine the distribution of ions on and near the solid surfaces. As long as the surfaces are more than one Debye length apart, and the ionic strength of the solution is lower than approximately 0.1 M (Diao and Espinosa-Marzal, 2016; Israelachvili, 2011), the surface forces can be described by the classical DLVO theory, which includes the repulsive Electrical Double Layer (EDL) and attractive van der Waals (vdW) forces (Israelachvili, 2011; Verwey, 1947) (see Chapter 3 for further discussion on surface forces).

Other mechanisms that have been suggested to describe the weakening effect of water are the interaction forces at the fracture tip, which are mostly repulsive due to hydration forces between hydrophilic calcite surfaces or the EDL repulsion (Croizé et al., 2010; Megawati et al., 2012; Risnes et al., 2005; Røyne et al., 2015). A recent experimental work by Bergsaker et al. (2016) shows the effect of ionic strength of the contacting aqueous solutions on subcritical crack propagation and strength of calcitic rocks. All these findings indicate that the nature of the interaction forces between calcite surfaces is associated with the molecular details of the contacting fluids with calcite interfaces, a phenomenon that is yet to be understood fully.

1.1.2 Compaction of chalk - Creep deformation

Compaction is a process of progressive loss of porosity and volume in sedimentary or fluid-saturated rocks under stress. The applied stress is provided by not only the overburden weight but also by the fluid production that can change the pore pressure and thus increase the vertical effective stress on the rock structure (Doornhof et al., 2006). Compaction may cause irreversible changes in the rock structure (intracrystalline deformations) such as grain dislocations/rearrangements relative to each other or grain sliding; break-

ing the grain cementations or causing grain indentation.

Deformation of carbonate rocks displays a strong dependency on the strain rate of the material (Brantut et al., 2014; Nicolas et al., 2016), but varies with the rock composition, depositional history and pore-fluid compositions (Doornhof et al., 2006; Zimmerman et al., 1986). The stress-strain relationship varies also from material to material. When the relationship between stress (σ) and strain (ε) is linear, the material is in an elastic regime, where the ratio between stress and strain is characterized by the material's Young's or elastic modulus (E) as such $\sigma = E\varepsilon$. A deformation is known as elastic if, when the applied stress returns to initial state, the material will return to its initial shape. If a material's initial shape (or condition) is not restored after one stress cycle, the deformation will not be elastic any longer but rather inelastic or plastic deformation.

In the outcrop chalks a common type of deformation is creep, a kind of plastic deformation. Creep is a time-dependent strain rate deformation that continues even after the stress change ceases (Risnes, 2001; Risnes and Nygaard, 1999).

Another mechanism that can account for the reduction in strength of chalks is the chemical dissolution at the stressed grain boundaries (Hellmann et al., 2002b). It is a type of plastic deformation and known as pressure solution creep. It has been extensively studied by (e.g. Croizé et al. (2010, 2013); Hellmann et al. (2002a,b); Madland et al. (2011); Nermoen et al. (2015)), and is found to depend strongly on chemical parameters like pH, ionic species and ionic strength of the pore fluid due to their effect on the surface charge.

Pressure solution

Pressure solution, or "intragranular pressure solution creep", is a chemical driven deformation mechanism playing a key role in the compaction of carbonates (Gratier et al., 1999; Hellmann et al., 2002b; Zhang and Spiers, 2005). It is a slow process that operates at single contacts between calcite surfaces at the micro-scale. Its main driving force is the chemical potential difference between stressed and unstressed parts of the solid, along with local chemi-

cal gradients. It involves (a) mineral dissolution at stressed parts of contact, (b) diffusion of ionic species through the pore space, and (c) precipitation on unstressed or less stressed surfaces (Croizé et al., 2010).

When a mineral surface is in equilibrium with its saturated solution, dissolution of the surface does not happen unless there is an increase in the magnitude of normal stress (F_n) (Lehneri and Bataille, 1984). This is known as stress-enhanced solubility, and is a driving force for changes in the surface chemical potential (μ),

$$\mu = f^s + F_n/\rho^s \tag{1.1}$$

where f^s is the Helmholtz surface free energy and ρ^s is the solid density (Lehneri and Bataille, 1984). Once the dissolution begins, it triggers mass transfer by diffusion towards larger pores with a lower solute concentration (Lehneri and Bataille, 1984; Putnis, 2015). The diffusive flow of the dissolved mineral out of the contact is a function of solute concentration (ϕ), and follows the Fick's diffusion law which in one dimension (x) is given as,

$$J_x = -D\frac{d\phi}{dx} \tag{1.2}$$

where D is the diffusion rate, which itself is a function of viscosity of the confined fluid film. For the diffusion to continue into the bulk, the pressure in the bulk should be lower than the pressure in the confined fluid film (Renards and Ortoleva, 1997; Rutter, 1983). The pressure in the confined fluid film is referred to as disjoining pressure.

The disjoining pressure (Π) was first introduced by Derjaguin (Derjaguin and Landau, 1941) in the 1930s (see the sketch in Figure 1.4). When the fluid film between two surfaces is in equilibrium with the bulk fluid, the disjoining pressure is determined by the Gibbs free energy (G) variation with distance (D) per unit area (A) at a constant cross-sectional area, temperature (T), and volume (V) (Butt et al., 2003),

$$\Pi = -\frac{1}{A}\left.\frac{\partial G}{\partial D}\right|_{A,T,V} \tag{1.3}$$

Figure 1.4: The disjoining pressure between two parallel surfaces, where P is the pressure in the film, and P_0 is the pressure of the bulk phase. This figure is a modified sketch from (Butt et al., 2003).

According to the DLVO (Derjaguin-Landau and Verwey-Overbeek) theory (Derjaguin and Landau, 1941; Verwey, 1947), van der Waals (vdW) and Electrical Double Layer (EDL) forces are involved in the disjoining pressure (Israelachvili, 2011). Attractive forces with their negative contribution to the disjoining pressure reduce the stability and thickness of the water film. This eventually leads to the collapse of the water film and, thus, migration of the dissolved ions into the bulk solution. Repulsive forces, on the other hand, have a positive contribution and increase the stability and thickness of the water film. This means that the disjoining pressure is larger than the liquid hydrostatic pressure and a significant force in the direction normal to the surfaces is required to remove the fluid film from the confined space.

The disjoining pressure of a confined water film between calcium carbonate surfaces has been measured in molecular dynamic simulation by Brekke-Svaland and Bresme (2018), who found a significant amount of ≈ 1 GPa at separations below a few nm.

1.2 Thesis objective and structure

If we can figure out how tight chalk grains can hold on to one another while the chemistry of the fluid between them is changed, by for instance changing the type and concentration of ionic species, we are one step closer to understanding the chemical and/or physio-chemical processes taking place during the chalk compaction and

subsequent seabed subsidence. The main objective of this thesis work has been to measure the interaction forces between two surfaces of calcite, being the main component of chalk, in aqueous solutions; and investigate the effect of salinity on the nm-ranged surface forces acting between the interacting surfaces. By this approach, we can get closer to quantifying the possible contribution of these nano-scale surface forces to the cohesion and macroscopic strength of fluid-saturated, calcite-bearing rocks. In this work, the source of calcite comes from both natural and in-house prepared polycrystalline calcite films, rough on the nm-scale, that are formed by atomic layer deposition. The aqueous solutions used are $CaCO_3$-saturated salt solutions and $CaCO_3$-saturated water. We have used two powerful tools in the field of *in situ* force measurements: the Atomic Force Microscope (AFM) and the Surface Force Apparatus (SFA). We have focused on measuring the effect of the salinity of various salt solutions on the surface properties of calcite and on the adhesion between two calcite surfaces. Throughout this work, we have studied the conditions under which the adhesion forces between two hydrophilic calcite surfaces become stronger, such that it may lead to materials with higher strength in aqueous solutions.

This thesis includes 6 chapters to support the scientific background and experimental work carried on to address the main goal of this project. The current chapter includes the motivation and objective of this project. Chapter 2 introduces the properties of calcite, with particular focus on the dynamic behaviour of calcite surfaces in the presence of water. Chapter 3 is devoted to the introduction of surface forces and a discussion of how they can be affected by the chemical composition of aqueous solutions, with their impact on the strength of calcite interfaces. Chapter 4 describes the experimental methods used in this thesis. Chapter 5 summarizes the main findings of the study, that are presented in more detail in the accompanying manuscripts. Finally, Chapter 6 sums up the main conclusions of this thesis, in addition to suggestions for future possible experiments that might add to the present knowledge on this topic.

In Manuscript I, we show that in addition to the ionic strength of the NaCl solutions, surface roughness plays a key role in controlling

the adhesive forces between two calcite surfaces. Later, I improved the experimental method by adding another technique called inverse imaging for further investigation of the surface roughness evolution, as presented in Manuscript III. Force measurements between two calcite surfaces with the SFA involved the development of a method to prepare and mount thin films of calcite on SFA, and measuring the interactions between them in air and aqueous solutions. This method and the results from the SFA experiments are published as Manuscript II and the related appendix.

Chapter 2

The dynamic calcite surface

Calcite is the most stable crystalline polymorph of calcium carbonate. It is a mineral of interest to scientists and engineers due to its diverse application from biology to geology, reservoir engineering and industry. In general, calcite is a thermodynamically stable mineral and found abundantly in nature: in geological settings, e.g., carbonate-bearing rocks, sedimentary carbonate platforms, chemical sediments in oceans, and marine organisms; in biology, it is the main constituent biomineral of the inner ear in humans (Verpy et al., 1999) and responsible for our sense of balance. It is found extensively in the so-called Brassica vegetables (Heaney et al., 1993) with high dietary benefits. Pearls and egg-shells also contain a substantial amount of calcium carbonate (Omari et al., 2016). Apart from its abundance in nature, calcite is utilized in a great deal of industrial materials and processes, e.g., paper, paint, plastic, food additives, pharmaceutical, cements used in road construction, and water treatments (Omari et al., 2016).

Calcite is a crystal with a trigonal-rhombohedral structure, with a unit cell of the form shown in Figure 2.1 (left). Among various crystallographic planes of calcite, the (104) cleavage plane (Skinner et al., 1994) is the most stable crystallographic plane as de Leeuw and Parker (1998) showed based on its minimum surface energy. However, the calcite (104) face displays a highly dynamic and reactive surface in contact with water molecules in air and aqueous

solutions (Stipp, 1999; Stipp et al., 1994, 1996).

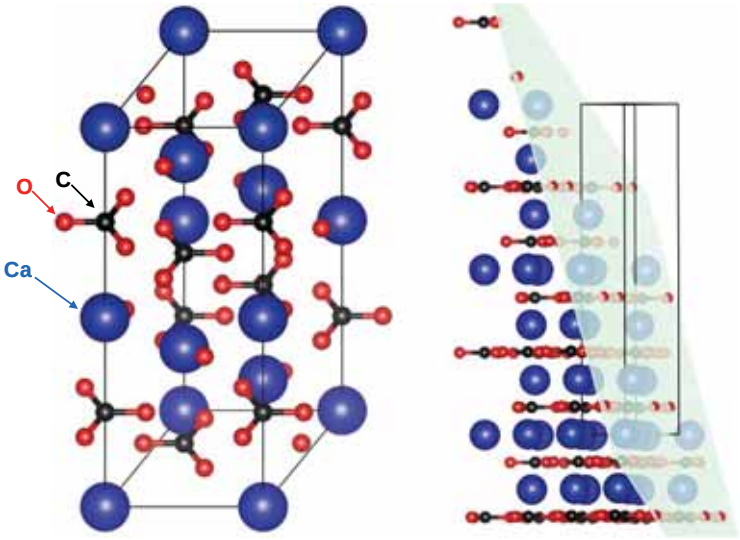

Figure 2.1: The unit cell structure of calcite (left), and cut by the (104) plane (right). Modified figure from (Bentz et al., 2017) with permission. Physical dimension of unit cell in a calcite lattice (lattice parameters) are, a = b = 0.498 nm, c = 1.706 nm, $\alpha = \beta = 90°$ and $\gamma = 120°$.

2.1 Reactivity of the calcite-water interface

Surface properties of calcite like topography, molecular structure and chemical composition of the surface are parameters that control the reactivity and dissolution of the calcite surfaces. Investigations of the surface properties of calcite are therefore of tremendous help in understanding a wide range of natural and engineering processes that are influenced by calcite dissolution and reactivity in aqueous solutions, such as the compaction of carbonate rocks.

By now, the detailed structure of the calcite surface has been revealed through extended number of studies, using atomic force

microscopy (AFM) (e.g., (Stipp, 1999; Stipp et al., 1994)), X-ray absorption spectroscopy (XPS) and low energy electron diffraction (LEED) (e.g., (Stipp, 1999; Stipp and Hochella, 1991)), and molecular dynamic simulations (Fenter et al., 2013). All these studies have concluded that calcite surfaces are dynamic in aqueous solutions, with continuous dissolution and recrystallization on the timescale of hours even in saturated solutions.

2.2 Calcite hydration

Calcite is composed of Ca^{+2} and CO_3^{-2} ions. The atomic arrangement of the cleavage plane (104) is same as the bulk structure (Heberling et al., 2011; Stipp, 1999), as shown in Figures 2.2 and 2.1(right). As seen in Figure 2.2, the surface rectangular unit cell with dimensions of 0.5 nm $\times$ 0.81 nm contains two carbonate groups that are rotated with respect to each other and with regard to the surface normal. Although it is not clear in a sketch on a two dimensional paper, the calcium and carbonate groups are in an alternate crystallographic orientation on the (104) calcite surface. This induces local surface charge variation with a high potential to adsorb water molecules, making the calcite surfaces highly hydrophilic (Bohr et al., 2010; Stipp, 1999). Stipp (1999) showed, through a detailed study of the calcite surface, that cleaving the calcite produces dangling bonds (or under-bonded atoms) on the surface that quickly bind to the hydrolyzed water (H and OH) in the air. As a result, a hydration layer or an adsorbed water layer develops at the termination of the calcite bulk structure on the cleavage plane (Stipp, 1999; Stipp and Hochella, 1991; Stipp et al., 1994).

The hydration layer on the calcite (104) surface has been elucidated using atomic force microscopy (AFM) (Bohr et al., 2010; Ricci et al., 2013; Rode et al., 2009; Stipp, 1999; Stipp et al., 1994) and MD simulations (Kerisit and Parker, 2004; Perry et al., 2007; Wolthers et al., 2012). It has been recently revealed that the hydration layer on calcite is not limited to a monolayer of water, but to comprise at least three layers, using amplitude modulation AFM by Marutschke et al. (2014), and even recently to five hydration layers

using high-resolution 3D AFM (Songen et al., 2018).

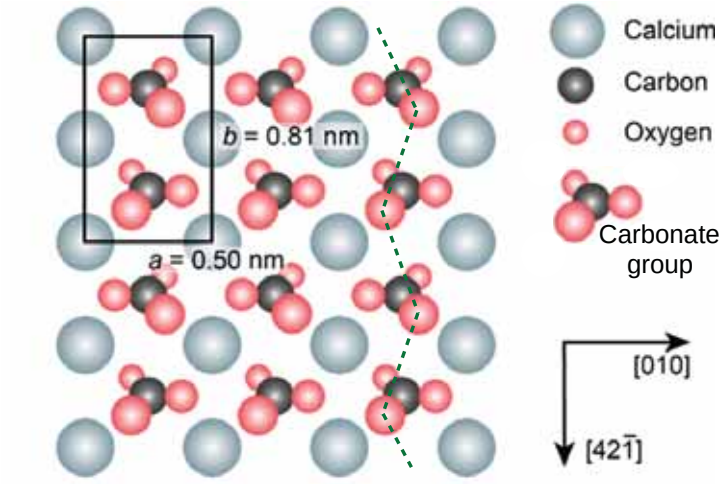

Figure 2.2: The calcite (104) surface, with a 2D rectangular unit cell with dimensions of 0.5 and 0.81 nm. Oxygen atoms in larger size are the protruding ones and their zigzag pattern (described by Stipp (1999)) is evidenced with the dotted lines. This sketch is modified from (Nalbach et al., 2017) with permission.

At a charged calcite surface in an electrolyte solution, there exists a layer with the a higher surface potential, formed by adsorbed ionic species that is known as the Stern layer (Ricci et al., 2013). At the Stern layer, Ca^{+2} and CO_3^{-2} ions are kept in the outer-sphere orientation with respect to the calcite surface by the hydrolysis species (Kirch et al., 2018; Stipp, 1999). The reactivity of calcite surfaces to aqueous solutions is defined by the hydrolysis species (de Leeuw and Parker, 1998; Gao et al., 2017; Heberling et al., 2011; Kerisit and Parker, 2004; Wolthers et al., 2012). For example, the loss of hydrolysis species by dehydration, along with the transportation of adsorbed species to inner-sphere coordination, with respect to the surface, result into precipitation on the surface (Stipp, 1999).

2.3 Dissolution and precipitation

Dissolution-precipitation of a mineral is a natural response of a mineral-fluid system to a nonequilibrium state. It is a coupling process that leads to the re-equilibration of the mineral with respect to the surrounding fluid, while lowering the surface free energy (Agudo and Putnis, 2012). Many factors, such as degree of supersaturation, pH, solution stoichiometry, the presence of impurities (such as biopolymers, (Karaseva et al., 2018)), pressure, and temperature influence the calcite dissolution-precipitation or/and growth mechanisms (Agudo and Putnis (2012), and references therein); (Morse et al., 2007; Renard et al., 2019; Ruiz-Agudo et al., 2014, 2016).

The supersaturation of a solution is the key determining factor in growth and dissolution processes. The tendency of a mineral to grow or dissolve is given by the saturation index (SI), which can be calculated from,

$$\mathrm{SI} = \log\Omega = \log(\mathrm{IAP}/\mathrm{K_{sp}}) \begin{cases} < 0, & \text{solution is undersaturated} \\ = 0, & \text{mineral \& solution in equilibrium} \\ > 0, & \text{solution is supersaturated} \end{cases} \tag{2.1}$$

where Ω is the supersaturation, and IAP and $\mathrm{K_{sp}}$ are ion activity and solubility products respectively. A mineral, for example calcite, dissolves in an undersaturated aqueous solution; and it recrystallizes in a supersaturated (with respect to the mineral) solution. For example, calcite starts to heterogeneously grow at active surface sites, i.e., step edges and/or kinks, in aqueous solutions at conditions with $0 < \mathrm{SI} < 0.2$ with respect to calcite (Teng et al., 2000). In addition, if the supersaturation increases ($\mathrm{SI} \approx 0.7$), the growth mechanism changes to surface nucleation (Teng et al., 2000).

The calcite (104) surface belongs to the F-face crystal category (Ruiz-Agudo et al., 2009), and is characterized by step patterns. Step edges parallel to the edges of calcite rhombohedron are the most stable step edges of calcite. They correspond to the $[\bar{4}41]$ and $[48\bar{1}]$ crystallographic directions (Fig. 2.3a). Calcite dissolution-

precipitation or/and growth at the (104) surface are typically parallel to these directions (Heberling et al., 2014). For instance, depending on the supersaturation index, these mechanisms continue as 1) nucleation and step growth advancement over the surface (Agudo and Putnis, 2012) (see Figs. 2.3b and 2.4), or/and 2) spiral growth (see Figs. 2.3c-d and 2.4) that are originated from crystal imperfections such as screw dislocations (Lakshtanov et al., 2018; Teng et al., 2000). Step and kink sites on calcite (104) surfaces that are originated from these growth spirals can grow endlessly depending on the supersaturation index (Fig. 2.3c-d) (Lakshtanov et al., 2018; Teng et al., 2000).

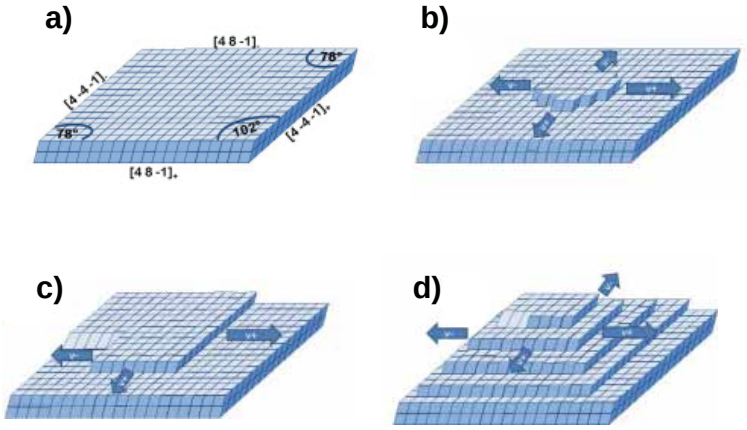

Figure 2.3: Growth processes at the calcite cleavage plane (104) rhombohedron. a) illustration of the structurally equivalent steps parallel to $[\bar{4}41]_{\pm}$ and $[48\bar{1}]_{\pm}$ directions; b) step growth advancement over the surface; c-d) growth spirals formation. This sketch is modified from (Heberling et al., 2014) with permission.

The processes mentioned above are mostly affected by the pH (which influences the surface charge) and chemical composition of the boundary layer at the calcite-fluid interface (Renard et al. (2019); Ruiz-Agudo et al. (2009) and references therein). For example, Ruiz-Agudo et al. (2009) observed a significant effect of Mg^{+2} concentration on the calcite dissolution rate: increasing the concentration of Mg^{+2} ($>$ 50mM) increased the dissolution rate by approx. an order

of magnitude, which is attributed to increasing the deepening rate and density of the etch pits.

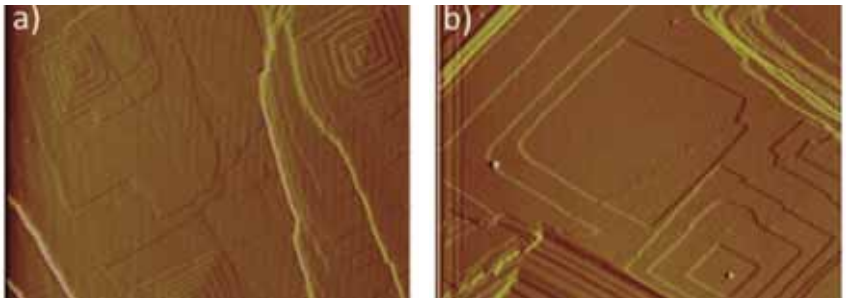

Figure 2.4: Growth processes on calcite (104) surface observed by AFM. a) spiral growth; b) 2D nucleation (after (Agudo and Putnis, 2012) with permission.)

Dissolution, precipitation, and growth of calcite, which in reality are time-dependent processes, (Stipp et al., 1994; Wojas et al., 2019), lead to progressive variation in surface topography and step roughening of calcite in aqueous solutions, that is often referred to surface roughness. Although surface roughness is a natural part of the calcite surfaces, its effect on surface forces between calcite surfaces is still remained insufficiently addressed.

Chapter 3

Interfacial Forces

When solid surfaces are in contact with aqueous solutions, they usually become charged through various processes, such as ion adsorption to the surface or dissociation from the surface (Butt et al., 2003). The electric field generated by the surface charges attracts the counter ions in the solution, and the resulting distribution of aqueous species at and near the solid surface. This mechanism plays a major role in determining the interaction between two neighbouring surfaces. For a wide range of systems, the DLVO theory, introduced by Derjaguin-Landau (Derjaguin and Landau, 1941) and Verwey-Overbeek (Verwey, 1947) in the late 1940s, can be used to describe the interactions between two charged surfaces in aqueous solutions. However, if the two surfaces come closer into small separations (a few molecular layers thick) the continuum DLVO theory is no longer valid. At this scale, the properties of the solvent (e.g., density, mobility and orientational order) differ from the related values in the bulk, and thus the solvation forces come into play with their additional dependency on the chemical and physical properties of the surfaces (e.g., hydrophobic or hydrophilic, rough or smooth, crystalline or amorphous surfaces) (Israelachvili, 2011).

3.1 DLVO theory

DLVO is a continuum theory that describes the interaction between two opposing surfaces as a sum of attractive van der Waals (vdW) and repulsive Electrical Double Layer (EDL) forces.

van der Waals force

For two parallel flat surfaces, the vdW contribution is given by,

$$F_{\mathrm{vdW}} = -\frac{A}{6\pi D^3} \tag{3.1}$$

where A, the non-retarded Hamaker constant, can be calculated using Lifshitz theory (Israelachvili, 2011; Lifshitz, 1956). For two identical surfaces in a medium (air or liquid), the Hamaker constant is obtained by the following equation,

$$A = \frac{3}{4}kT\left(\frac{\epsilon_1 - \epsilon_3}{\epsilon_1 + \epsilon_3}\right)^2 + \frac{3h\nu_e}{16\sqrt{2}}\frac{(n_1^2 - n_3^2)^2}{(n_1^2 + n_3^2)^{3/2}} \tag{3.2}$$

where n_1 and ϵ_1 are refractive index and dielectric permitivity for both identical interacting surfaces, and n_3 and ϵ_3 are refractive index and dielectric permitivity for the intervening medium. Because A is always positive for identical surfaces, the vdW contribution for these systems is always attractive.

Electrical double layer forces

The so-called Electrical Double Layer (EDL) is a representative structure used to describe the charge distribution near charged surfaces in an electrolyte solution (Israelachvili, 2011). Several models have been proposed to describe the EDL model, including the Helmholtz model (Helmholtz, 1853), the Gouy-Chapman model (Chapman, 1913; Gouy, 1910) and the Stern model. In the Stern model (Stern, 1924), the EDL contains two parts with a "Stern layer" as the inner part and a "Diffuse layer" as the outer part. The Stern layer consists of ionic species adsorbed to the surface.

The diffuse layer is right above the Stern layer, where the ions are free to bounce around, balancing between the thermal diffusion and Coulomb attraction, while electrically screening the Stern layer. The Debye length (κ^{-1}) is the characteristic dimension of the diffuse layer and is a function of the ionic strength of the solution (Israelachvili, 2011).

The EDL interaction force between two parallel flat surfaces can be described as (Israelachvili, 2011),

$$F_{\mathrm{EDL}} = \left(\frac{\kappa^2}{2\pi}\right) Z e^{-\kappa D} \tag{3.3}$$

where, κ is the reciprocal Debye length and Z is an interaction parameter, which for a monovalent electrolyte (e.g., NaCl solution) is given as a function of the surface potential (Israelachvili, 2011),

$$Z = 64\pi\epsilon_0\epsilon(kT/e)^2 \tanh^2(e\psi_0/4kT)$$

here, ψ_0 is the surface potential, which for calcite is a function of the pH, Ca^{2+} concentration (Foxall et al., 1979; Stipp, 1999) and P_{CO_2} (Wolthers et al., 2008).

As an example, consider two calcite flat surfaces in a NaCl solution. Figure 3.1 shows the calculated DLVO interactions for various NaCl concentrations assuming a surface potential of either 15 or 20 mV, corresponding to expected surface potentials for pH between 8 and 9 (Wolthers et al., 2008, Figure 3B). As expected, the position and height of the EDL repulsive barrier changes by increasing salt concentration. At high salt concentration, the interaction becomes purely attractive. However, for ionic strengths larger than approximately 100 mM and surface separations shorter than the Debye length (Diao and Espinosa-Marzal, 2016; Israelachvili, 2011), the continuum DLVO theory breaks down and other effects, such as hydration effects and specific ion interactions, become more pronounced (Donaldson et al., 2015; Pashley and Israelachvili, 1984; Ricci et al., 2013; Zachariah et al., 2016).

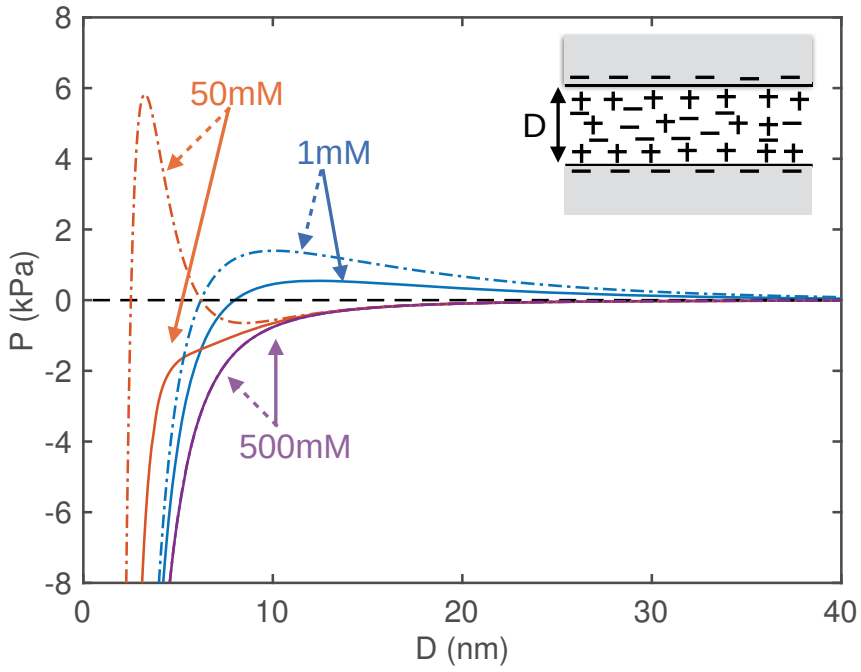

Figure 3.1: Calculated DLVO for two flat, smooth calcite surfaces in NaCl solution, with separation D, using combination of Equations 3.1 and 3.3. By reducing the Debye length (measured as $\kappa^{-1} = \frac{0.304}{\sqrt{[c]}}$ for NaCl (as 1:1 electrolyte)), the EDL repulsive forces shrinks eventually. In this measurement ψ_0 is assumed to be 20 mV for dotted lines and 15 mV for solid lines. The inset shows a sketch of two interacting surfaces in an electrolyte solution with separation D.

3.2 Hydration forces

When the separation between two opposing surfaces becomes very small, confinement may influence the liquid density distribution and interaction between the solute molecules and surfaces as a function of surface separation (Israelachvili, 2011). These interactions can lead to measurable forces described as solvation forces, or, in the presence of water molecules, hydration forces. Hydration forces are a function of distance and more pronounced at separations below

the Debye length (Israelachvili, 2011). They can be monotonically repulsive between hydrophilic atomically rough surfaces (Donaldson et al., 2015; Espinosa-Marzal et al., 2012; Israelachvili, 2011), or oscillatory for smooth and rigid surfaces (Diao and Espinosa-Marzal, 2016; Israelachvili and Pashley, 1983). Hydration forces are often categorized as primary or secondary hydration forces (Parsegian and Zemb, 2011; Parsons et al., 2011). Primary hydration forces are short-ranged and due to binding of the water molecules to the surface, resulting in the development of low entropy water layers. Secondary hydration forces are weaker and longer ranged than the primary hydrations. They are assumed to be due to hydration of solute molecules near the surface, above the absorbed water layer (Parsegian and Zemb, 2011).

SFA measurements on mica surfaces by Pashley and Israelachvili (1984) and Pashley (1981) showed that the strength of hydration forces is correlated with the ion hydration, such that more hydrated ions give rise to stronger hydration forces. In fact, the strength of hydration increases in order of

$$Mg^{2+} > Ca^{2+} > Li^{+} \approx Na^{+} > K^{+} > Cs^{+}$$

as discussed by Israelachvili (2011). Recent SFA and AFM measurements have also shown that the repulsive hydration forces between calcite surfaces (Diao and Espinosa-Marzal, 2016) and mica surfaces (Baimpos et al., 2014; Donaldson et al., 2015) are related to a high population of counterions in different hydration states in the water layer absorbed to surface.

To summarize, the hydration repulsion between two hydrophilic surfaces in small separations (below the characterized Debye length), can be described as an exponentially decaying repulsive force, as given by Israelachvili (2011)

$$W(D) = W_0 e^{-D/\lambda} \tag{3.4}$$

where D is the separation, λ is the decay length, typically on the order of a few nm (0.5-2 nm for mica and silica (Donaldson et al., 2015)), and W_0 depends on the surface hydration (Donaldson et al., 2015; Pashley, 1981; Pashley and Israelachvili, 1984).

3.3 Ion-ion correlation forces

When a large number of ions are adsorbed on surfaces in an electrolyte solution, the possible correlation between ions on opposing surfaces give rise to additional interaction forces. Ion-ion correlation can generate a net attractive force between two charged opposing surfaces due to 1) correlation between ions on one surface and ions on the other surface, and 2) strong correlation between counterions on the same surface, mostly in divalent solutions, that leads to a reduction in the thickness of the diffuse layer upon approach of the opposing surface and therefore decreases the EDL repulsion (Labbez et al., 2009). Attractive ion-ion correlation forces are not limited to divalent solutions, as Franks (2002) showed a strong attraction between silica surfaces in KCl and CsCl. A similar result was obtained by Baimpos et al. (2014) between two mica surfaces in CsCl, attributed to ion-ion correlation forces.

3.4 Effect of surface roughness

Surface roughness, often characterized by asperities in different scales, has a significant impact on adhesion and friction between two macroscopic surfaces. It is interesting to know that even the smallest, nanometer-sized asperities can be enough to make the interaction between two surfaces go from adhesive (in the absence of roughness) to repulsive (Persson et al., 2005). This is because both, roughness decreases the area of contact between the surfaces (see Figure 3.2), and elastic deformation of the highest asperities gives rise to repulsive surface forces (Eom et al., 2017; Parsons et al., 2014) by disturbing the arrangement of surface species. Asperities may come into contact long before the midplane of two surfaces can touch at $D = 0$.

Calcite surfaces are among those minerals that display some degree of roughness at the molecular scales. Although many studies have been carried out to address the role of surface roughness in surface force measurements (Benz et al., 2006; Eom et al., 2017; Parsons et al., 2014; Persson and Scaraggi, 2014; Persson et al.,

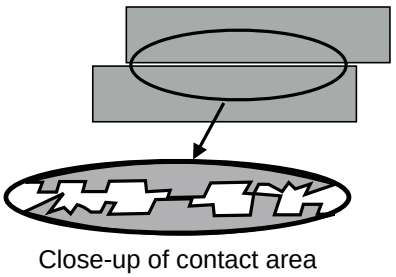

Figure 3.2: Schematic of contact for two presumably flat calcite surfaces with nano-scale roughness characterized by steps and kinks. The surfaces look flat on large scale but rough in the smaller scale, seen by magnification here.

2005; Persson, 2006; Persson and Gorb, 2003; Thormann, 2017), its effect on the interactions between calcite surfaces has been poorly addressed. The water wettability of calcite has been shown to be influenced by the surface roughness (Ulusoy and Yekeler, 2005; Ulusoy et al., 2004). Chen et al. (2017) observed increased wettability and enhanced oil desorption from the calcite surfaces by increasing calcite surface roughness. Recent modeling work by Wolthers et al. (2012) indicates that the surface topography of calcite is directly related to the reactivity of calcite surfaces in aqueous solutions.

Changes in roughness may occur because of the dynamic nature of calcite surfaces in contact with aqueous solutions (Stipp et al., 1994), which can thus influence the forces between calcite surfaces (as discussed in the previous chapter). Moreover, contacting surface asperities give rise to an exponentially decaying repulsive forces, that although varied in magnitude and range, can potentially be interpreted as hydration repulsion (Brant and Childress, 2004; Eom et al., 2017) which could complicate the interpretations of force measurements.

Chapter 4

Experimental techniques for measuring surface forces

> Doing physics is much more enjoyable than just learning it. Maybe "doing it" is the right way of learning, at least as far as I am concerned.
>
> Gerd Binnig

This chapter covers the scientific background for two common experimental methods used for surface force measurements at nano-scale. It also describes the experimental setups and procedures employed in this thesis to measure the surface interactions between calcite surfaces in aqueous solutions.

4.1 Atomic Force Microscopy

The Atomic Force Microscopy (AFM), Figure 4.1, was invented in 1986 by Binnig and Quate (1986), right after the invention of the Scanning Tunneling Microscope (STM). In the early years, AFM measurements were mainly focused on reducing the forces between sample and tip to obtain better resolution images, which required the need to understand the interaction forces between AFM probe

and the sample (Butt et al., 2005). Later, the force measurement technique has been widely extended for not only high-resolution AFM images but also to studying the properties of the sample, tip and an intervening medium. These forces are a function of separation between a tip and a sample, in addition to the material properties of two interacting surfaces.

4.1.1 AFM force measurement technique

4.1.1.1 Overview

In force measurements with AFM, the tip that is attached to cantilever (with spring constant k_c) moves relative to the surface of a sample in the normal direction by a piezoelectric translator. During this movement, the possible deflection of the cantilever (Z_c) due to interaction force between the tip and surface, is recorded versus the piezo position (Z_p), and makes a set of curves, one upon approach and one on retraction, as shown in Figure 4.2. These curves are converted to force-distance curves and typically known as the "force curves".

The force corresponding to a given deflection is found using the Hooke's law,

$$F = k_c Z_c \tag{4.1}$$

where k_c is the cantilever spring constant and a function of material properties (characterized by Young's modulus) and cantilever dimensions (Butt et al., 2005).

The tip-sample separation, D, is found as $D = Z_c + Z_p$. $D = 0$ is a matter of definition and chosen as the contact point, the position where the surface separation shows negligible change when increasing the applied force.

A representative measured force-distance curve for calcite surfaces in NaCl solution is shown in Figure 4.3, where the measured interaction force is adhesive. (Note: Z_c - Z_p and force-distance curves in Figures 4.2 and 4.3 are not corresponding and are only chosen for demonstration).

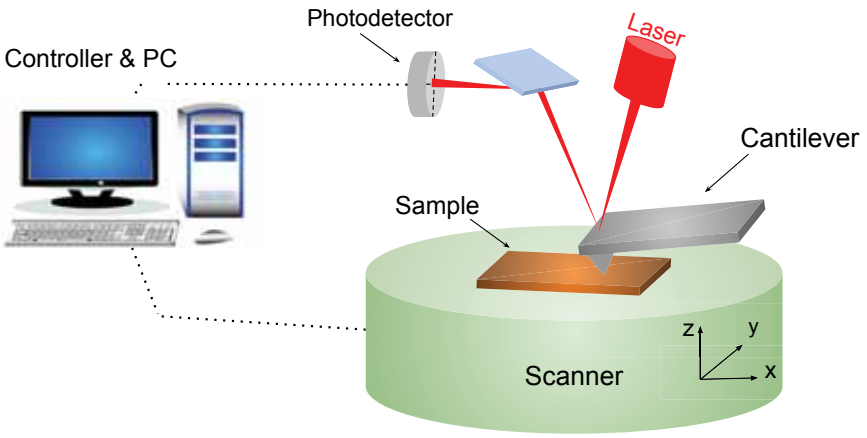

Figure 4.1: Schematic illustration of a typical AFM operation. As illustrated, the data is collected by the photodetector detecting the reflection of the laser from the end of the cantilever, and processed by a signal processor and a controller.

4.1.1.2 Calibration of the cantilever

Before each force measurement by the AFM, the cantilever spring constant, k_c, is measured; which usually results in a slightly different value than provided by the manufacturer. This is because of the non-homogeneous thickness and Young's modulus of cantilevers (Butt et al., 2005). Therefore it is necessary to calibrate the k_c and the sensitivity (slope of the linear part of the contact region, as seen in Figure 4.2) of the cantilevers before each experiment.

In this study, to calibrate the cantilever spring constant, we used the thermal tune calibration method (Hutter and Bechhoefer, 1993). The thermal tune calibration is a method based on small force impulses provided by the thermal fluctuations, in air or fluid, of a cantilever. These fluctuations are measured and analyzed by the AFM software through a noise spectrum plot (fluctuations vs. frequency). The amplitude of this spectrum at a certain temperature depends on the cantilever spring constant (k_c), which is obtained

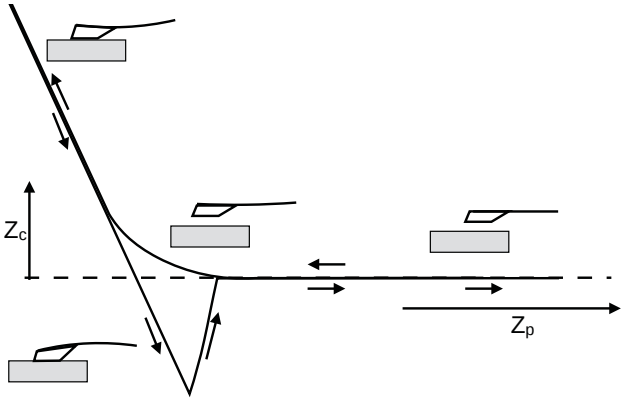

Figure 4.2: A typical cantilever deflection (Z_c) upon approach to the surface and retraction vs. position of piezo (Z_p). The sketch is inspired from (Butt et al., 2005), and modified to a flat probe with relatively similar geometry used in all measurements of this work.

by fitting a Lorentz function to the spectrum (see e.g., (Hutter and Bechhoefer, 1993, Figure 3)).

A force-distance curve at the start of each experiment is used to determine the sensitivity of the cantilevers. The sensitivity depends on the cantilever properties and the optical path of the laser light in the experimental environment. We, therefore performed this stage of the calibration every time we exchanged the fluid during our experiments (see Manuscript I (Javadi and Røyne, 2018) for more detail on the fluid exchange process). Sensitivity calibration is done by measuring a set of output voltages and the corresponding cantilever deflection (in nanometers). When an AFM is in contact with a hard surface (e.g., Figure 4.2), the cantilever deflection is increasing linearly in the repulsive contact region. By choosing that linear part of the contact region (where the approach curve meets the retract curve), the AFM software can determine the factor to convert the voltage into nanometer, named as sensitivity with (nm/V) as its unit. A typical sensitivity is up to 100 nm/V, depending on the environment (air or liquid). We measured values between 50 and 85 nm/V for all experiments presented in this work.

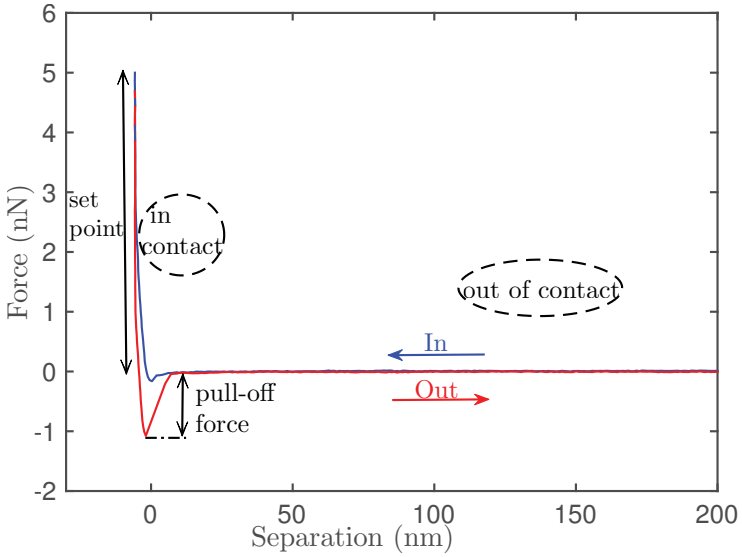

Figure 4.3: Force-distance curve between two calcite surfaces in 800 mM NaCl solution. This figure shows the pull-off force, which is the measure of adhesive strength based on the force used in pulling the cantilever off the surface. Set point refers to the applied normal force, which equals to 5 nN in this measurement. This figure is adopted from (Javadi and Røyne, 2018).

4.1.2 Colloidal probe technique

An important breakthrough in AFM force measurements came in the work of Ducker et al. (1991) and Butt (1991) with the introduction of the so-called "colloidal probe technique". In this technique the cantilever is modified by attaching a particle/fragment to the end of a tipless cantilever, replacing the typical sharp tip of the AFM. This technique has made the AFM force measurements more applicable for different materials, and for *in situ* measurements. With this technique, depending on the shape and size of the attached particles, highly sensitive quantitative analyze of surface forces have become more feasible (Butt et al., 2005).

Ducker et al. (1991) introduced their method by glueing silica spheres, with 3.5 μm radius, to a cantilever for long-range repulsive force measurements between two silica surfaces in NaCl solu-

tions. Shortly after, Butt (1991) used the same method and glued alumina and diamond shards and glass beads for force measurements against mica and glass planar surfaces, showing that the colloidal probe technique is not limited to only spherical particles. The probe can be fabricated in various sizes and shapes depending on the measurement requirements. Force measurements with the colloidal probe technique is now a well established technique, through which the measurements of interaction between surfaces with various chemical compositions have been studied by several groups using either commercial or *in situ* fabricated colloidal AFM probes (Biggs et al., 2005; Jiang and Turner, 2016; Levenson and Emmanuel, 2017; Liu et al., 2016; Pourchet et al., 2013; Røyne et al., 2015). There are multiple methods to develop and fabricate the AFM microprobes in addition to those that are commercially available (see e.g., http://www.nanosensors.com/products-catalog and (Butt et al., 2005)).

In this thesis, we use the colloidal probe technique to *in situ* fabricate a calcite probe for measuring the interaction between two calcite surfaces, as fully described in Section 4.3.

4.1.3 Challenges with AFM force measurements in liquids

During surface force measurements, in addition to van der Waals, electrical double layer, hydrophobic forces (between two hydrophobic surfaces), and hydration repulsion forces (between two hydrophilic surfaces), one must consider that due to the relative motion of surfaces and the liquid, hydrodynamic forces contribute to the observed interactions between two surfaces.

Hydrodynamic forces, like friction forces, belong to a group of forces that only appear as "a reaction to motion" (Israelachvili, 2011). During force measurements with colloidal probe technique in liquids, the cantilever moves up and down with respect to the surface. Unless this movement is at low speed, the extension and retraction parts of the force curves will have different baselines due to the hydrodynamic drag (Butt et al., 2005). The baseline refers

to $Z_c = 0$ and $Z_p = D$ in the non-contact region as seen in Figure 4.2. The hydrodynamic force is, also, a function of distance; it is repulsive upon approach and attractive upon retraction, which might be confused with other types of interfacial forces.

During the force measurements with AFM colloidal probe in aqueous solutions, the hydrodynamic forces must be taken into account unless the approach and retract velocities are slow enough to eliminate the effect of these forces. In this study, we measured no hydrodynamic effect at velocities below 500 nm/s. All experiments presented here have been performed at 150 nm/s $\leq$ v $\leq$ 200 nm/s to avoid any possible hydrodynamic effect.

4.2 Surface Force Apparatus

The Surface Force Apparatus (SFA) measures interaction forces between surfaces in fluids (air or liquid) at nN resolution based on optical interferometry (Israelachvili and Tabor, 1972; Tabor and Winterton, 1968). The SFA has the potential to measure both the interfacial forces and surface deformations. SFA also provides information on the thickness of the fluid film confined between the two surfaces. The quantitative measure of surface separation, in addition to visualizing the surfaces during force measurements, make the SFA superior over the AFM. However, the SFA is limited to flexible, transparent surfaces due to the geometry of the sample holders (Figure 4.4).

In the SFA, the separation (D) between two interacting surfaces, the interaction forces (F), and the surface shape (deformations) are measured by analyzing the optical interference fringes that result from, white light passing through the opposing surfaces (Figure 4.4). The transmitted light is the result of multiple beam reflections between the semi-reflective samples, and observed in a spectrometer as interferometric "Fringes of Equal Chromatic Orders" (FECO) (Israellachvili, 2013).

The multiple beam interferometry technique is based on placing two transparent materials, with a semi-reflective backside coating (e.g., 45 - 55 nm thick films of deposited gold or silver), in a close

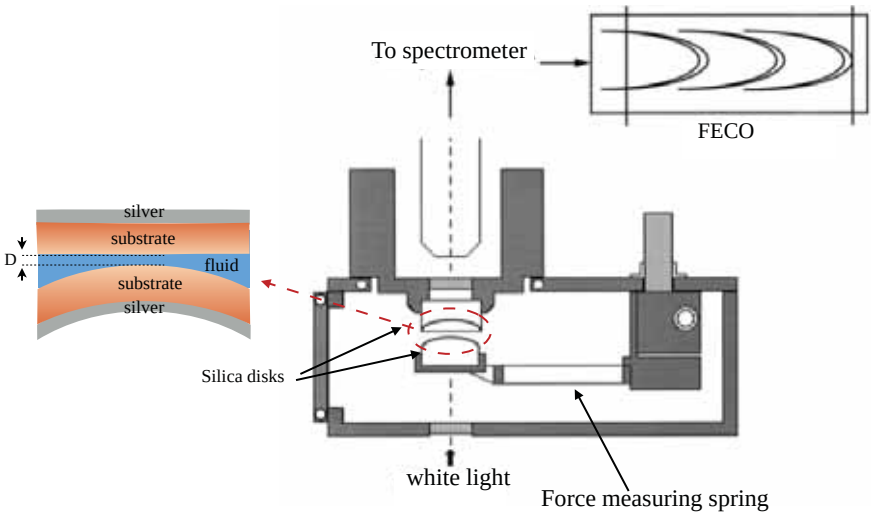

Figure 4.4: Schematic sketch of the SFA. The cross-section of the contact is highly magnified here for illustration of the opposing surfaces in fluid mounted on silica disks (typically with radius of 1 cm) for measurement. This sketch is reproduced from (Fröberg et al., 1999) with permission.

vicinity. The transmitted light, with discrete wavelength λ_{n}^{0}, that has gone through multiple reflections between the surfaces is converged with an optical lens, and measured as fringes (FECO) in a spectrometer. The wavelength of the transmitted light is characterized as λ_{n}^{0} when two surfaces are in contact and as $\lambda_{\mathrm{n}}^{\mathrm{D}}$ when they are separated. In a typical SFA measurement with mica $\lambda_{\mathrm{n}}^{\mathrm{D}}$ is measured by (Israellachvili, 2013),

$$\tan(2\pi\mu \mathrm{D}/\lambda_{\mathrm{n}}^{\mathrm{D}}) = \frac{2\bar{\mu}\sin\left(\frac{(1-\lambda_{\mathrm{n}}^{0})/\lambda_{\mathrm{n}}^{\mathrm{D}}}{(1-\lambda_{\mathrm{n}}^{0})/(\lambda_{\mathrm{n-1}}^{0})}\pi\right)}{(1+\bar{\mu}^{2})\cos\left(\frac{(1-\lambda_{\mathrm{n}}^{0})/(\lambda_{\mathrm{n}}^{\mathrm{D}})}{(1-\lambda_{\mathrm{n}}^{0})/(\lambda_{\mathrm{n-1}}^{0})}\pi\right) \pm (\bar{\mu}^{2}-1)} \tag{4.2}$$

where $\bar{\mu} = \mu_{\mathrm{mica}}/\mu$ with μ_{mica} as the refractive index of mica at λ_n^D and μ is the refractive index of the fluid between two mica surfaces. Plus sign (+) refers to the odd fringes ($n = 1, 3, 5, ..$) and minus sign

(-) for even fringes ($n = 0, 2, 4, ..$). The great benefit of this method is that the thickness of mica films does not need to be known, as long as both films have the same thickness. This method is usually ideal for experiments with symmetrical layers and known order of contact fringes (small separations) (Israelachvili, 1973; Tadmor et al., 2003).

In this study, we use an open source software Reflcalc (Reithmeier and Erbe, 2010) to calculate the surface separations between in-house customized deposited calcite surfaces (see Section 4.3.2) in the SFA. More details regarding force measurements between calcite surfaces are given in Manuscript II (Dziadkowiec et al., 2018) and in the supporting information document.

During force runs in the SFA, the lower surface is moved relative to the upper surface using a motor. Forces acting between the surfaces cause the force measuring spring, on which the lower surface is fixed, to bend (it is a "double-spring cantilever" with $k \approx 2000 N/m$ (Israellachvili, 2013)), (see Figure 4.4). The change in separation (displacement) measured by the optical interferemeter is linearly proportional to the applied force, based on the Hooke's law ($F = kD$). The measured force between curved surfaces is normalized by the surface radius R. It corresponds to the interaction free energy per unit area, G, between two flat surfaces, based on approximation by Derjaguin (in 1934) (Israelachvili, 2011),

$$\frac{F}{R} = 2\pi G \tag{4.3}$$

this equation is valid while the surface separation is much smaller compared to R.

4.3 Experimental methods

The results of all experiments performed for this work are presented as two publications (Dziadkowiec et al., 2018; Javadi and Røyne, 2018), and one manuscript in preparation. The first manuscript builds on preliminary AFM experiments at the University of Copenhagen and presents results from experiments with the AFM, JPK system, installed in the Physics department at the University of

Oslo. The study described in the second manuscript involved installing the SFA in the Physics department from scratch, along with my own designed temperature controller box and the enclosure. In addition, an extended number of trials took place for sample preparation for the SFA that resulted in the successful method presented briefly in Section 4.3.2 and with more detail in the Manuscript II, a practical method for measuring interactions between calcite surfaces in various aqueous solutions with SFA. The third manuscript is inspired by the other two studies, in which we present the result of combining two experimental methods, AFM colloidal probe and inverse imaging, to investigate the calcite surface roughness evolution as the effect of various aqueous solutions and find a link between calcite dissolution and/or recrystallization processes and measured surface forces. Following is mainly focused on describing these experimental methods.

4.3.1 Using calcite in the AFM

In this work, we use a JPK NanoWizard®4 Bioscience AFM. We keep it in force spectroscopy mode for force measurements and in QI-mode (Quantitative Imaging) for the imaging. This AFM is placed on an inverted Olympus IX71 microscope. In addition, there is a stand-alone operation TopViewOptics^{TM}to provide a clear top view of the sample. We use this tool for the probe fabrication procedure as well as during entire experiments to monitor the sample.

4.3.1.1 Materials

We use Iceland spar calcite for all performed AFM measurements in this work. Prior to each experiment, we cleave the calcite to an approx. 5×5 mm crystal and glue it to a glass slide using a UV-curing adhesive (Casco Glaslim). We customized a fluid cell as such we can exchange the fluid easily during experiments (Figure 4.5). For that, we use a plastic ring (20 mm inner diameter, 6.5 mm height, final capacity approx. 3.5 ml) and embedded inlet and outlet ports connecting to plastic tubing. In order to fix the fluid cell, we use Reprorubber self-cure rubber. To avoid fluid evaporation, we

use a silicon membrane to loosely seal the top of the fluid cell.

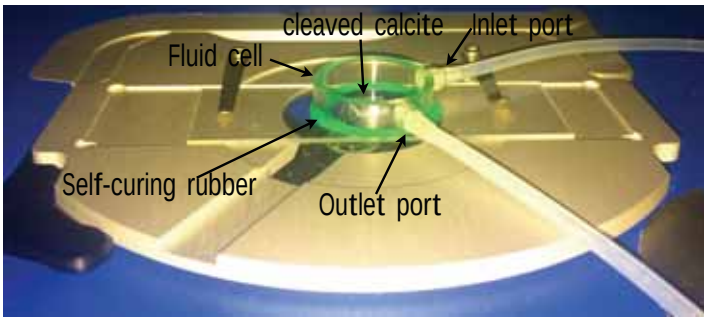

Figure 4.5: Cleaved calcite inside a custom made fluid cell with one inlet and one outlet for fluid exchange. It is fixed to the JPK AFM stage that was used for all measurements.

Solutions used for all experiments were made using various concentrations of NaCl (VWR, 100.2%), $MgSO_4$ (MERCK, 98%), and $MgCl_2$ hexahydrate (MERCK, 99-101%) in pre-saturated $CaCO_3$ solutions using $CaCO_3$ powder (MERCK) and deionized (type II) water. All solutions were made at least two weeks before every experiment, and left stationary to reach to the equilibrium state. Solutions are kept 12h before experiments inside the AFM enclosure for thermal equilibration. The measurement of pH-value for each solution shows no significant change before and after each experiment (averaged value of 8-9). These measurements are all in good agreement with our calculations using PHREEQC for open and closed systems (see Manuscript I: (Javadi and Røyne, 2018)). The difference between open and closed systems is the exchange of CO_2 with the atmosphere, as such it is none for the closed systems.

4.3.1.2 AFM-probe modification

The AFM calcite probe plays the role of the second calcite surface in our measurements, and is placed against the cleaved surface. We adapt the method of fabrication from (Røyne et al., 2015), as shown in Figure 4.6. Cleaving calcite leaves a surface full of small calcite fragments. Among those we choose a fragment with 40-70 μm in length and 15-20 μm in width.

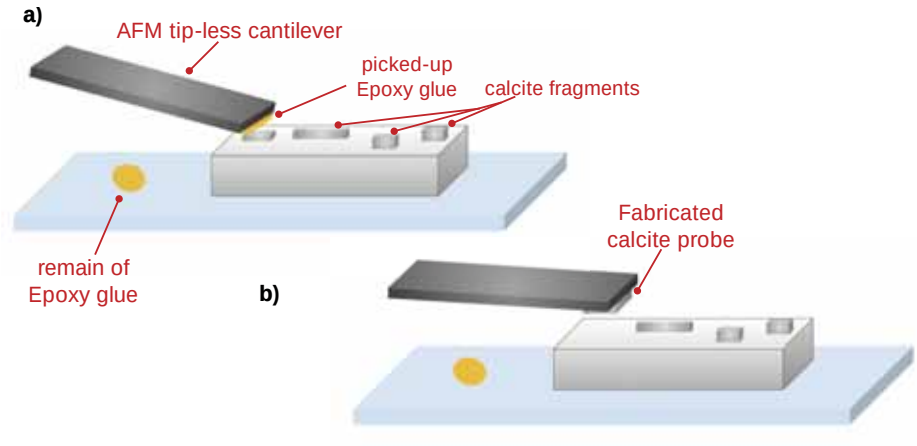

Figure 4.6: A, not to scale, sketch to illustrate the preparation of calcite probe. a) Freshly cleaved calcite crystal with small fragments on surface, glued to a microscope glass slide with a drop of epoxy glue by its side. AFM tipless cantilever is already picked up the glue and ready to engage to the suitable calcite fragment. b) After 16 hours the Epoxy glue is cured and calcite fragment is attached to the cantilever, ready to start the measurement. The fluid cell is not sketched here, in order to simplify the illustration.

A tipless cantilever (All In One-TL, 15 kHz, 0.2 N/m) is moved over a drop of two component epoxy glue (Epoxy Universal 335, DANA LIM, mixing ratio 1:1), that is placed close to the crystal, brought down to pick up a tiny drop, and moved back to the position of the chosen particle (Figure 4.6a). The cantilever is then brought into contact with the calcite fragment and left at a constant applied force overnight, approx. 12-16h, to set. Figure 4.6b shows a ready-to-use calcite probe. In order to ensure two parallel interacting surfaces, all measurements are performed without moving the calcite probe from its initial position. Before each glueing process, we measure the spring constant of the cantilever and the sensitivity with the methods described in Section 4.1.1.2. Figure 4.7 shows a SEM image of one calcite probe after the experiment.

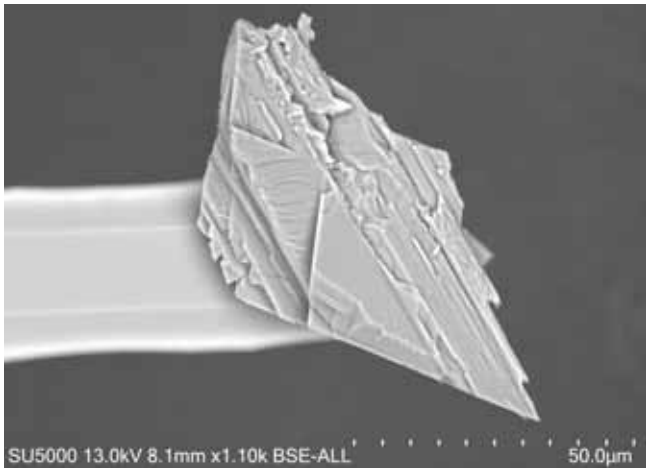

Figure 4.7: SEM image of a representative calcite probe, after the experiment, with surface area $\approx 1520\ \mu m^2$. This is imaged by a Hitachi SU5000 FE-SEM, at 13 kV acceleration voltage.

4.3.1.3 Inverse imaging

We study the possible variation in surface topography of the calcite probe as a function of time and chemical composition of fluid using "inverse imaging", a method that was first introduced by Montelius and Tegenfeldt (1993), for imaging and characterizing an *in situ* deposited silver probe. Several people have reported using this technique for biological applications, e.g. (Stewart et al., 2013), but to the best of our knowledge, this method has not been used for characterization of calcite surfaces. The result of this study is presented as Manuscript III.

In this method, we use the self-curing rubber (mentioned above) to fix a cantilever (RTESP-300, 300 kHz, 40 N/m), tip pointing upward, on the glass-bottomed of the fluid cell. The cantilever chip is placed next to a $\approx 3\times3$ mm cleaved calcite crystal as shown in Figure 4.8. The probe modification follows the method described above except for the size of the calcite crystal. We had to cleave a smaller crystal in order to fit in the fluid cell adjacent to the inverted cantilever.

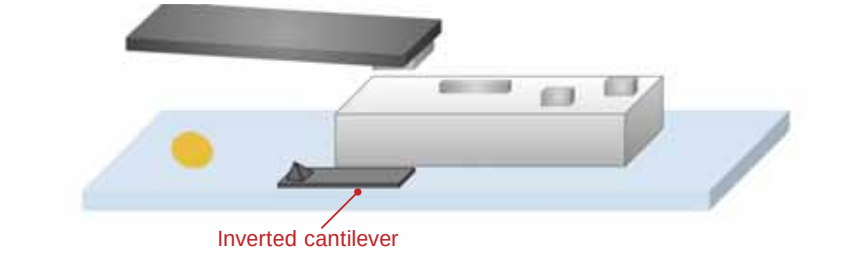

Figure 4.8: Illustration of inverted cantilever next to the cleaved calcite, additional procedure to the probe modification (Figure 4.6). The whole setup is placed in the previously introduced fluid cell. The sketch is not to scale.

4.3.2 Using calcite in the SFA

Muscovite mica with its molecularly smooth surface is known to be an ideal material for SFA measurements (Alcantar et al., 2003a; Anzalone et al., 2006; Baimpos et al., 2014; Donaldson et al., 2015; Heuberger et al., 2017). However, SFA experiments have not been limited to only mica surfaces. In addition to biological surfaces (Leckband, 1995; Sivasankar et al., 1999; Yang et al., 2012), Benz et al. (2006) used SFA for measuring the surface roughness effect on adhesion between polymeric surfaces; and Alcantar et al. (2003b) for adhesion of "ductile" metal surfaces. Due to their brittle nature, calcite surfaces had not been used in the SFA before. Only recently Chen et al. (2017) used synthesized discontinuous calcite surfaces for studying the calcite reactivity in SFA measurements, and wettability of calcite in the context of oil recovery in EOR systems.

In this work, we use the SFA (SFA2000; SurfaceForce LLC, USA) (Israelachvili et al., 2010), equipped with a spectrometer (Princeton Instruments IsoPlane SCT320 with a PIXIS2048B camera) for MBI and a camera (Thorlabs DCC1645C) for surface topography observations (resolution of 0.015 μm/pixel). The primary goal of this project was to develop a method for using calcite surfaces in the SFA and then measuring the adhesive properties of calcite in brine. We tested different ways of calcite preparation for the SFA, among which calcite deposition using Atomic Layer Vapor Deposition (ALVD) method was proved most suitable. With this method

polycrystalline calcite films, 100-200 nm thick, were grown on gold-coated cleaved mica films with 1-10 μm thickness. This method is adapted from Nilsen et al. (2004). In summary, the growth of calcite films happens by frequently pulsing the precursors: $Ca(thd)_2$ (Hthds2,2,6,6-tetramethylheptan-3,5-dione) as a Ca source, Ozone gas and CO_2 in a reaction chamber. An inert gas (N_2) flows, with a constant rate, into the chamber between each pulse of precursors to control the reactor pressure. The deposition reaction takes place in the gas phase but the growth of calcite films happens on the substrates placed in the reaction chamber. Gold-coated mica films are those solid substrates for our samples. The deposition temperature ranged between 250 and 300° C (Dziadkowiec et al., 2018). Further details are given in Manuscript II (Dziadkowiec et al., 2018).

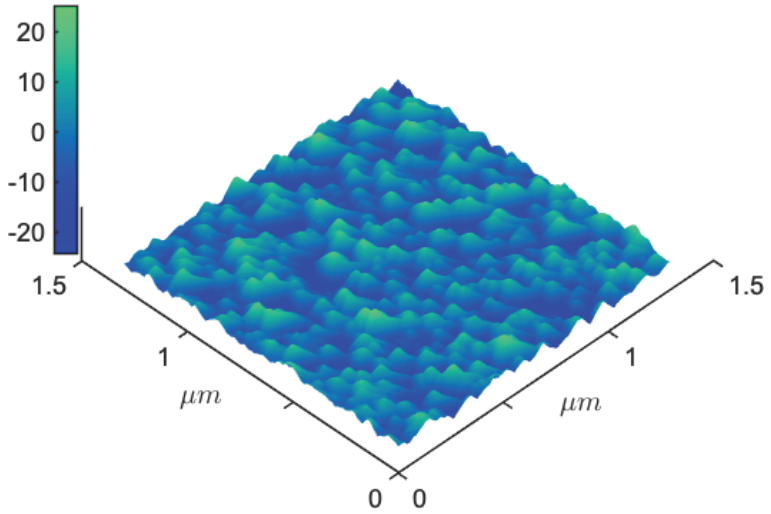

Figure 4.9: Topography measurement of ALD deposited calcite film on Mica at 300°C, shown as AFM height map (rms = 4.3 nm).

Following our goal, the deposited calcite films could be easily mounted on the SFA cylindrical disks. After each deposition, we performed X-ray diffraction (XRD) analysis that confirmed the films were composed of calcite, mostly oriented in the (104) direction (see Manuscript II: (Dziadkowiec et al., 2018)). The only drawback of these deposited films was the uncontrolled surface roughness. The

surface roughness was characterized as rms values and measured by the AFM before and after the SFA experiments (see also the Manuscript II for the discussion on surface roughness). As an example Figure 4.9 shows one of the calcite films deposited on mica at 300° C with thickness ≈100 nm and rms value of 4.3 nm.

Chapter 5

Results and discussion

The full results of the thesis work are presented as two publications and one manuscript in preparation. The first manuscript, titled "Adhesive forces between two cleaved calcite surfaces in NaCl solutions: The importance of ionic strength and normal loading", builds entirely on AFM experiments. The second manuscript, titled "Surface Force Apparatus measurements of interaction between rough and reactive calcite surfaces", introduces a practical method for measuring interactions between calcite surfaces in various aqueous solutions using the SFA. For further experimental details, see Chapter 4.

In the first two manuscripts, we found significant effects of calcite surface topography (or roughness) and nm-scale crystallization processes on the interfacial forces between calcite grains in aqueous solutions, with their possible effect on the observed decrease of cohesion in the saturated carbonate bearing rocks. Therefore, it was important to extend our measurements to a further detailed investigation of surface roughness evolution, and finding visual evidence on the effect of roughness on the interaction between calcite surfaces in brines. For that reason, we introduce the inverse imaging technique with AFM, for the first time using calcite, in Manuscript III titled "Direct observation of AFM calcite probe: Implication for calcite roughness evolution measurement". With this technique, we can measure the surface forces between the calcite probe and an opposing calcite surface while measuring the topography variation

in the surface of the calcite probe.

In this chapter, I have summarized and discussed the main results of the thesis. Further details are given in the attached manuscripts. The most significant results of the thesis work relate to how the adhesion between two calcite surfaces are affected by fluid chemistry, applied normal force, time, contact area and roughness.

5.1 Main results

5.1.1 Effect of fluid chemistry

By using the AFM, we measured the interaction forces between two freshly cleaved calcite surfaces in $CaCO_3$-saturated solutions with varying NaCl concentration. In these measurements, we consistently observed that the interaction between calcite surfaces changed from repulsive to adhesive when the concentration of NaCl exceeded about 100 mM (see Figure 5.1(right) for an exemplary result). With continuing increase in salinity, the measured adhesion (quantified as the force required to separate two surfaces from an adhesive contact) was observed to increase with increasing the NaCl concentration. In agreement with recent studies by Diao and Espinosa-Marzal (2016) and Røyne et al. (2015), we also measured strong repulsion in low NaCl concentration and water ($CaCO_3$-saturated solution). Similar results were achieved through our SFA measurements in $CaCO_3$-saturated solutions.

5.1.2 Effect of applied normal load

In AFM experiments, the measured adhesion was found to increase when the applied normal force was increased in the range from 5 to 30 nN. This behavior is fitted, for all experiments, to a linear function of the form $F_{ad} = \alpha F_n + F_{ad}^0$, where F_{ad} is the measured pull-off force (adhesion) and F_n is the applied normal force. Figure 5.1(left) shows the data collapse onto this linear curve, where $F_{ad} - F_{ad}^0$ is plotted against αF_n.

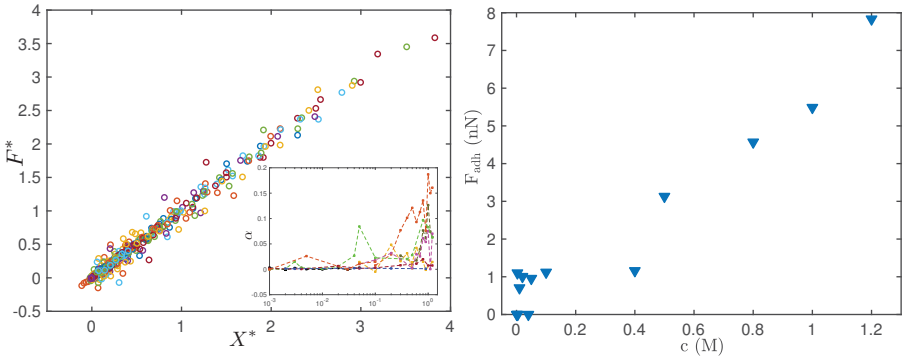

Figure 5.1: The effect of applied normal load (left) and NaCl concentration (right) on adhesive forces between two calcite surfaces during AFM measurements. **Left:** this plot shows the collapse of adhesion vs. applied normal load when $F^* = F_{ad} - F^0_{ad}$ is plotted vs. $X^* = \alpha F_n$. The inset shows the slope (α) of the fitting curve against concentration (x-axis is plotted in log-scale). **Right:** an exemplary result (calcite probe surface area = 650 μm^2) of measured adhesion that increases with NaCl concentration. The left plot is modified from (Javadi and Røyne, 2018).

5.1.3 Effect of time and surface roughness

Because of the dynamic nature of calcite in contact with water molecules (Stipp et al., 1996), we expected the actual contact area between the contacting surfaces to change continuously, and to observe such effect as a variation in the measured adhesion with time in our AFM experiments. We only observed a slow change in measured adhesion (F_{ad}) with time, with no consistent increasing or decreasing trend. Figure 5.2 shows an exemplary result of F_{ad} for one set of two interacting calcite surfaces in NaCl solution of 500 mM concentration. The applied force (F_n) is in the range of 5 to 30 nN for each loop. The upward trend illustrated in Figure 5.2 is not a consistent trend for all our measurements.

In our SFA measurements, we measured the interaction forces between similar (calcite-calcite (CC)) and dissimilar (calcite-mica (CM)) surfaces in water (saturated $CaCO_3$ solutions). Depending on the calcite surface roughness, we measured adhesion and repulsion between calcite and mica in $CaCO_3$ solutions and only repulsion

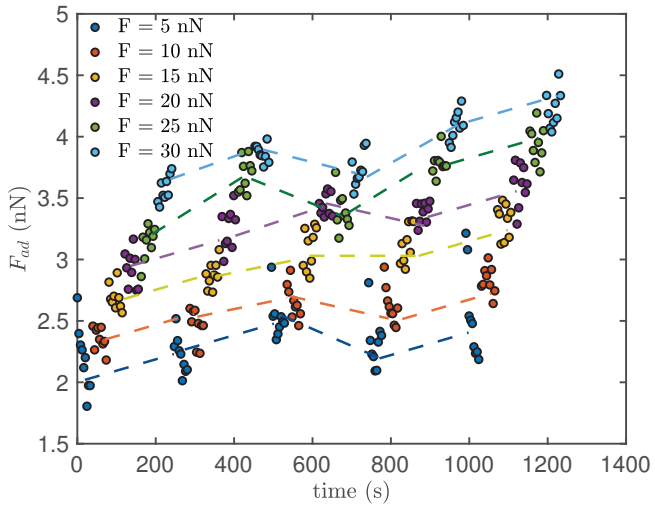

Figure 5.2: Measured adhesion with time in NaCl solution with 500 mM concentration. Measured adhesion (F_{ad}) increases with F_n in each loop and mostly return to their initial state (for low values of F_n). The dotted line is a sketch to illustrate the variation trend of F_{ad} with time at each applied load value. This plot is modified from (Javadi and Røyne, 2018).

between calcite surfaces independent on surface roughness. Both the magnitude and onset of attractive and repulsive forces are expected to depend on the surface roughness (Teng et al., 2011; Valtiner et al., 2012). Therefore, to quantify the variation in surface roughness during the experiments, we introduced an exponential decay length (λ) of the approach part of the repulsive force curves (fitted to $F(D) = F_0 \exp(-D/\lambda)$) to be an indirect measure of surface roughness (Parsons et al., 2014). Figure 5.3 shows the repulsive forces as a function of distance (D) between CC and CM surfaces in $CaCO_3$ solutions, where the magnitude and onset of the repulsive forces are strongly influenced by the calcite surface roughness (which is measured by λ).

We observed increasing adhesion with applied force between calcite and mica surfaces, in $CaCO_3$-solutions, with time. This was correlated directly with the decrease of calcite surface roughness, as discussed later.

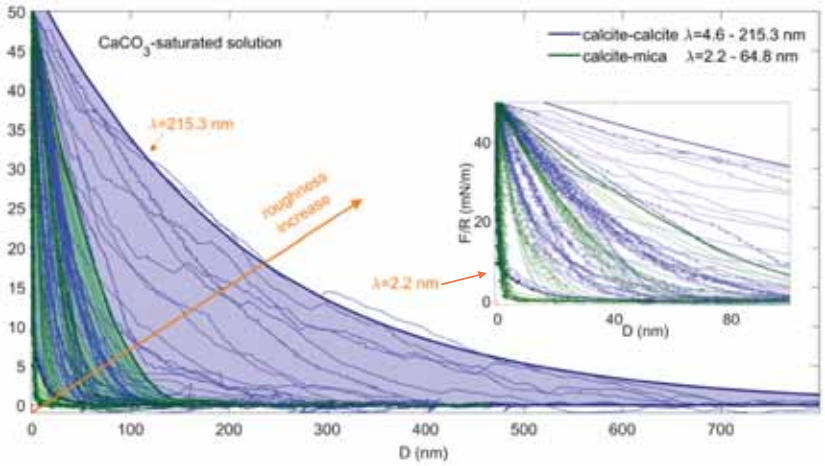

Figure 5.3: Repulsive forces is plotted against the distance between two calcite surfaces (blue) and between calcite and mica (green) in $CaCO_3$-saturated solutions. In this figure, only the force curves on approach are shown. D = 0 is located at the applied load of ≈50 mN/m for all force curves. The shadings mark approximate ranges of the measured force. The inset shows a closer approach to the D region between 0 and 100 nm. Figure is from (Dziadkowiec et al., 2018).

In our AFM experiments, we optically measured surface area of each modified calcite probe before the experiments. These values are referred to as nominal surface area in this work. Through our measureents, we observed no correlation between measured adhesion and the nominal contact area. This is because the actual contact area for rough surfaces, e.g. calcite, is a function of number, size and height of asperities; and surface forces are measured depending on the geometry, density (Bhattacharjee et al., 1998; Huang et al., 2010) and height distribution of asperities (Eom et al., 2017; Parsons et al., 2014). This makes the actual contact area being always smaller than the nominal area (Prokopovich and Perni, 2010). Hoek and Agarwal (2006) have also observed a similar behavior for the rough polyamide membranes, where the average interaction energy was measured as a function of surface area, size and density of surface asperities.

Based on our measurements with both AFM and SFA, progres-

sive variation in calcite surface topography with time, due to nm-recystallization upon equilibration with pore fluid of varied chemistry, influences the measured adhesion between two calcite surfaces and consequently their mechanical strength. We therefore, introduced an additional method to quantify this effect using "inverse imaging" technique with AFM, that is described in Chapter 4. Through these measurements, we observed that the surface roughness, which is characterized by λ, is decreasing with time in $MgSO_4$, $MgCl_2$ and NaCl solutions with ionic strength of 1.2 M. Figure 5.4 shows an exemplary result of the average values for variation of measured λ in $MgSO_4$ and NaCl solutions with time. These results indicate that the calcite surfaces might become smoother with time in the electrolyte solutions used here.

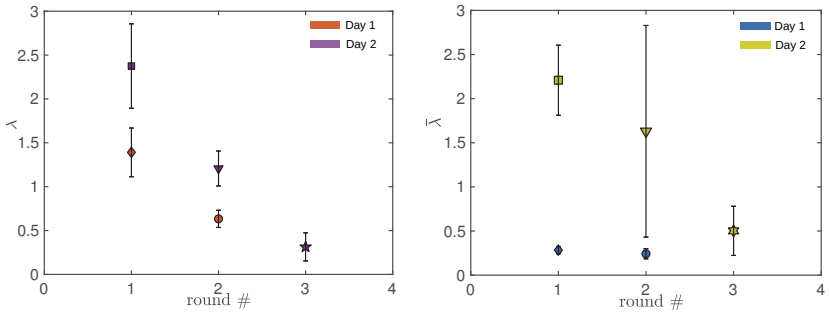

Figure 5.4: The averaged λ is plotted against number of measurement rounds (i.e., elapsed time) in $MgSO_4$ (left) and NaCl (right) with the same ionic strength of 1.2 M. Different color in each plot represents one day of measurement, and each marker stands for $\bar{\lambda}$ of one round of ≈200 force curves.

5.2 Discussion

We measured adhesion between calcite surfaces in NaCl solutions around 100 mM, and found that by increasing the concentration the adhesion becomes stronger. Possible explanations for this observation include the decreased level of water activity (Kohns et al., 2016; Mutisya et al., 2017) or the DLVO theory through which the

higher salt concentration is linked with decreased electrical double layer repulsion and the dominance of van der Waals attractive forces. However, since in our PHREEQC calculations we found a minor change in water activity between low and high salt concentrations; and the ionic strength is beyond what should be the limit of the DLVO theory (Smith et al., 2016), these assumptions cannot be valid for our measurements. Instead, we propose that progressively weak secondary hydration and strong ion-ion correlation forces are the key mechanisms leading to stronger adhesion measured in higher-concentration solutions. In this study, we attributed the measured repulsion between calcite surfaces in water to both repulsive secondary hydration forces and to the roughness effect. The secondary hydration forces are long ranged repulsive forces due to hydration of solute molecules near the surface at small separations (see Chapter 3). Both the hydration force and roughness effects add an exponentially repulsive component to the total interaction force between the surfaces (Eom et al., 2017); thus, it was not straightforward to distinguish between these two contributions. We used the model suggested by Parsons et al. (2014) to semi-quantify the roughness effect (Section 5.1.3), through which we showed that the hydration repulsion is lowering in magnitude as roughness increases, because only the highest asperities in contact will reach separations small enough to experience the nm-ranged interaction.

Assessing how the strength of contact-bonds, for rough calcite surfaces, in aqueous solutions may be influenced by normal load and salinity of the pore fluid can be relevant for carbonate rocks and geological environments, where calcite surfaces are under a various amount of pressure and in contact with percolating fluids. In our AFM experiments, the measured adhesion increased linearly with increasing the applied force (Figure 5.1(left)). The possible explanation may lie in the surface roughness. For rough surfaces, we may assume that the microscopic contribution to the macroscopic, effective interfacial energy, γ, can be expressed as the sum of the product of contact-bond strengths, β, and actual area, σ, of all contacting asperities that define the real surface area. Both parameters, β and σ, may change with time (t) and applied normal load (F_n):

$$\gamma(F_n, t) = \Sigma_i \beta_i(F_n, t)\sigma_i(F_n, t) \tag{5.1}$$

Elastic processes take place only if, the required force to separate two adhesive surfaces is independent of both time and applied load. In that case, the macroscopic surface energy on approach, γ_A, equals that on retraction, γ_r: $\gamma_A = \gamma_r$ (point A to B in Figure 5.5). When γ is not constant, the measured adhesion force will depend on the time and maximum applied load at the contact, point B to C vs. D to E in Figure 5.5.

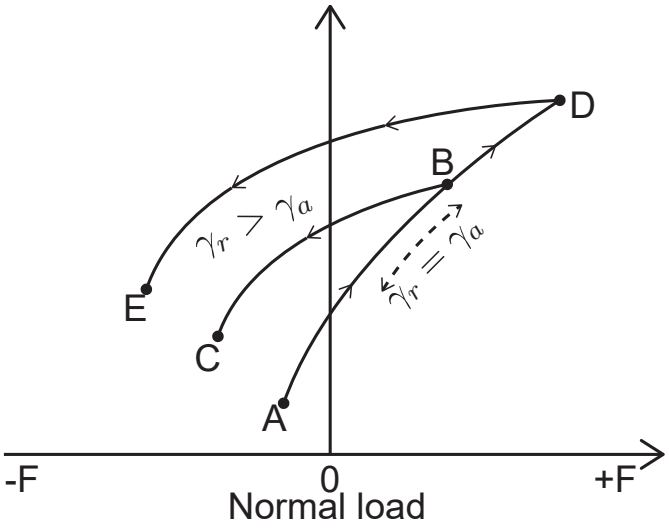

Figure 5.5: "Adhesion hysteresis", from (Javadi and Røyne, 2018), presenting reversible and irreversible cycles. Upon approach of adhesive surfaces, they jump into contact at A and move along the path to B with increasing normal load. In the case of constant interfacial energy ($\gamma_A = \gamma_r$), unloading follows the same path back to A and the force measured at separation is independent of the maximum applied load. If $\gamma_A > \gamma_r$, separation follows the path from B to C. The measured force of adhesion in this case depends on the maximum applied load (C vs. E).

When two rough surfaces are brought into contact under an applied normal load, time-dependent processes can lead to 1) chemical

strengthening of contact bonds (increased β in our case), and when unloading they will return to their original state, which was mostly what we observed in our measurements; and/or 2) asperity creep through dissolution-precipitation processes, a process that increases the contact area and consequently the measured adhesion forces. In the latter case, unloading will not return the surfaces to their original state, which is in contrary to what we observed through our AFM experiments (see Figure 5.2). In these measurements, the slight dependency on time and strong dependency on applied force of β take into account any possible chemical strengthening of asperities that might result from diffusion of ions or from slow chemical reactions. Such a phenomenon can have a significant effect in frictional strengthening of granular faults that are controlled by the contact strength-driven grain boundary friction (Chen and Spiers, 2016).

For rough loaded surfaces, the total contact area, σ in Equation 5.1, is the sum of areas of individual contacting surface asperities. Time and load-dependent "asperity creep" through dissolution and precipitation processes can increase the real area of contact (Gratier et al., 2009; Renard et al., 2012) that give rise to increased measured adhesion. This is an irreversible process that leads to the strengthening of natural faults in carbonates, and is related to the chemical reactivity of the interfaces (Renard et al., 2012). Here, through our AFM measurements, we measure a slight variation in the measured adhesion, in NaCl solutions, with time in a non-monotonic fashion (Figure 5.2). Although this might be the indication of irreversible changes in contact area (pressure solution), we observed no evidence of a consistent flattening of asperities nor plastic deformation of contacts with time. We propose that the variation in adhesion and the corresponding contact area is mostly attributed to the local recrystallization of single asperities in a multiple asperity system, i.e., rough calcite surfaces.

In our SFA experiments, we expected dissolution of rough contacting calcite surfaces to be influenced by the applied pressure, because of 1) pressure solution due to higher solubility of the stressed solid (Gibbs, 1878), and 2) plastic deformation due to flattening or breaking the higher asperities. We observed a larger volume

changes, of small crystals within the contact, in the CC (two interacting calcite surfaces) system than CM (calcite and mica interacting surfaces). We assumed that the contact area in CC was smaller than the CM system, due to calcite roughness. Therefore, in the CC system the stress transmitted at the discrete contacts is much higher than in the CM under the same load, which result into a much bigger extent of breakage or flattening of the highest asperities. However, since the surface roughness causes inhomogeneous stress distribution on the surface (Rutter and Elliott, 1976), it was not possible to quantify the dissolution as a function of applied force. Therefore, we barely observed any correlation between the applied load and the dissolution rate.

Increasing adhesion with applied force between calcite and mica surfaces, in $CaCO_3$-solutions, with time, through the SFA experiments, was correlated directly with the decrease of calcite surface roughness. This is suggested to be due to the progressive increase of real contact areas between the surfaces, caused by gradual pressure-driven deformation of calcite surface asperities during repeated loading and unloading cycles. This could be related to the healing processes for frictional interfaces as described, in detail, by Renard et al. (2012). We also show that the interface chemical reactivity of calcite is a function of the initial topography of the surfaces. Initially smoother surfaces show more roughening progress, which is shown by stronger measured repulsive forces.

Moreover, in our observations through the "inverse imaging" technique with AFM, we found that calcite surfaces became smoother with time in Mg^{+2}-salt and NaCl solutions (Figure 5.4). This effect might be significant for the calcite crack healing in the presence of Mg^{2+} that was observed by (Bergsaker et al., 2016). This could be due to the surface morphological changes that could have been a driving force to form a solid bond and increase the adhesion between surfaces separated by a nanometer-wide fracture. The observed increased adhesion might be because of a larger contact area, which is expected from smoother surfaces that was also observed in our SFA experiments.

In the oil and gas industry, the tertiary or EOR (Enhanced Oil Recovery) method is a group of techniques designed to increase the

oil recovery rate from an oil field, where the traditional oil extraction techniques are no longer effective. Depending on the initial wetting state of a chalk reservoir, injection of water can promote oil recovery if the reserve is initially water-wet (like the Ekofisk field). In addition to the initial wettability state of the reservoir, the chemical composition of the injected fluid (Fathi et al., 2010; Risnes et al., 2003; Zhang et al., 2006) plays an important role in determining the oil recovery efficiency. Seawater injection into the oil reservoir has been proved to be one exemplary successful EOR method (Puntervold, 2008).

Several studies have supported the hypothesis that electrostatic interactions between the calcite surfaces and hydrocarbons' components define whether the surface repels or adsorbs the oil molecules by making changes in the surface charge (Hassenkam et al., 2009; Pedersen et al., 2016; Skovbjerg et al., 2013). Therefore, it is expected that controlling the electrostatic forces by, for instance, adjusting the salinity of contacting fluid will be an effective mechanism to desorb the oil from calcite surfaces and produce oil more effectively (Pedersen et al., 2016). For example, Liu et al. (2016) observed that injection of NaCl solution (low and high concentrations) into a carbonate rock increases the oil desorption rate from calcite surfaces. They explained this result by increased solubility of calcite in high concentration NaCl solution, which in turn increases the local pH, leading to more negatively charged calcite surfaces and hence repulsive forces between the calcite and the oil. For low NaCl concentrations, they relate the high-rate oil desorption to the EDL repulsive forces between oil and calcite surfaces. The EDL repulsion in a confined fluid film has a large range for solutions of low salinity, which can help stabilize a thicker fluid film [1]. This can make min-

[1] As discussed in Chapter 1, the stability and thickness of the water film are controlled by the disjoining pressure (Bergeron and Radke, 1995). If the disjoining pressure of the water film between the oil and the mineral surface is low, the water film can collapse, so that oil comes into contact with the pore wall and makes the rock more oil-wet. The wettability can change from water wet to oil wet by absorption of active components in the oil to the Ca^{2+}-sites of the surface (Hiorth et al., 2010). On the other hand, if the disjoining pressure is higher, the water film can remain intact between the oil and the pore wall,

eral surfaces become more water-wet, with tendency to repel the oil molecules (Awolayo et al., 2014; Derkani et al., 2018; Fathi et al., 2010; Hiorth et al., 2010; Liu et al., 2016; Myint and Firoozabadi, 2015; Puntervold, 2008; Shariatpanahi et al., 2011; Strand et al., 2006, 2008; Wang and Fu, 2018; Zhang et al., 2006). However, this mechanism is still being debated because of, 1) the heterogeneous surface properties of chalk (or calcite), leading to inhomogeneous wetting of the surface (Hassenkam et al., 2009; Matthiesen et al., 2014); and 2) the wide range polar and non-polar components present in oil (Gomari and Hamouda, 2006; Pedersen et al., 2016).

In this work, we showed that repulsive forces in water and low NaCl concentration solutions between calcite surfaces increase due to secondary hydration forces and roughness effect. Repulsive forces, apart from enhacing the repulsion between calcite surfaces, have a positive contribution in disjoining pressure that create a more stable water film confined between two surfaces (or making the calcite surfaces more water-wet). Therefore, the contact between oil droplets and rock surfaces become more prevented; thus increasing the oil recovery. Water wettability of the calcite surfaces has been also found to increase with the surface roughness by Ulusoy and Yekeler (2005). This observation was further emphasized by Chen et al. (2017) for EOR systems, in which dilute electrolyte solutions enhanced oil desorption from calcite surfaces both by affecting the colloidal forces (EDL, hydration, and vdW forces) and by increasing the surface roughness.

so that the rock is still water-wet.

Chapter 6

Conclusions and outlook

6.1 Conclusions

Through our investigation of the adhesive properties of calcite interfacse as a function of pore fluid chemistry at the nano-scale, we aimed to understand the chemical or/and physio-chemical processes responsible for the loss of macroscopic strength of water saturated carbonate, mainly chalk, rocks. We show that the strength of the contact bonds at the grain boundaries may be influenced by both the salinity of the confined fluid and the applied external force. In our AFM measurements, the chemical strengthening of the contact bonds appear to be more profound than the time and stress-induced surface deformation of calcite that could have been interpreted as pressure solution (known as a physio-chemical process (Hellmann et al., 1996)) or "asperity creep". Instead, we suggest that the strengthening of the contact-bonds is mostly due to the combination of applied normal stress, that increases the population of surface asperities in contact, and disturbs the calcite hydration layer by populating it with a high number of partially dehydrated cations, and increasing attractive ion-ion correlation forces. Our findings, i.e. the possible variation in local topography at contacts, together with a strong dependence on the ionic strength of the solution, might explain the inconsistent behavior of calcite rocks in NaCl solutions, as reported by different authors (Fathi et al., 2010,

2012; Liu et al., 2016).

Our findings, through the SFA force measurements, indicate that the observed low mechanical strength of water-saturated carbonate rocks may be explained by the strong hydration repulsion between calcite grains that can be additionally enhanced with the progressive nm-scale recrystallization of the calcite surfaces in water. The force of crystallization upon mineral growth produces mechanical repulsive effects that prevent the mineral surfaces with high surface roughness to develop adhesive contacts in water. We show that nm-scale rough surfaces give rise to repulsive effects due to asperity deformations that may be stronger than hydration effects.

In this thesis, we discuss that the dynamic calcite surfaces give rise to the *water weakening* phenomenon due to a progressive variation in the surface topography in contact with water molecules. We therefore suggest that surface roughening of calcite in water could be an additional mechanism to describe the *water weakening* and compaction phenomena due to their significant effect on increasing the repulsion between calcite surfaces and thus decreasing the cohesion between calcite grains in saturated carbonate rocks. Our findings also show that the chemical processes (i.e. progressively weaker secondary hydration and stronger ion-ion correlation forces) taken place at the local contacts are dominant explanation for the strength of calcium carbonate bearing rocks in NaCl solutions (with concentration > 100 mM).

Due to the molecular scale surface roughness of calcite surfaces, the contact area between the calcite grains is expected to be only a fraction of the nominal contact area. The surface roughness increases because of nm-scale recrystallization, which decreases the contact area; and, thus, impacts the measured surface forces. Therefore, a quantitative data set on contact topography and surface roughness evolution would be required for further investigations of the effect. Accordingly, we introduce an inverse imaging technique with AFM to monitor the *in situ* fabricated calcite probe, which is one of the contacting surfaces. With this technique, we aim to find the coupling between calcite recrystallization and measured surface forces in aqueous solutions, in particular, Mg^{2+}-salt solutions. Although we, currently, do not have enough results to draw a clear

conclusion, we believe that this technique is a powerful tool to study the coupling between the calcite surface roughness evolution and surface forces, which could have implications for crack healing and the mechanical strength of calcite-bearing rocks.

6.2 Suggestions for future work

Although the problem of compaction and *water weakening* of chalk has been studied for almost 30 years, our understanding about the role of interfacial fluids in deformation of porous carbonate sediments is still far from complete. This thesis shows that, apart from the chemistry of pore fluid, the surface topography of calcite, at nm to μm scale, has a significant role on surface forces and consequently in the chemical and physio-chemical processes responsible for the chalk compaction. Therefore, more detailed studies of possible changes in the roughness of calcite as a function of time, chemical composition, pH of solutions, temperature, and atmospheric CO_2 are of immediate interest.

In the same framework of the first manuscript, it would be interesting to study the interaction between calcite and silica in NaCl and $CaCl_2$ solutions, by moving a calcite AFM probe towards a smooth silica surface. This result could be compared with our first manuscript and the recent study by Diao and Espinosa-Marzal (2016) in which the repulsive forces between a smooth calcite surface and spherical silica probe were measured in $CaCl_2$ solutions and attributed to the hydration forces, in addition to the effect of confinement that induces pressure solution and recrystallization. Additionally, it might be possible to perform the reflective interference contrast microscopy (RICM) method (Li et al., 2017) alongside these measurements. With this method, measurement of change in contacting asperities might be possible by correlating the light intensity at the contacts with the corresponding height measurements from the AFM. This result leads to a better understanding of the roughness evolution as the influence of confinement and fluid chemistry.

Calcite is a dynamic surface (Stipp et al., 1996) and the conclu-

sive changes in surface roughness in aqueous solutions need to be investigated further in relation to surface forces and consequently water weakening. We suggest that the inverse imaging technique with AFM can be used for a quantitative investigation of contact topography and surface roughness. This method can be performed alone, similar to the work presented by the third manuscript or alongside the RICM method.

This thesis contains a feasible method for calcite measurements with SFA, therefore a more detailed study of forces between calcite surfaces is suggested for a better understanding of the strength of calcitic rocks in various chemical pore fluids.

Above all, I believe that there are many opportunities to extend this study and continue with the experiments initiated here. Changing only one of these parameters will be enough to open a new pathway for more explorations, which reminds me of a quote from a British mathematician, A de Morgan (1806-1871):

> *Great fleas have little fleas upon their backs to bite ém,*
> *and little fleas have lesser fleas and so ad infinitum.*
> *And the great fleas themselves, in turn,*
> *have greater fleas to go on;*
> *while these again have greater still, and greater still, and so on.*

Bibliography

E. R. Agudo and C. V. Putnis. Direct observations of mineral fluid reactions using atomic force microscopy: the specific example of calcite. *Mineralogical Magazine*, 76(1):227–253, 2012.

N. A. Alcantar, J. N. Israelachvili, and J. Boles. Forces and ionic transport between mica surfaces: implications for pressure solution. *Geochimica et Cosmochimica Acta*, 67(7):1289–1304, 2003a.

N. A. Alcantar, C. Park, J. M. Pan, and J. N. Israelachvili. Adhesion and coalescence of ductile metal surfaces and nanoparticles. *Acta materialia*, 51(1):31–47, 2003b.

M. P. Andersson, K. Dideriksen, H. Sakuma, and S. L. S. Stipp. Modelling how incorporation of divalent cations affects calcite wettability - Implications for biomineralisation and oil recovery. *Scientific Reports*, 6(28854), 2016.

A. Anzalone, J. Boles, G. Greene, K. Young, J. N. Israelachvili, and N. Alcantar. Confined fluids and their role in pressure solution. *Chemical Geology*, 230(3-4):220–231, 2006.

A. Awolayo, H. Sarma, and A. M. AlSumaiti. A laboratory study of ionic effect of smart water for enhancing oil recovery in carbonate reservoirs. In *SPE EOR Conference at Oil and Gas West Asia*, Muscat, Oman, 31 March-2 April 2014.

T. Baimpos, B. R. Shrestha, S. Raman, and M. Valtiner. Effect of interfacial ion structuring on range and magnitude of electric double layer, hydration, and adhesive interactions between mica

surfaces in 0.05-3 M Li^+ and Cs^+ electrolyte solutions. *Langmuir*, 30(15):4322–4332, 2014.

D. P. Bentz, C. F. Ferraris, S. Z. Jones, D. Lootens, and F. Zunino. Limestone and silica powder replacements for cement: Early-age performance. *Cement and Concrete Composites*, 78:43–56, April 2017.

M. Benz, K. J. Rosenberg, E. J. Kramer, and J. N. Israelachvili. The deformation and adhesion of randomly rough and patterned surfaces. *The Journal of Physical Chemistry B*, 110(24):11884–11893, 2006.

V. Bergeron and C. J. Radke. Disjoining pressure and stratification in asymmetric thin-liquid films. *Colloid and Polymer Science*, 273:165–174, 1995.

A. S. Bergsaker, A. Røyne, A. Ougier-Simonin, J. Aubry, and F. Renard. The effect of fluid composition, salinity, and acidity on subcritical crack growth in calcite crystals. *Journal of Geophysical Research: Solid Earth*, 121(3):1631–1651, 2016.

S. Bhattacharjee, C. H. Ko, and M. Elimelech. DLVO interaction between rough surfaces. *Langmuir*, 14:3365–3375, 1998.

S. Biggs, D. C. Prieve, and R. R. Dagastine. Direct comparison of atomic force microscopic and total internal reflection microscopic measurements in the presence of nonadsorbing polyelectrolytes. *Langmuir*, 21(12):5421–5428, 2005.

G. Binnig and C. F. Quate. Atomic force microscope. *Physical Review Letters*, 56(9), 1986.

M. J. Blandamer, J. B. Engberts, P. T. Gleeson, and J. C. Reis. Activity of water in aqueous systems; a frequently neglected property. *Chemical Society Reviews*, 34(5):440–58, 2005.

T. L. Blanton. Deformation of chalk under confining pressure and pore pressure. *Society of Petroleum Engineers*, 21(01), 1981.

J. Bohr, R. A. Wogelius, P. M. Morris, and S. L. S. Stipp. Thickness and structure of the water film deposited from vapour on calcite surfaces. *Geochimica et Cosmochimica Acta*, 74(21):5985–5999, 2010.

J. A. Brant and A. E. Childress. Membrane-Colloid interactions: Comparison of extended DLVO predictions with AFM force measurements. *Environmental Engineering Science*, 19(6):413–427, 2004.

N. Brantut, M. J. Heap, P. Baud, and P. G. Meredith. Mechanisms of time-dependent deformation in porous limestone. *Journal of Geophysical Research: Solid Earth*, 119(7):5444–5463, 2014.

G. Brekke-Svaland and F. Bresme. Interactions between hydrated calcium carbonate surfaces at nanoconfinement conditions. *The Journal of Physical Chemistry C*, 122(13):7321–7330, 2018.

H. J. Butt. Measuring electrostatic, van der Waals, and hydration forces in electrolyte solutions with an atomic force microscope. *Biophysical Journal*, 60(6):1438–1444, 1991.

H. J. Butt, K. Graf, and M. Kappl. *Physics and Chemistry of Interfaces*. Wiley, 2003.

H. J. Butt, B. Cappella, and M. Kappl. Force measurements with the atomic force microscope: Technique, interpretation and applications. *Surface Science Reports*, 59(1-6):1–152, 2005.

D. L. Chapman. A contribution to the theory of electrocapillarity. *Philosophical Magazine*, 25(148):475–481, 1913.

J. Chen and C. J. Spiers. Rate and state frictional and healing behavior of carbonate fault gouge explained using microphysical model. *Journal of Geophysical Research: Solid Earth*, 121(12): 8642–8665, 2016.

S.-Y. Chen, Y. Kaufman, K. Kristiansen, D. Seo, A. M. Schrader, M. B. Alotaibi, H. A. Dobbs, N. A. Cadirov, J. R. Boles, S. C. Ayirala, J. N. Israelachvili, and A. A. Yousef. Effects of salinity

on oil recovery (the Dilution Effect): Experimental and theoretical studies of crude oil/brine/carbonate surface restructuring and associated physicochemical interactions. *Energy and Fuels*, 31(9): 8925–8941, 2017.

M. O. Ciantia, R. Castellanza, G. B. Crosta, and T. Hueckel. Effects of mineral suspension and dissolution on strength and compressibility of soft carbonate rocks. *Engineering Geology*, 184:1–18, 2015.

D. Croizé. *Mechanical and chemical compaction of carbonates - An experimental study*. PhD thesis, Department of Geosciences, University of Oslo, 2010.

D. Croizé, F. Renard, K. Bjørlykke, and D. K. Dysthe. Experimental calcite dissolution under stress: Evolution of grain contact microstructure during pressure solution creep. *Journal of Geophysical Research*, 115(B9), 2010.

D. Croizé, F. Renard, and J. P. Gratier. Compaction and porosity reduction in carbonates: A review of observations, theory, and experiments. *Advances in Geophysics*, 54:181–238, 2013.

N. H. de Leeuw and S. C. Parker. Surface structure and morphology of calcium carbonate polymorphs calcite, aragonite, and vaterite: An atomistic approach. *Journal of Physical Chemistry B*, 102: 2914–2922, 1998.

P. Delage, C. Schroeder, and Y. J. Cui. Subsidence and capillary effects in chalks. *arxiv:0803.1308*, 2008.

B. Derjaguin and L. Landau. Theory of the stability of strongly charged lyophobic sols and of the adhesion of strongly charged particles in solutions of electrolytes. *Progress in Surface Science*, 43:1–4, 1941.

M. H. Derkani, A. J. Fletcher, W. Abdallah, B. Sauerer, J. Anderson, and Z. J. Zhang. Low salinity waterflooding in carbonate reservoirs. *Colloids and Interfaces*, 2(2):20, 2018.

M. D'Heur. Porosity and hydrocarbon distribution in the north sea chalk reservoirs. *Marine and Petroleum Geology*, 1(3):211–238, 1984.

Y. Diao and R. M. Espinosa-Marzal. Molecular insight into the nanoconfined calcite-solution interface. *Proceedings of the National Academy of Sciences*, 113(43):12047–12052, 2016.

J. Donaldson, S. H., A. Røyne, K. Kristiansen, M. V. Rapp, S. Das, M. A. Gebbie, D. W. Lee, P. Stock, M. Valtiner, and J. N. Israelachvili. Developing a general interaction potential for hydrophobic and hydrophilic interactions. *Langmuir*, 31(7):2051–2064, 2015.

D. Doornhof, T. G. Kristiansen, N. B. Nagel, P. D. Pattillo, and C. Sayers. Compaction and subsidence. *Oilfield Review*, 18(3): 50–68, 2006.

W. A. Ducker, T. J. Senden, and R. M. Pashley. Direct measurement of colloidal forces using an atomic force miscroscope. *Nature*, 353 (6341):239–241, 1991.

J. Dziadkowiec, S. Javadi, J. E. Bratvold, O. Nilsen, and A. Røyne. Surface Forces Apparatus measurements of interactions between rough and reactive calcite surfaces. *Langmuir*, 34(25):7248–7263, 2018.

N. Eom, D. F. Parsons, and V. S. J. Craig. Roughness in surface force measurements: Extension of DLVO theory to describe the forces between hafnia surfaces. *Journal of Physical Chemistry B*, 121(26):6442–6453, 2017.

R. M. Espinosa-Marzal, T. Drobek, T. Balmer, and M. P. Heuberger. Hydrated-ion ordering in electrical double layers. *Physical Chemistry Chemical Physics (PCCP)*, 14(17):6085–6093, 2012.

S. J. Fathi, T. Austad, and S. Strand. "Smart Water" as a wettability modifier in chalk: The effect of salinity and ionic composition. *Energy and Fuels*, 24(4):2514–2519, 2010.

S. J. Fathi, T. Austad, and S. Strand. Water-based enhanced oil recovery (EOR) by "Smart Water" in carbonate reservoirs. In *SPE International*. Society of Petroleum Engineers, January 2012.

P. Fenter, S. Kerisit, P. Raiteri, and J. D. Gale. Is the calcite–water interface understood? Direct comparisons of molecular dynamics simulations with specular X-ray reflectivity data. *The Journal of Physical Chemistry C*, 117(10):5028–5042, 2013.

T. Foxall, G. C. Peterson, H. M. Rendall, and A. L. Smith. Charge determination at calcium salt/aqueous. *Chemical Society, Faraday Transactions 1: Physical Chemistry in Condensed Phases*, 1979.

G. V. Franks. Zeta potentials and yield stresses of silica suspensions in concentrated monovalent electrolytes: isoelectric point shift and additional attraction. *Journal of Colloid and Interface Science*, 249(1):44–51, 2002.

J. C. Fröberg, O. J. Rojas, and P. M. Claesson. Surface forces and measuring techniques. *International Journal of Mineral Processing*, 56:1–30, 1999.

Z. Gao, C. Li, W. Sun, and Y. Hu. Anisotropic surface properties of calcite: A consideration of surface broken bonds. *Colloids and Surfaces A: Physicochemical and Engineering Aspects*, 520:53–61, 2017.

J. W. Gibbs. On the equilibrium of heterogeneous substances. *American Journal of Science*, 16(96):441–458, 1878.

K. A. R. Gomari and A. A. Hamouda. Effect of fatty acids, water composition and pH on the wettability alteration of calcite surface. *Journal of Petroleum Science and Engineering*, 50(2): 140–150, 2006.

G. Gouy. On the formation of electrical charges at the surface of an electrolyte. *Journal of Physique*, (9):457, 1910.

J. Gratier, R. Guiguest, F. Renard, L. Jenatton, and D. Bernard. A pressure solution creep law for quartz from indentation experiments. *Journal of Geophysical Research*, 114(B3), 2009.

J. P. Gratier, F. Renard, and P. Labaume. How pressure solution creep and fracturing processes interact in the upper crust to make it behave in both a brittle and viscous manner. *Journal of Structural Geology*, 21:1189–1197, 1999.

M. Gutierrez, L. E. Øino, and K. Høeg. The effect of fluid content on the mechanical behaviour of fractures in chalk. *Rock Mechanics and Rock Engineering*, 33(2):93–117, 2000.

T. Hassenkam, L. L. Skovbjerg, and S. L. S. Stipp. Probing the intrinsically oil-wet surfaces of pores in north sea chalk at subpore resolution. *Proceedings of the National Academy of Sciences (PNAS)*, 106(15):6071–6, 2009.

T. Hassenkam, A. Johnsson, K. Bechgaard, and S. L. S. Stipp. Tracking single coccolith dissolution with picogram resolution and implications for CO_2 sequestration and ocean acidification. *Proceedings of the National Academy of Sciences (PNAS)*, 108(21): 8571–6, 2011.

R. Heaney, C. Weaver, S. Hinders, B. Martin, and P. Packard. Absorbability of calcium from brassica vegetables: broccoli, bok choy, and kale. *Journal of Food Science*, 58:1378–1380, 1993.

F. Heberling, T. P. Trainor, J. Lutzenkirchen, P. Eng, M. A. Denecke, and D. Bosbach. Structure and reactivity of the calcite-water interface. *Journal of Colloid and Interface Science*, 354(2): 843–57, 2011.

F. Heberling, D. Bosbach, J.-D. Eckhardt, U. Fischer, J. Glowacky, M. Haist, U. Kramar, S. Loos, H. S. Müller, T. Neumann, C. Pust, T. Schäfer, J. Stelling, M. Ukrainczyk, V. Vinograd, M. Vučak, and B. Winkler. Reactivity of the calcite–water-interface, from molecular scale processes to geochemical engineering. *Applied Geochemistry*, 45:158–190, 2014.

T. Heggheim, M. V. Madland, R. Risnes, and T. Austad. A chemical induced enhanced weakening of chalk by seawater. *Journal of Petroleum Science and Engineering*, 46(3):171–184, 2005.

R. Hellmann, J. Gratier, and P. Renders. Deformation of chalk by pressure solution. In *V.M. Goldschmidt Conference*, volume 1, page 248, Heidelberg, 1996. GoldSchmidt, V.M. Goldschmidt.

R. Hellmann, P. Gaviglio, P. Renders, J. Gratier, S. Békri, and P. Adler. Experimental pressure solution compaction of chalk in aqueous solutions: Part 2: deformation examined by SEM, porosimetry, synthetic permeability and X-ray computerized tomography. *Water-Rock Interactions, Ore Deposits, and Environmental Geochemistry*, A tribute to David A. Crerar (R. Hellmann, and SA Wood, Eds.)(7):153–178, 2002a.

R. Hellmann, P. Renders, J. Gratier, and R. Guiguet. Experimental pressure solution compaction of chalk in aqueous solutions part 1. deformation behavior and chemistry. *Water-Rock Interactions*, (7):129–152, 2002b.

H. V. Helmholtz. About some laws of distribution of electric currents in physical conductors with application to the brutish-electrical experiments. *Annual Physics (Leipzig)*, 165:211–233, 1853.

M. P. Heuberger, Z. Zachariah, N. D. Spencer, and R. M. Espinosa-Marzal. Collective dehydration of ions in nano-pores. *Physical Chemistry Chemical Physics (PCCP)*, 19(21):13462–13468, 2017.

A. Hiorth, L. M. Cathles, and M. V. Madland. The impact of pore water chemistry on carbonate surface charge and oil wettability. *Transport in Porous Media*, 85(1):1–21, 2010.

E. M. Hoek and G. K. Agarwal. Extended DLVO interactions between spherical particles and rough surfaces. *Journal of Colloid and Interface Science*, 298(1):50–8, 2006.

X. Huang, S. Bhattacharjee, and E. M. Hoek. Is surface roughness a "scapegoat" or a primary factor when defining particle-substrate interactions? *Langmuir*, 26(4):2528–37, 2010.

J. L. Hutter and J. Bechhoefer. Calibration of atomic-force microscope tips. *Review of Scientific Instruments*, 64(7):1868–1873, 1993.

J. N. Israelachvili. Thin film studies using multiple-beam interferometry. *Journal of Colloid and Interface Science*, 44(2):259–272, 1973.

J. N. Israelachvili. *Intermolecular and Surface Forces*. Elsevier, 3rd edition, 2011.

J. N. Israelachvili and R. M. Pashley. Molecular layering of water at surfaces and origin of repulsive hydration forces. *Nature*, 306: 249–250, 1983.

J. N. Israelachvili and D. Tabor. The measurement of van der waals dispersion forces in the range 1.5 to 130 nm. *Proceedings of the Royal Society Lond. A*, 331(1584):19–38, 1972.

J. N. Israelachvili, Y. Min, M. Akbulut, A. Alig, G. Carver, W. Greene, K. Kristiansen, E. Meyer, N. Pesika, K. Rosenberg, and H. Zeng. Recent advances in the surface forces apparatus (sfa) technique. *Reports on Progress in Physics*, 73(3):036601, 2010.

J. N. Israellachvili. *Surface Force Apparatus: user manual for SFA 3 and SFA 2000 with attachements*. SurForceLLC, 2013.

S. Javadi and A. Røyne. Adhesive forces between two cleaved calcite surfaces in NaCl solutions: The importance of ionic strength and normal loading. *Journal of Colloid and Interface Science*, 532: 605–613, 2018.

Y. Jiang and K. T. Turner. Measurement of the strength and range of adhesion using atomic force microscopy. *Extreme Mechanics Letters*, 9:119–126, 2016.

O. N. Karaseva, L. Z. Lakshtanov, D. V. Okhrimenko, D. A. Belova, J. Generosi, and S. L. S. Stipp. Biopolymer control on calcite precipitation. *Crystal Growth and Design*, 18(5):2972–2985, 2018.

S. Kerisit and S. C. Parker. Free energy of adsorption of water and calcium on the {10 $\bar{1}$ 4} calcite surface electronic supplementary information (esi) available: free energy calculations. *Chemical Communications*, (1):52, 2004.

A. Kirch, S. M. Mutisya, V. M. Sánchez, J. M. de Almeida, and C. R. Miranda. Fresh molecular look at Calcite–Brine nanoconfined interfaces. *The Journal of Physical Chemistry C*, 122(11):6117–6127, 2018.

M. Kohns, M. Schappals, M. Horsch, and H. Hasse. Activities in aqueous solutions of the alkali halide salts from molecular simulation. *Journal of Chemical and Engineering Data*, 61(12):4068–4076, 2016.

C. Labbez, B. Jonsson, M. Skarba, and M. Borkovec. Ion-ion correlation and charge reversal at titrating solid interfaces. *Langmuir*, 25(13):7209–7213, 2009.

K. S. Lackner, C. H. Wendt, D. P. Butt, E. L. J. JR., and D. H. Sharp. Carbon dioxide disposal in carbonate minerals. *Energy*, 20(11):1153–1170, 1995.

L. Z. Lakshtanov, D. V. Okhrimenko, O. N. Karaseva, and S. L. S. Stipp. Limits on calcite and chalk recrystallization. *Crystal Growth and Design*, 18(8):4536–4543, 2018.

D. Leckband. The surface force apparatus - a tool for probing molecular protein interactions. *Nature*, 376:617–618, 1995.

F. K. Lehneri and J. Bataille. Nonequilibrium thermodynamics of pressure solution. *Pure and Applied Geophysics*, 122(1):53–85, 1984.

Y. Levenson and S. Emmanuel. Repulsion between calcite crystals and grain detachment during water–rock interaction. *Geochemical Perspectives Letters*, pages 133–141, 2017.

L. Li, F. Kohler, A. Røyne, and D. Dysthe. Growth of calcite in confinement. *Crystals*, 7(12):361, 2017.

E. M. Lifshitz. The theory of molecular attractive forces between solids. *Soviet Physics JETP*, 2(1):73–83, 1956.

X. Liu, W. Yan, E. H. Stenby, and E. Thormann. Release of crude oil from silica and calcium carbonate surfaces: On the alternation of surface and molecular forces by high- and low-salinity aqueous salt solutions. *Energy and Fuels*, 30(5):3986–3993, 2016.

M. V. Madland, A. Hiorth, E. Omdal, M. Megawati, T. Hildebrand-Habel, R. I. Korsnes, S. Evje, and L. M. Cathles. Chemical alterations induced by rock–fluid interactions when injecting brines in high porosity chalks. *Transport in Porous Media*, 87(3):679–702, 2011.

C. Marutschke, D. Walters, D. Walters, I. Hermes, R. Bechstein, and A. Kuhnle. Three-dimensional hydration layer mapping on the (10.4) surface of calcite using amplitude modulation atomic force microscopy. *Nanotechnology*, 25(33):335703, 2014.

J. Matthiesen, N. Bovet, E. Hilner, M. P. Andersson, D. A. Schmidt, K. J. Webb, K. N. Dalby, T. Hassenkam, J. Crouch, I. R. Collins, and S. L. S. Stipp. How naturally adsorbed material on minerals affects low salinity enhanced oil recovery. *Energy and Fuels*, 28 (8):4849–4858, 2014.

M. Megawati, A. Hiorth, and M. V. Madland. The impact of surface charge on the mechanical behavior of high-porosity chalk. *Rock Mechanics and Rock Engineering*, 46(5):1073–1090, 2012.

L. Montelius and J. O. Tegenfeldt. Direct observation of the tip shape in scanning probe microscopy. *Applied Physics Letters*, 62 (21):2628–2630, 1993.

J. W. Morse, R. S. Arvidson, and A. Lüttge. Calcium carbonate formation and dissolution. *Chemical Review*, 107:342–381, 2007.

S. M. Mutisya, A. Kirch, J. M. de Almeida, V. M. Sánchez, and C. R. Miranda. Molecular dynamics simulations of water confined in calcite slit pores: An NMR spin relaxation and hydrogen bond

analysis. *The Journal of Physical Chemistry C*, 121(12):6674–6684, 2017.

P. C. Myint and A. Firoozabadi. Thin liquid films in improved oil recovery from low-salinity brine. *Current Opinion in Colloid and Interface Science*, 20(2):105–114, 2015.

M. Nalbach, P. Raiteri, S. Klassen, S. Schäfer, J. D. Gale, R. Bechstein, and A. Kühnle. Where is the most hydrophobic region? Benzopurpurine self-assembly at the calcite–water interface. *The Journal of Physical Chemistry C*, 121(43):24144–24151, 2017.

A. Nermoen, R. I. Korsnes, A. Hiorth, and M. V. Madland. Porosity and permeability development in compacting chalks during flooding of nonequilibrium brines: Insights from long-term experiment. *Journal of Geophysical Research*, 120(5):2935–2960, 2015.

A. Nermoen, R. I. Korsnes, E. V. Storm, T. Stødle, M. V. Madland, and I. L. Fabricius. Incorporating electrostatic effects into the effective stress relation — Insights from chalk experiments. *Geophysics*, 83(3):MR123–MR135, 2018.

A. Nicolas, J. Fortin, J. B. Regnet, A. Dimanov, and Y. Guéguen. Brittle and semi-brittle behaviours of a carbonate rock: influence of water and temperature. *Geophysical Journal International*, 206 (1):438–456, 2016.

M. R. Nielsen, K. K. Sand, J. D. Rodriguez-Blanco, N. Bovet, J. Generosi, K. N. Dalby, and S. L. S. Stipp. Inhibition of calcite growth: Combined effects of Mg^{2+} and SO_4^{-2}. *Crystal Growth and Design*, 16(11), 2016.

O. Nilsen, H. Fjellvåg, and A. Kjekshus. Growth of calcium carbonate by the atomic layer chemical vapour deposition technique. *Thin Solid Films*, 450(2):240–247, 2004.

NPD. Ekofisk. Norwegian Ministry of Petroleum and Energy, July 2019. URL `https://www.norskpetroleum.no/en/facts/field/ekofisk/`.

M. M. A. Omari, I. S. Rashid, N. A. Qinna, A. M. Jaber, and A. A. Badwan. Calcium carbonate. *Profiles of Drug Substance, Excipients, and Related Methodology*, 41:31–132, 2016.

N. S. Ottosen and M. Ristinmaa. *The Mechanics of Constituitive Modeling*. Elsevier Science, 2005.

V. A. Parsegian and T. Zemb. Hydration forces: Observations, explanations, expectations, questions. *Current Opinion in Colloid and Interface Science*, 16(6):618–624, 2011.

D. F. Parsons, M. Bostrom, P. Lo Nostro, and B. W. Ninham. Hofmeister effects: interplay of hydration, nonelectrostatic potentials, and ion size. *Physical Chemistry Chemical Physics (PCCP)*, 13(27):12352–67, 2011.

D. F. Parsons, R. B. Walsh, and V. S. Craig. Surface forces: surface roughness in theory and experiment. *Journal of Chemical Physics*, 140(164701), 2014.

R. Pashley. DLVO and hydration forces between mica surfaces in Li^+, Na^+, K^+, and Cs^+ electrolyte solutions: A correlation of double-layer and hydration forces with surface cation exchange properties. *Colloid and Interface Science*, 83(2):531–546, 1981.

R. M. Pashley and J. N. Israelachvili. DLVO and hydration forces between mica surfaces in Mg^{2+}, Ca^{2+}, Sr^{2+}, and Ba^{2+} chloride solutions. *Colloid and Interface Science*, 97(2):446–455, 1984.

N. R. Pedersen, T. Hassenkam, M. Ceccato, K. N. Dalby, K. Mogensen, and S. L. S. Stipp. Low salinity effect at pore scale: Probing wettability changes in middle east limestone. *Energy and Fuels*, 30(5):3768–3775, 2016.

T. D. Perry, R. T. Cygan, and R. Mitchell. Molecular models of a hydrated calcite mineral surface. *Geochimica et Cosmochimica Acta*, 71(24):5876–5887, 2007.

B. N. Persson and M. Scaraggi. Theory of adhesion: role of surface roughness. *Journal of Chemical Physics*, 141(124701), 2014.

B. N. Persson, O. Albohr, U. Tartaglino, A. I. Volokitin, and E. Tosatti. On the nature of surface roughness with application to contact mechanics, sealing, rubber friction and adhesion. *Journal of Physics: Condensed Matter*, 17(1):R1–R62, 2005.

B. N. J. Persson. Contact mechanics for randomly rough surfaces. *Surface Science Reports*, 61(4):201–227, 2006.

B. N. J. Persson and S. Gorb. The effect of surface roughness on the adhesion of elastic plates with application to biological systems. *Journal of Chemical Physics*, 119(21):11437–11444, 2003.

S. Pourchet, I. Pochard, F. Brunel, and D. Perrey. Chemistry of the calcite/water interface: Influence of sulfate ions and consequences in terms of cohesion forces. *Cement and Concrete Research*, 52: 22–30, 2013.

P. Prokopovich and S. Perni. Multiasperity contact adhesion model for universal asperity height and radius of curvature distributions. *Langmuir*, 26(22):17028–36, 2010.

T. Puntervold. *Waterflooding of carbonate reservoirs*. PhD thesis, Department of Petroleum Engineering, University of Stavanger, 2008.

A. Putnis. Transient porosity resulting from fluid–mineral interaction and its consequences. *Reviews in Mineralogy and Geochemistry*, 80(1):1–23, 2015.

M. Reithmeier and A. Erbe. Dielectric interlayers for increasing the transparency of metal films for mid-infrared attenuated total reflection spectroscopy. *Physical Chemistry Chemical Physics (PCCP)*, 12(44):14798–14803, 2010.

F. Renard, S. Beauprêtre, C. Voisin, D. Zigone, T. Candela, D. K. Dysthe, and J.-P. Gratier. Strength evolution of a reactive frictional interface is controlled by the dynamics of contacts and chemical effects. *Earth and Planetary Science Letters*, 341-344: 20–34, 2012.

F. Renard, A. Røyne, and C. V. Putnis. Timescales of interface-coupled dissolution-precipitation reactions on carbonates. *Geoscience Frontiers*, 10(1):17–27, 2019.

F. Renards and P. Ortoleva. Water films at grain-grain contacts: Debye-hückel, osmotic model of stress, salinity, and mineralogy dependence. *Geochimica et Coesmochimica Acta*, 61(10):1963–1970, 1997.

M. Ricci, P. Spijker, F. Stellacci, J. F. Molinari, and K. Voitchovsky. Direct visualization of single ions in the Stern layer of calcite. *Langmuir*, 29(7):2207–2216, 2013.

R. Risnes. Deformation and yield in high porosity outcrop chalk. *Physics and Chemistry of the Earth (A)*, 26(1-2):53–57, 2001.

R. Risnes and O. Flaageng. Mechanical properties of chalk with emphasis on chalk-fluid interactions and micromechanical aspects. *Oil and Gas Science and Technology*, 54(6):751–758, 1999.

R. Risnes and V. Nygaard. Elasticity in high porosity outcrop chalk. In *Second Euroconference on Rock Physics and Rock Mechanics*, Edinburgh, Scotland, 1999. Heriot-Watt University.

R. Risnes, H. Haghighi, R. I. Korsnes, and O. Natvik. Chalk–fluid interactions with glycol and brines. *Tectonophysics*, 370(1-4):213–226, 2003.

R. Risnes, M. Madland, M. Hole, and N. Kwabiah. Water weakening of chalk—Mechanical effects of water–glycol mixtures. *Journal of Petroleum Science and Engineering*, 48:21–36, 2005.

S. Rode, N. Oyabu, K. Kobayashi, H. Yamada, and A. Kühnle. True Atomic-Resolution imaging of $\{10\bar{1}4\}$ calcite in aqueous solution by frequency modulation Atomic Force Microscopy. *Langmuir*, 25:2850–2853, 2009.

A. Røyne, J. Bisschop, and D. K. Dysthe. Experimental investigation of surface energy and subcritical crack growth in calcite. *Journal of Geophysical Research*, 116(B4), 2011.

A. Røyne, K. N. Dalby, and T. Hassenkam. Repulsive hydration forces between calcite surfaces and their effect on the brittle strength of calcite-bearing rocks. *Geophysical Research Letters*, 42(12):4786–4794, 2015.

E. Ruiz-Agudo, C. V. Putnis, C. Jiménez-López, and C. Rodriguez-Navarro. An atomic force microscopy study of calcite dissolution in saline solutions: The role of magnesium ions. *Geochimica et Cosmochimica Acta*, 73(11):3201–3217, 2009.

E. Ruiz-Agudo, C. V. Putnis, and A. Putnis. Coupled dissolution and precipitation at mineral–fluid interfaces. *Chemical Geology*, 383:132–146, 2014.

E. Ruiz-Agudo, H. E. King, L. D. Patiño-López, C. V. Putnis, T. Geisler, C. Rodriguez-Navarro, and A. Putnis. Control of silicate weathering by interface-coupled dissolution-precipitation processes at the mineral-solution interface. *Geology*, 44(7):567–570, 2016.

E. H. Rutter. Pressure solution in nature, theory and experiment. *Journal of Geological Society*, 140:725–740, 1983.

E. H. Rutter and D. Elliott. The kinetics of rock deformation by pressure solution. *Philosophical Transactions of the Royal Society*, A(283):203–219, 1976.

S. F. Shariatpanahi, S. Strand, and T. Austad. Initial wetting properties of carbonate oil reservoirs: Effect of the temperature and presence of sulfate in formation water. *Energy and Fuels*, 25(7): 3021–3028, 2011.

E. D. Shchukin. Surfactant effects on the cohesive strength of particle contacts: Measurements by the cohesive force apparatus. *Journal of Colloid and Interface Science*, 256(1):159–167, 2002.

S. Sivasankar, W. Brieher, N. Lavrik, B. Gumbiner, and D. Leckband. Direct molecular force measurements of multiple adhesive interactions between cadherin ectodomains. *Proceedings of*

the National Academy of Sciences (PNAS), 96(21):11820–11824, 1999.

A. J. Skinner, J. P. LaFemina, and H. J. F. Jansen. Structure and bonding of calcite: a theoretical study. *American Mineralogist*, 79:205–214, 1994.

L. L. Skovbjerg, D. V. Okhrimenko, J. Khoo, K. N. Dalby, T. Hassenkam, E. Makovicky, and S. L. S. Stipp. Preferential adsorption of hydrocarbons to nanometer-sized clay on chalk particle surfaces. *Energy and Fuels*, 27(7):3642–3652, 2013.

A. M. Smith, A. A. Lee, and S. Perkin. The electrostatic screening length in concentrated electrolytes increases with concentration. *Journal of Physical Chemistry Letter*, 7(12):2157–63, 2016.

H. Songen, B. Reischl, K. Miyata, R. Bechstein, P. Raiteri, A. L. Rohl, J. D. Gale, T. Fukuma, and A. Kuhnle. Resolving point defects in the hydration structure of calcite (10.4) with Three-Dimensional Atomic Force Microscopy. *Physical Review Letters*, 120(11):116101, 2018. doi: 10.1103/PhysRevLett.120.116101.

O. Stern. The theory of the electrolytic double-layer. *Z. Elekrochemie und Angewandte Physikaliche Chemie*, 30:508, 1924.

M. P. Stewart, A. W. Hodel, A. Spielhofer, C. J. Cattin, D. J. Muller, and J. Helenius. Wedged AFM-cantilevers for parallel plate cell mechanics. *Methods*, 60(2):186–94, 2013.

S. L. S. Stipp. Toward a conceptual model of the calcite surface: hydration, hydrolysis, and surface potential. *Geochimica et Cosmochimica Acta*, 63(19-20):3121–3131, 1999.

S. L. S. Stipp and M. F. Hochella. Structure and bonding environments at the calcite surface as observed with X-ray photoelectron spectroscopy (XPS) and low energy electron diffraction (LEED). *Geochimica et Cosmochimica Acta*, 55:1723–1736, 1991.

S. L. S. Stipp, C. M. Eggleston, and B. S. Nielsen. Calcite surface structure observed at microtopographic and molecular scales with

atomic force microscopy (AFM). *Geochimica et Coesmochimica Acta*, 58(14):3023–3033, 1994.

S. L. S. Stipp, W. Gutmannsbauer, and T. Lehmann. The dynamic nature of calcite surfaces in air. *American Mineralogist*, 81:1–8, 1996.

S. Strand, E. J. Høgnesen, and T. Austad. Wettability alteration of carbonates-effects of potential determining ions (Ca^{2+} and SO_4^{-2}) and temperature. *Colloids and Surfaces A: Physicochemical and Engineering Aspects*, 275(1-3):1–10, 2006.

S. Strand, T. Austad, T. Puntervold, E. Høgnesen, M. Olsen, and S. M. F. Barstad. "Smart water" for oil recovery from fractured limestone: A preliminary study. *Energy and Fuels*, 22:3126–3133, 2008.

J. E. Sylte, L. K. Thomas, D. W. Rhett, D. D. Bruning, and N. B. Nagel. Water induced compaction in the Ekofisk Field. Number SPE-56426-MS, Houston, Texas, 3-6 October 1999. SPE Annual Technical Conference and Exhibition, Society of Petroleum Engineers.

D. Tabor and R. H. S. Winterton. Surface forces: Direct measurement of normal and retarded van der Waals forces. *Nature*, 219: 1120–1121, 1968.

R. Tadmor, N. Chen, and J. N. Israelachvili. Thickness and refractive index measurements using multiple beam interference fringes (FECO). *Journal of Colloid and Interface Science*, 264(2):548–553, 2003.

F. Teng, H. Zeng, and Q. Liu. Understanding the deposition and surface interactions of gypsum. *The Journal of Physical Chemistry C*, 115(35):17485–17494, 2011.

H. Teng, P. Dove, and J. D. Yoreo. Kinetics of calcite growth: Surface processes and relationships to macroscopic rate laws. *Geochimica et Coesmochimica Acta*, 64(13):2255–2266, 2000.

E. Thormann. Surface forces between rough and topographically structured interfaces. *Current Opinion in Colloid and Interface Science*, 27:18–24, 2017.

U. Ulusoy and M. Yekeler. Correlation of the surface roughness of some industrial minerals with their wettability parameters. *Chemical Engineering and Processing: Process Intensification*, 44(5): 555–563, 2005.

U. Ulusoy, C. Hiçyılmaz, and M. Yekeler. Role of shape properties of calcite and barite particles on apparent hydrophobicity. *Chemical Engineering and Processing: Process Intensification*, 43(8):1047–1053, 2004.

M. Valtiner, X. Banquy, K. Kristiansen, G. W. Greene, and J. N. Israelachvili. The electrochemical surface forces apparatus: The effect of surface roughness, electrostatic surface potentials, and anodic oxide growth on interaction forces, and friction between dissimilar surfaces in aqueous solutions. *Langmuir*, 28(36):13080–13093, 2012.

E. Verpy, M. Leibovici, and C. Petit. Characterization of Otoconin-95, the major protein of murine otoconia, provides insights into the formation of these inner ear biominerals. *Proceedings of the National Academy of Sciences (PNAS)*, 96:529–534, 1999.

E. Verwey. Theory of the stability of Lyophobic colloids. *Journal of Physical Chemistry*, 51(3):631–636, 1947.

J. A. D. Waal. *On the Rate Type Compaction Behavior of Sandstone Reservoir Rock*. PhD thesis, Department of Applied science, Delft University of Technology, May 1986.

L. Wang and X. Fu. Data-driven analyses of low salinity water flooding in sandstones. *Fuel*, 234:674–686, 2018.

N. A. Wojas, A. Swerin, V. Wallqvist, M. Jarn, J. Schoelkopf, P. A. C. Gane, and P. M. Claesson. Iceland spar calcite: Humidity and time effects on surface properties and their reversibility. *Journal of Colloid and Interface Science*, 541:42–55, 2019.

M. Wolthers, L. Charlet, and P. V. Cappellen. The surface chemistry of divalent metal carbonate minerals; a critical assessment of surface charge and potential data using the charge distribution multi-site ion complexation model. *American Journal of Science*, 308:905–941, 2008.

M. Wolthers, D. Di Tommaso, Z. Du, and N. H. de Leeuw. Calcite surface structure and reactivity: molecular dynamics simulations and macroscopic surface modelling of the calcite-water interface. *Physical Chemistry Chemical Physics (PCCP)*, 14(43): 15145–15157, 2012.

X. Yang, F. Teng, H. Zeng, and Y. Liu. Impact of cranberry juice on initial adhesion of the EPS producing bacterium burkholderia cepacia. *Biofouling*, 28(5):417–431, 2012.

J. Young, P. Brown, and J. Lees. International nanoplankton association. Nanotax3 website, April 2017. URL `http://www.mikrotax.org/Nannotax3`.

Z. Zachariah, R. M. Espinosa-Marzal, N. D. Spencer, and M. P. Heuberger. Stepwise collapse of highly overlapping electrical double layers. *Physical Chemistry Chemical Physics (PCCP)*, 18(35): 24417–27, 2016.

P. Zhang, M. Tweheyo, and T. Austad. Wettability alteration and improved oil recovery in chalk: The effect of calcium in the presence of sulfate. *Energy and Fuels*, 20:2056–2062, 2006.

X. Zhang and C. J. Spiers. Compaction of granular calcite by pressure solution at room temperature and effects of pore fluid chemistry. *International Journal of Rock Mechanics and Mining Sciences*, 42(7-8):950–960, 2005.

R. W. Zimmerman, W. H. Somerton, and M. S. King. Compressibility of porous rocks. *Journal of Geophysical Research: Solid Earth*, 91(B12):12765–12777, 1986.

Manuscript 1

Adhesive forces between two cleaved calcite surfaces in NaCl solutions: The importance of ionic strength and normal loading

Shaghayegh Javadi and Anja Røyne
Journal of Colloid and Interface Science, 532C (**2018**), pp. 605-613.

Author contribution: Shaghayegh Javadi designed and performed all experiments, analyzed and interpreted the data and wrote the manuscript. Anja Røyne supervised the project; contributed to design of the experiments, advised on experimental methods, contributed to data analysis, interpretation, and manuscript writing.

Journal of Colloid and Interface Science 532 (2018) 605–613

Contents lists available at ScienceDirect

Journal of Colloid and Interface Science

journal homepage: www.elsevier.com/locate/jcis

Adhesive forces between two cleaved calcite surfaces in NaCl solutions: The importance of ionic strength and normal loading

Shaghayegh Javadi [a,c,b,*], Anja Røyne [b]

[a] The National IOR center of Norway, University of Stavanger, Norway
[b] Department of Physics, University of Oslo, Norway
[c] Department of Energy Resources, University of Stavanger, Norway

GRAPHICAL ABSTRACT

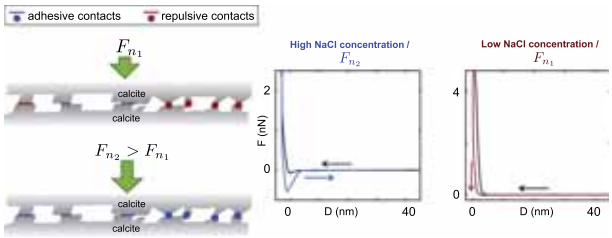

ARTICLE INFO

Article history:
Received 29 November 2017
Revised 31 July 2018
Accepted 9 August 2018
Available online 10 August 2018

Keywords:
Nano-scale interaction
Nano-confinement of calcite
Normal stress
Surface roughness
Adhesion forces
Ionic strength

ABSTRACT

The mechanical strength of calcite bearing rocks is influenced by pore fluid chemistry due to the variation in nano-scale surface forces acting at the grain contacts or close to the fracture tips. The adhesion of two contacting surfaces, which affects the macroscopic strength of the material, is not only influenced by the fluid chemistry but also by the surface topography. In this paper, we use Atomic Force Microscope (AFM) to measure the interfacial forces between two freshly cleaved calcite surfaces in $CaCO_3$-saturated solutions with varying NaCl concentration. We show that calcite contacts become stronger with increasing NaCl concentration (>100 mM), as a result of progressively weaker secondary hydration and increasing attraction due to instantaneous ion-ion correlation. Moreover, we discuss the effect of normal applied force (F_n) and surface roughness on the measured adhesion forces (F_{ad}). We show that the measured pull-off force (adhesion) is linearly correlated with the magnitude of F_n, where an increase in applied force results in increased adhesion. This is attributed to a larger number of contacting surface asperities and thus increase in real contact area and the contact-bond strength. We discuss that the possible variation in local topography at contacts, together with strong dependence on ionic strength of the solution, can explain the inconsistent behavior of calcite rocks in NaCl solutions.

1. Introduction

Calcite is an abundant mineral in nature. It is a crystalline polymorph of calcium carbonate with a cleavage plane along the $(1\,0\,\bar{1}\,4)$ direction [1–3]. Calcite plays a key role in biomineralization and it is a constituent of shells and skeletons of many marine

* Corresponding author at: Department of Physics, University of Oslo, Norway.
E-mail address: shaghayegh.javadi@fys.uio.no (S. Javadi).

https://doi.org/10.1016/j.jcis.2018.08.027
0021-9797/

invertebrates [4]. Moreover, it is one of the most common rock-forming minerals of importance to hydrocarbon recovery, CO_2 sequestration [5,6] and nuclear waste storage [7]. Calcite is the main constituent mineral of chalk (>99%). Chalk deposits form many of the world's oil and gas reservoirs, such as the North Sea oil reserves, where they alone account for 25 million barrels of oil since the 1970s [8].

Chalk reservoirs are prone to strong compaction, due to water injection associated with Enhanced Oil Recovery (EOR) projects [9–13]. The mechanical behavior of chalk and calcite-bearing rocks is known to be influenced by the pore fluid chemistry [9,14–17], an effect that is often referred to as water-weakening (the significant loss of mechanical strength of chalk in water-saturated rocks [12,18]). Several mechanisms have been proposed to describe this phenomenon, such as pressure solution [19,20], chemical influences [19], invading the capillary bridges/menisci by water flooding [21], time-dependent water adsorption on calcite surfaces [11,22] and subcritical crack growth at the grain boundaries [23]. In the early 2000s, Risnes et al. [12,18] proposed that water activity is a key parameter behind the strength loss in chalk in aqueous solutions. Hellmann et al. [13] suggested that water-weakening may be also related to the repulsive forces due to adsorbed water molecules on adjacent calcite surfaces. These two hypotheses were further supported by atomic force microscope (AFM) experiments by Røyne et al. [24], in which adhesion between two surfaces depended on water activity, with strong repulsion measured in pure water.

At the nano-scale, repulsive and attractive forces operate between two calcite surfaces that are separated by a thin fluid film. Surface forces between two charged surfaces in an electrolyte solution can be described by the Derjaguin-Landau and Verwey-Overbeek (DLVO) theory [25,26] that includes van der Waals (vdW) and Electrical Double Layer (EDL) forces [27,28]. However, at separations significantly shorter than the Debye length, and for solutions with high ionic strength (>0.1 M) [28,29], where specific ion interactions and hydration effects become exceedingly important, [30–36] the DLVO theory cannot accurately describe the interaction between surfaces in aqueous solutions. The AFM direct force measurements by Røyne et al. [24] shows that the observed repulsion in water is due to hydration forces acting between two hydrophilic calcite surfaces. A similar experiment by Pourchet et al. [37] indicates that attractive forces act between calcite surfaces in high pH and higher ionic strength solutions (0.12 M), which were attributed to the ion-ion correlation forces. Both hydration and ion-correlation forces are not included in the DLVO theory.

Several studies have shown that the degree of water weakening is also affected by the salinity of the pore fluid [12,18,38]. The salinity of the solution affects both the EDL component of the DLVO forces, and the water activity [39,40]. It also changes the calcite dissolution kinetics in aqueous solutions [41–44].

In general, calcite and other natural mineral surfaces display some degree of roughness at a molecular scale. Several studies have shown that surface roughness affects the water wettability of calcite [45,46] and oil desorption from calcite surfaces [47]. It, also, influences the interfacial forces between mineral surfaces in molecular scale. This is because of the actual contact area is always smaller than the nominal surface area (see Fig. 1) [48–57]. For rough surfaces, contacting surface asperities give rise to an exponentially decaying repulsive force upon loading [58], which can potentially be interpreted as hydration repulsion, as in the past studies [58,59].

Calcite surfaces are dynamic in aqueous solutions, with continuous dissolution and recrystallization on the timescale of hours even in saturated solutions, as shown by Stipp et al. [60,61]. We, therefore, expect the distribution and geometry of surface asperities to change with time, which in turn influence the magnitude of repulsive mechanical effects due to asperity deformation. Recently Dziadkowiec et al. [62] performed force measurement experiments between two rough calcite surfaces (with nm-scaled asperities), using the Surface Force Apparatus (SFA). They observed repulsive forces with a decay length that increases with time, which was explained by repulsive hydration forces combined with continuous recrystallization and roughening of the calcite films in saturated $CaCO_3$ solutions.

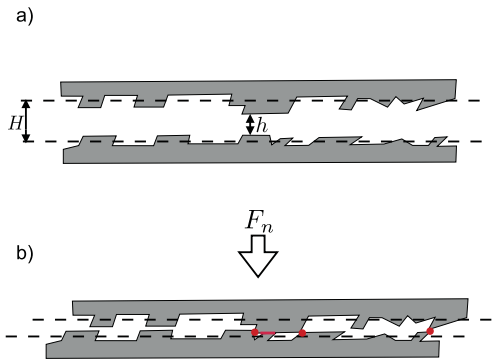

Fig. 1. A simple sketch of two opposing, cleaved calcite surfaces with nano-scale roughness characterized by steps and terraces on the (1 0 1 4) surface. (a) Dotted lines represent the midline of surface asperities with H as the surface separation, and "h" is the distance between highest asperities. (b) When two surfaces pushed into contact by an applied normal load (F_n), a discrete number of asperities are forced into contact, as represented by the red dots and lines. The sum of these discrete areas of contact are referred to the actual area of contact for rough, contacting surfaces. (For interpretation of the references to color in this figure legend, the reader is referred to the web version of this article.)

The effect of NaCl on the interaction between calcite surfaces is of interest because both Na^+, and Cl^- are the two most abundant monovalent ions in seawater. The influence of NaCl on the strength of carbonate rocks [15,16,63] and EOR systems has been extensively investigated in surface science and reservoir engineering, e.g. [64–66]. Liu et al. [64] observed that injection of NaCl solution (low and high concentrations) into a carbonate rock increases the oil desorption rate from calcite surfaces. They explained this result by increased solubility of calcite in high concentration NaCl solution, which in turn increases the local pH, leading to more negatively charged calcite surfaces and hence repulsive forces between the calcite and the oil. For low NaCl concentrations, they relate the high-rate oil desorption to the EDL repulsive forces between oil and calcite surfaces. Interestingly, in contrast, Fathi et al. [65,66] showed that oil recovery improves when the NaCl (named as non-active salt) is removed from the seawater. This effect was attributed to a high population of Na^+ and Cl^- near the calcite surfaces that prevents the potential determining cations/anion (Mg^{2+}, Ca^{2+} and SO_4^{-2}) to reach to the surface. As a result, a more positively charged calcite surface attracts oil to a higher extent. However, they show that surface reactivity and ultimately wettability of the surface varies with the temperature as well as the solution ionic strength. This shows the increased complexity of the calcite-brine-calcite system once the oil is present. In fact, the type and history of mineral surfaces, and the components of oil and brine are inevitable parameters and shall thus be considered when investigating such a system.

In this study, we aim to understand the role of ionic strength in compaction of calcite-bearing rocks, and its potential relation to the nm-range forces between calcite surfaces. To achieve this, we use the colloidal probe AFM with a calcite probe against a freshly

cleaved calcite surface. We investigate the pull-off force between two calcite surfaces, as a measure of the adhesion and surface energy between two surfaces, [41,67] in NaCl solutions with concentrations ranging from 1 mM to 1.2 M, pre-saturated with calcium carbonate. We additionally address, indirectly, the effect of applied normal force (F_n) on the pull-off forces and its relation to intrinsic roughness of natural cleaved calcite surfaces.

2. Experimental method

2.1. Force measurement using AFM

To measure forces between two calcite surfaces we use a JPK NanoWizard® 4 Bioscience AFM, in force spectroscopy mode. The AFM is situated on an inverted Olympus IX71 microscope. The approach and retract velocities are set to 200 nm/s, where we observe negligible hydrodynamic effects. The maximum applied normal load, or set point (Fig. 2), is varied from 5 to 30 nN in steps of 5 nN. For each approach-retract curve, we record one value for the pull-off (adhesion) force (Fig. 2). The temperature inside the AFM enclosure is continuously monitored, and found to be stable at 24.5 ± 0.5 °C.

2.2. Sample preparation

2.2.1. Calcite surface and fluid cell

Each experiment is performed with a freshly cleaved Iceland spar calcite crystal. A 5 × 5 mm crystal is first glued to a glass slide using a UV-curing adhesive (Casco Glaslim) and cleaved *in situ*. To make the fluid cell, we use a plastic ring (20 mm inner diameter, 6.5 mm height, final capacity approx. 3.5 ml) with inlet and outlet ports connected to plastic tubing, and fix it around the sample using a self-cure rubber (Reprorubber). The fluid cell is loosely sealed at the top by a silicone membrane to reduce the fluid evaporation rate. Fig. 3a–c show the production of calcite probe and assembling the fluid cell (with calcite crystal in) on the AFM stage.

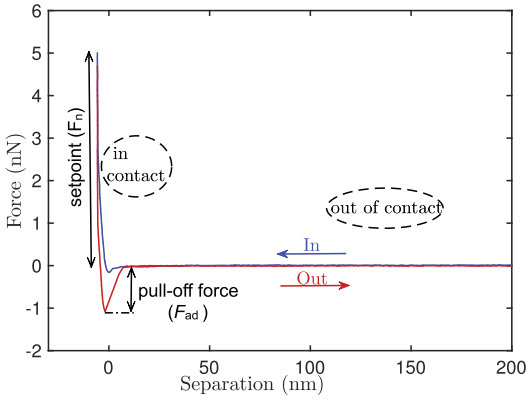

Fig. 2. One representative force curve measured in 800 mM NaCl solution, with setpoint F_n = 5 nN. The approach curve (blue line) shows a sudden small vdW attraction at short distance, and repulsion closer to or at the contact. The measurement shows a characteristic jump-out upon retraction (red line) and the minimum value of this curve, called the pull-off force, is used as a measure of the adhesive interaction of the surfaces. The non-contact area shows the force zero line obtained by fitting a straight line to the corresponding data points of the cantilever deflection versus piezo position curve. In this description, some terminologies are used from [24,68]. (For interpretation of the references to color in this figure legend, the reader is referred to the web version of this article.)

2.2.2. AFM-probe modification

We adapt the method described by [24] (see Fig. 3a–b) for AFM-tip fabrication. A suitable calcite fragment (size between 40–70 μm in length and 15–25 μm in width) is identified under the microscope. A tipless cantilever (All In One-TL, 15 kHz, 0.2 N/m) is moved over a drop of two component epoxy glue (Epoxy Universal 335, DANA LIM, mixing ratio 1:1), picks it up and moves back to the position of the chosen particle. The cantilever is then brought into contact with the particle and left at a constant applied force overnight to set (12–16 h). In order to ensure two parallel interacting surfaces, all measurements are made without moving the particle from its initial position. Before each gluing process, we measure the spring constant of the cantilever using the thermal tune calibration method [69]. In addition, we measure the cantilever sensitivity using a contact based force-distance curve, after each solution injection.

2.2.3. Solutions

Solutions are made using various concentrations of NaCl (VWR, 100.2%) (see Table 2) in deionized (type II) water. All solutions are saturated with $CaCO_3$ (excess powder of $CaCO_3$ in deionized water). The $CaCO_3$ powder (MERCK) is heat treated at 300 °C in a clean laboratory environment to minimize any possible organic contamination. All solutions are shaken and left stationary for at least 2 weeks to equilibrate. Before each measurement, we place the vials containing the solutions inside the AFM enclosure for at least 12 h, for thermal equilibration. The pH of each solution is measured before and after the experiment (see Table 1), and shows no significant change. We compare these results with pH-values calculated using PHREEQC [70], for open systems (OS) in equilibrium with atmospheric CO_2 ($\log(pCO_2) = -3.5$), and for closed systems (CS) with no exchange of CO_2 with the atmosphere. Most of the measured values are between those calculated for OS and CS. This shows that the equilibrium with atmospheric CO_2 and calcite had not been fully reached; however, since the pH did not change during the measurement, we do not expect this process to influence our results. We also calculate the equilibrium Ca^{2+} concentration and find it to be of negligible influence on the ionic strength for NaCl concentrations higher than 5 mM.

2.3. Procedure

Once the calcite probe is fabricated, we start the experiment by performing a few force measurements in air, and then injecting the first solution (see Fig. 4 for the workflow of a typical experiment). We allow the system to equilibrate for 15 min after each fluid injection. To separate the effect of salt concentration and elapsed time, we inject the solutions in random order. Experiments continue for at least 10 h unless they have to be aborted because of a lost particle during measurement, or a piece of dust becomes permanently trapped between the surfaces after fluid injection. The AFM probe is stored in a sealed container after each successful measurement to be imaged by a Scanning Electron Microscope (SEM, TM3030Plus), after no more than one week (Fig. 3d-left). The results of EDS analysis do not show any precipitation of secondary minerals on these surfaces. We, also, use a white light interferometer (WLI) optical profiler (GTK-contour Bruker) to measure the topography of the calcite probes. Each surface is characterized by steps and terraces and the rms-values (root mean squared) indicate the height differences between microscopic terraces over the total surface area (see Fig. 3d for the SEM and WLI scans of a representative particle).

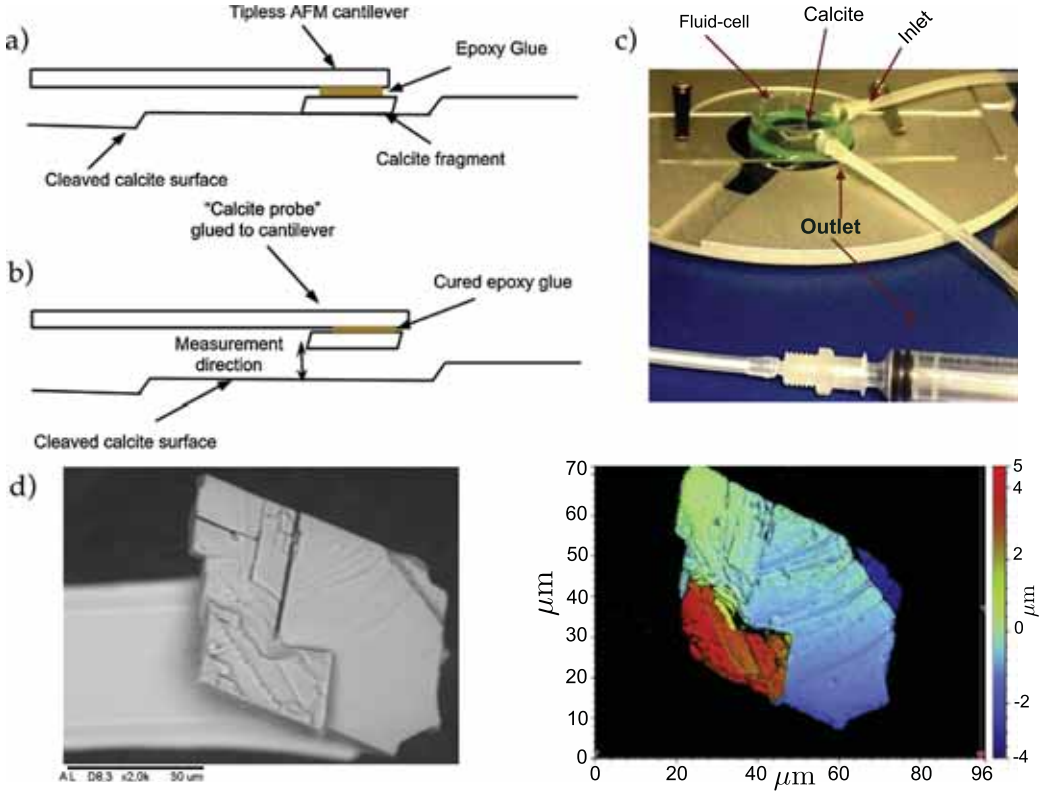

Fig. 3. AFM-tip modification procedure. (a) Freshly cleaved calcite crystal with small fragment on surface, and cantilever with a drop of Epoxy glue is about to be in contact. (b) After 16 h the cured Epoxy glue yields attached particle to cantilever. By separating them from the surface, we can start the measurement. (c) AFM-stage with a mounted fluid cell containing a cleaved calcite ready for the tip-fabrication process. Fluid exchange happens through the inlet/outlet tubes. (d-left) SEM image of a representative particle, after the experiment, with rms = 583 nm over A = 1352 μm^2. (d-right) WLI scan showing the surface topography of the same particle.

Table 1
Measured pH after the experiment (with ±0.1 deviation for all used solutions) and PHREEQC simulation results for open (OS) and closed systems (CS). The equilibrium concentration of $Ca^{+2}$is also calculated by PHREEQC in both OS and CS. The ionic strength for the highest concentration is calculated as 1290 mM (including Ca^{+2} and CO_3^{-2}).

NaCl (mM)	Measured pH(after exp. in OS)	Calculated pH (CS)	Calculated pH (OS)	Calculated Ca^{2+}(OS) (mM)	Calculated Ca^{2+}(CS) (mM)
0	9.00	9.91	8.27	0.48	0.12
1	8.96	9.91	8.28	0.49	0.13
2	8.42	9.91	8.28	0.50	0.13
3	9.03	9.91	8.28	0.51	0.14
4	8.38	9.91	8.29	0.52	0.14
5	8.36	9.91	8.29	0.54	0.14
10	8.27	9.92	8.30	0.56	0.15
20	8.50	9.92	8.31	0.60	0.17
30	8.16	9.92	8.32	0.63	0.19
40	8.67	9.92	8.33	0.66	0.20
50	8.14	9.92	8.33	0.68	0.21
100	8.87	9.92	8.35	0.76	0.26
200	8.00	9.91	8.36	0.87	0.34
300	8.09	9.90	8.36	0.96	0.40
400	8.50	9.89	8.37	1.02	0.45
500	8.22	9.88	8.36	1.07	0.49
600	8.34	9.87	8.36	1.11	0.53
700	8.23	9.86	8.36	1.15	0.56
800	9.78	9.86	8.35	1.18	0.58
900	8.75	9.85	8.35	1.21	0.60
1000	9.80	9.85	8.35	1.23	0.63
1100	7.86	9.84	8.34	1.25	0.65
1200	8.23	9.84	8.34	1.27	0.66

Table 2
List of particles, used solutions (shown by marker (×)), measured surface area by optical camera before experiment (A_{op}) and SEM after the experiment (A_{SEM}) and measured roughness (rms) by white light interferometer (WLI) for each particle. There is no information on A_{SEM} and rms for particles that were lost at the end or during the experiment. Zero value for NaCl concentration represents a saturated $CaCO_3$ solution only.

P (#)	A_{op} (μm^2)	A_{SEM} (μm^2)	rms (nm)	NaCl (mM) 0	1	2	3	4	5	10	20	30	40	50	100	200	300	400	500	600	700	800	900	1000	1100	1200
1	918	788													×	×	×	×	×	×	×	×	×	×	×	×
2	2562	1242												×	×	×	×	×	×	×	×	×	×	×	×	×
3	1905													×	×	×	×	×	×	×	×	×	×	×	×	
4	564													×	×	×	×	×	×	×	×	×	×	×	×	×
5	1099				×	×	×	×	×	×	×	×	×	×													
6	650	499	443		×	×	×	×		×	×		×	×	×			×	×				×		×		×
7	1195	958	761	×	×			×	×		×	×		×	×		×			×			×		×	×
8	693	708		×		×	×						×			×			×					×		
9	1489	1017	931	×	×				×	×		×		×	×		×		×		×		×		×	

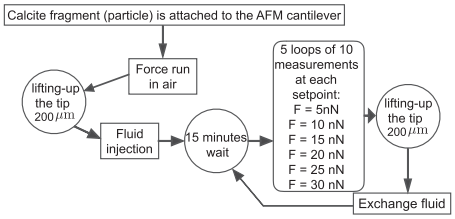

Fig. 4. Flowchart of the experimental procedure.

3. Results

The measured pull-off forces (F_{ad}) from all experiments are summarized in Fig. 5, plotted as cumulative distributions for each concentration and particle (p_1 - p_9), where the results of different applied forces are plotted as different colored lines. Each panel is marked with a number representing the order of fluid injections (t_i, where $i = 1, 2, \ldots, 14$).

3.1. Effect of NaCl concentration

As seen in Fig. 5, the general trend for each experimental day (particle) is that the measured pull-off forces increase with increasing concentration of NaCl. At low concentrations (below

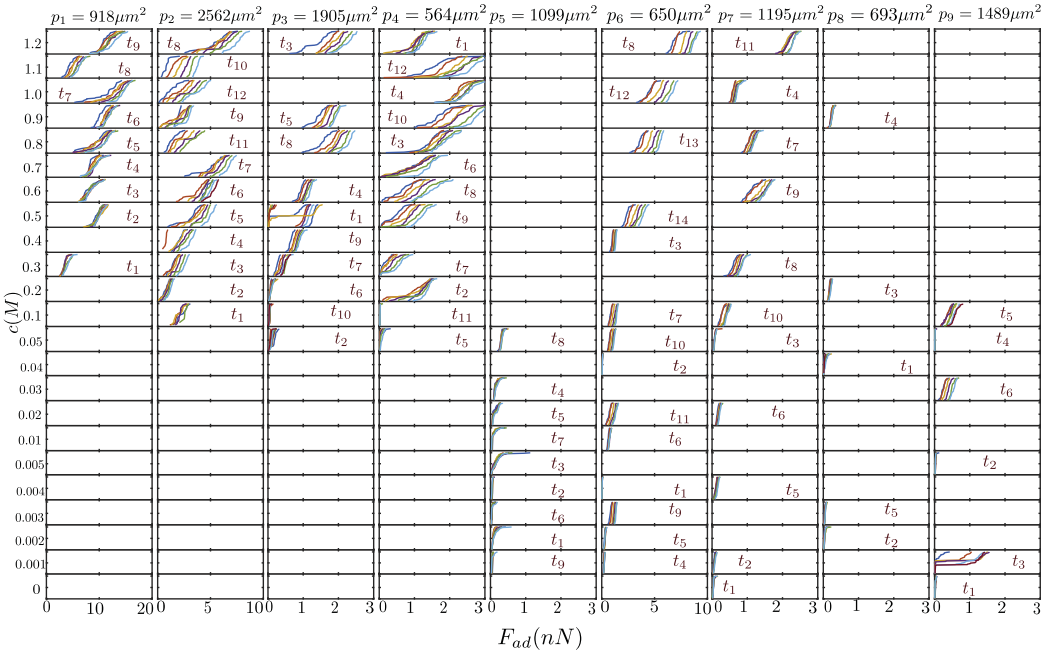

Fig. 5. Cumulative measured adhesion for all experimental days and salt concentrations. y-axis stands for experimental NaCl concentration and x-axis for measured adhesion, whose limitation depends on the maximum measured F_{ad} for each day. Different colors show the measured values at different applied force (F_n). In these plots, t_i represent the injection order, where $i = 1, 2, \ldots, 14$. (For interpretation of the references to color in this figure legend, the reader is referred to the web version of this article.)

100 mM), F_{ad} is either zero or very low in almost all measurements, consistent with the observations of Røyne et al. [24]. At higher concentrations, F_{ad} is non-zero in all cases.

In some experiments, the increase in F_{ad} with concentration is not monotonic. Abrupt changes in F_{ad} can take place when the solution is exchanged. This is clear, in Fig. 5, for particle p_2, where F_{ad} is reduced from t_7 (0.7 M) to t_9 (0.9 M) and then behaves the same for the rest of the measurements. We believe that these sudden changes can be caused by lateral movement of the cantilever [67] relative to the cleaved surface, or, less likely, by surface contamination (small particle(s) of calcite or other dust) getting caught between the surfaces, undetected by the subsequent force curves.

3.2. Effect of applied force

As seen in Fig. 6, for all experiments, the measured pull-off force increases with increasing applied normal stress. This behavior can be fitted, for all experiments, to a linear function of the form,

$$F_{ad} = \alpha F_n + F_{ad}^0 \quad (1)$$

where F_{ad} is the measured pull-off force and F_n is the setpoint (applied normal force). Fig. 6 shows the results of all experiments collapsed onto a single curve by rescaling with the fitted parameters, where the slope of the fitting curve increases between 0.01 and 0.19, independently of concentration (Fig. 6, top-left inset).

3.3. Effect of time

Given that calcite surfaces are known to be dynamic in aqueous solutions [71], with continuous dissolution and recrystallization at the nano-scale, we expect that the actual area of contact (the sum of discrete nano-asperities) could change through time. Since the measured pull-off forces reflect the number of asperities in contact, we can detect such variation by looking at a possible gradual change in measured pull-off forces as a function of time. Fig. 7 shows the result of F_{ad} for p_6 in 500 mM NaCl solution. Each of the clusters represents the measured F_{ad} values in each loop (following the procedure as shown in Fig. 4), where the results of different F_n are plotted in different colored circles. We observe a slow change with time in F_{ad} for each F_n. However, there is no consistent trend: sometimes we see increase in F_{ad} with time, sometimes decrease. The trend can change from increasing to decreasing or vice versa.

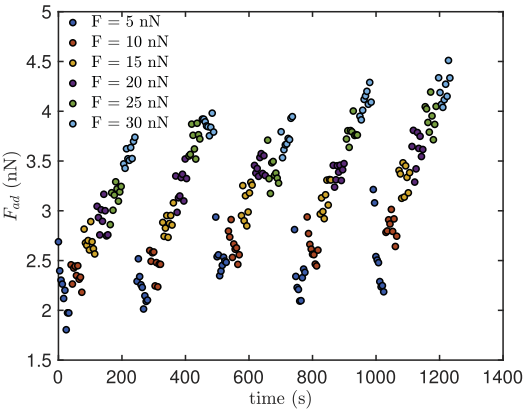

Fig. 7. Measured adhesion with time for p_6 in 500 mM NaCl solution. Adhesion forces increase by F_n in each loop, and mostly return to their initial state (at low value of F_n) for the next loop.

3.4. Effect of particle size

Fig. 8 shows the measured pull-off force for 6 different particles at three values of applied force, F_n = 5, 20 and 30 nN in NaCl concentration of 1200 mM. There is no clear correlation between nominal particle area and measured pull-off force, indicating that surface roughness and actual area of contact, are more important parameters than the nominal surface area. Note that this result is independent of the fluid composition and setpoint values.

We could expect that the magnitude of the pull-off force in air would be a measure of the actual area of contact, which would mean that normalizing by the adhesion in air, should give a measure of adhesive energy per unit area. However, this normalization does not reduce the variation in adhesion values for different particles for any given salt concentration nor setpoint. This is probably because the pull-off force in air is dominated by the breaking of

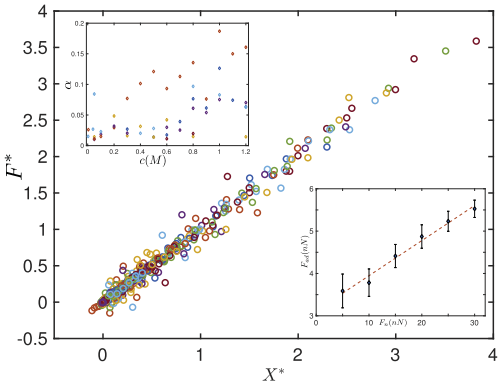

Fig. 6. Data collapse of pull-off force vs. applied normal load, for all experiments, with $X^* = \alpha F_n$ and $F^* = F_{ad} - F_{ad}^0$. The insets represent, (top-left) the slope (α) of the fitting curve vs. concentration (x-axis is plotted in logarithmic scale), and (right-bottom) a representative result for p_6 in NaCl 800 mM solution.

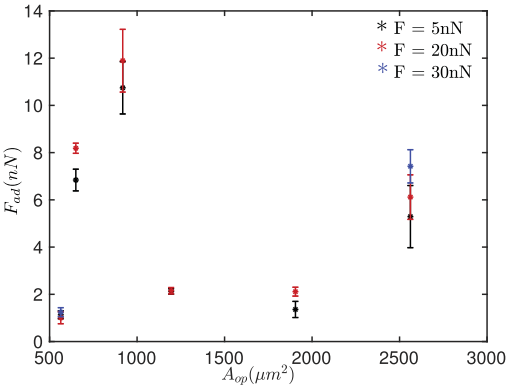

Fig. 8. We see no correlation between pull-off force and surface area. This plot shows the measured pull-off force vs. surface area (optical measured values) for different particles in 1200 mM NaCl solution at 3 different values for F_n.

capillary bridges, which is more influenced by the specific contact geometry than the actual area of contact.

4. Discussion

Our results can be summarized as follows: (1) the interactions between calcite surfaces goes from repulsive to adhesive at NaCl concentrations around 100 mM, and the adhesive interaction (pull-off force) increases with salt concentration; (2) for adhesive interactions, pull-off forces increase with increasing applied normal load; and (3) the pull-off forces change slightly with time in a non-monotonic fashion.

When two surfaces are in an electrolyte solution, the interaction potential between them determines the compressive force necessary to push them into adhesive contact. Fig. 9 shows the disjoining pressure, force per area for two flat calcite surfaces, given by DLVO theory as the sum of van der Waals (vdW) and electric double layer (EDL) forces [28]:

$$F_{\mathrm{vdW}} = -\frac{A}{6\pi D^3} \quad \text{and} \quad F_{\mathrm{EDL}} = \left(\frac{\lambda^2}{2\pi}\right) Z e^{-\lambda D} \tag{2}$$

where λ is the Debye length and Z is the interaction constant calculated by $Z = 64\pi\epsilon_0\epsilon(kT/e)^2\tanh^2(e\psi_0/4kT)$ [28]. ψ_0 is the surface potential and a function of the pH of solution, Ca^+ concentration [43,44] and P_{CO_2} [72]. For a monovalent electrolyte, Z differs between 1.95×10^{-18} and 3.47×10^{-18} J m^{-1}, where ψ_0 is expected to vary between 15 and 20 mV throughout the experiment for pH between 8 and 9 [72, Figure B]. A is the non-retarded Hamaker constant, calculated based on Lifshitz theory through [28],

$$A = \frac{3}{4}kT\left(\frac{\epsilon_1 - \epsilon_3}{\epsilon_1 + \epsilon_3}\right)^2 + \frac{3h\nu_e}{16\sqrt{2}}\frac{(n_1^2 - n_3^2)^2}{(n_1^2 + n_3^2)^{3/2}}$$

where $n_1 = 1.48$ and $\epsilon_1 = 8$ are refractive index and dielectric permittivity of calcite [29], and $n_3 = 1.33$ and $\epsilon_3 = 80$ are the refractive index and dielectric permittivity of water. $h = 6.6 \times 10^{-34}$ m^2 kg/s is the Planck constant and $\nu_e = 3 \times 10^{15}$ s^{-1} is the main electronic absorption frequency in the UV [28]. In general, the DLVO interaction energy is affected by the ionic strength of the electrolyte solution [53]. Increasing salt concentration, changes the position and height of EDL repulsive barrier. As the salt concentration increases, the van der Waals attractive forces contribution overcomes the EDL repulsive forces (Fig. 9).

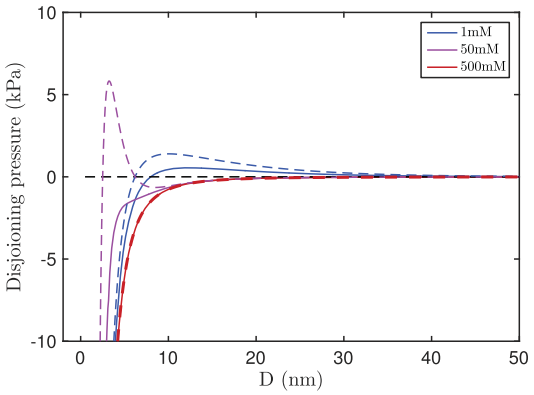

Fig. 9. Calculated DLVO for two flat, smooth calcite surfaces in NaCl solution with a few values of ionic strength, Eq. (2). It shows a higher repulsive barrier by reducing the Debye length and its diminishing effect at low values. Dotted lines: for ψ_0 = 20 mV, and Solid lines: for ψ_0 = 15 mV.

At first glance, this could explain the increased adhesion we see at high salt concentration. However, two observations do not fit this hypothesis: (1) as noted by Røyne et al. [24], the magnitude of the EDL repulsive barrier for calcite surfaces in low ionic strength solution is very small, and unlikely to explain the purely repulsive behavior observed under these conditions; and (2) the observed pull-off forces increase in magnitude even as the ionic strength is increased beyond what should be the limit of the DLVO theory [29,31,48,73–75].

An increase in the measured pull-off force can be explained by a decrease in any repulsive barrier present (due to EDL or hydrophilic repulsion), to an increase in the adhesive interaction (van der Waals or ion correlation forces), or both.

It has been suggested by Blandamer et al. [40] that water activity, which is known as the effective mole fraction of water (a_w), defined by the product of activity coefficient (γ_w) times by mole fraction of water (x_w) in that solution, $a_w = \gamma_w x_w$, controls water adsorption and thereby hydrophilic repulsion. By increasing the concentration of ions in solutions, water molecules become more involved with ion-dipole interactions in the bulk fluid that gives rise to hydrated ionic species. This affects surface water absorption on both hydrophilic surfaces, and results in less required force to make adhesive contacts due to the decrease in both magnitude and onset of the hydration forces [50]. Risnes et al. [12] and Rostom et al. [38] also showed that the strength of carbonate rocks and fracture threshold of calcite are affected by the salinity level of pore fluid and attributed this to the level of water activity in the solution [39,76,77]. However, in our system the difference between water activity at highest and lowest values is trivial ($0.95 \leqslant a_w \leqslant 1$, calculated by PHREEQC). The increased adhesion we observe is unlikely to be a function of decreased water adsorption. As shown by Heuberger et al. [78], secondary hydration forces due to compressed dehydrated ions ("two-stage collective ion dehydration" in high salt concentration) might be more important in modifying the repulsive interaction between contacting asperities than simply water adsorption directly onto the calcite surface. We propose that the increase in pull-off force for increasing salt concentration can be explained by a combination of reduced repulsion (weak secondary hydration [29,36,78–80]) and increased attraction between contacting asperities due to instantaneous ion-ion correlation at high salt concentration [35].

The adhesive interaction energy of rough surfaces is not characterized by the macroscopic, nominal area of contact (Fig. 8), but rather by the actual contact area, which is a function of the distribution of asperities on the contacting surfaces [81,82], and in the first approximation, increases linearly with applied compressive normal stress [83]. For rough surfaces, the area of contact depends on the number, size and height of asperities (see Fig. 1) and surface forces are measured depending on the geometry, density [53,54,84] and height distribution of contacting surfaces [49,58].

For rough, inorganic surfaces, the macroscopic, effective interfacial energy γ may be expressed as the sum of the product of contact-bond strengths, β, and actual area, σ, of all contacting asperities that define the real surface area, both of which may change with time (t) and applied normal load (F_n):

$$\gamma(F_n, t) = \Sigma_i \beta_i(F_n, t)\sigma_i(F_n, t) \tag{3}$$

For purely elastic processes, the force required to separate two adhesive surfaces will be independent of both time and applied load as long as the macroscopic surface energy on approach equals that on retraction, $\gamma_R = \gamma_A$ (point A to B in Fig. 10). When γ is not constant (Eq. (3)), the measured adhesion force will depend on the maximum applied load at the contact and time, point B to C vs. D to E, Fig. 10.

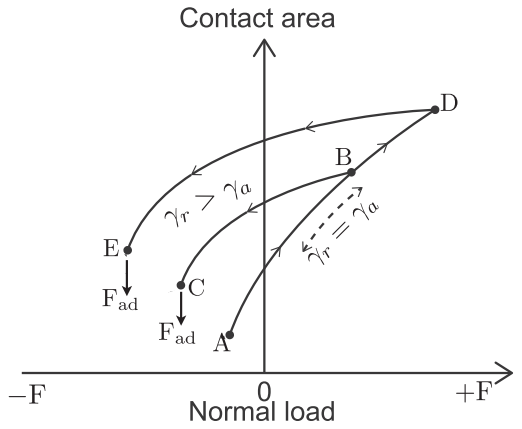

Fig. 10. "Adhesion hysteresis", modified from Israelachvili [28], presenting reversible and irreversible cycles. Upon approach of adhesive surfaces, they jump into contact at A and move along the path to B with increasing normal load. In the case of constant interfacial energy ($\gamma_R = \gamma_A$), unloading follows the same path back to A and the force measured at separation is independent of the maximum applied load. If $\gamma_R > \gamma_A$, separation follows the path from B to C. The measured force of adhesion in this case depends on the maximum applied load (C vs E).

Here, the contact-bond strength β will be given by the fluid chemistry as discussed above, while F_n determines whether a given contact will be pushed past any repulsive barrier into adhesive contact. Therefore, when repulsive barriers are small enough to be overcome, the number of asperities that make it into adhesive contact, and correspondingly the measured pull-off force will be a function of the applied normal load. This is consistent with what we observe. The time dependence of β takes into account any possible chemical strengthening of asperities that might result from diffusion of ions or slow chemical reactions.

Irreversible changes in σ can take place through nonelastic processes such as twinning [23,85] or breakage of asperities upon pressure, or through stress-induced dissolution and re-precipitation (pressure solution) [29,49,84,86–88] of highly stressed asperities and increase in size of contact area, σ ("asperity creep"). However, all these processes cause a permanent change in the surface topography that would remain present as a different measured pull-off force when lower loads are applied. We observe otherwise; as seen in Fig. 7, the pull-off force returns to the initial value when the setpoint (normal load) is reduced. The slow, non-monotonic change in F_{ad} indicates that there is no consistent flattening of asperities and increase of actual contact area with time. Therefore, we propose that the slow changes in F_{ad} with time may be caused by slow lateral drift or recrystallization.

5. Conclusion

Our measurements show a significant effect of normal load and salinity of the contacting solution on the adhesion of calcite surfaces. We discuss the effect of roughness on pull-off force measurements in NaCl solutions, and categorize it into mechanisms responsible for (1) strengthening the contact-bonds, that is discussed to be mostly due to the combination of weak secondary repulsion and ion-ion correlation forces along with the applied normal stress that generate strong contact-bonds at high salt concentration, and (2) variation in the contact area that is mostly attributed to the local recrystallization of single asperities in a multiple asperity system. The measured pull-off force increases with the applied normal stress, indicating that the population of asperities generate the total contact area which differs from nominal surface area of contacting surfaces. In agreement with [24], we measured strong repulsion in low concentration and $CaCO_3$ solutions due to the repulsive hydration forces.

Previous studies suggested that water activity is the key parameter in the strength of calcium carbonate bearing rocks [10,12,24] and single calcite crystals in salt solutions [38]. Based on our measurements, the strengthening process can be explained through progressively weaker secondary hydration and stronger ion-ion correlation forces in NaCl solutions with higher concentration than 100 mM. In addition, we see no indication of consistent flattening of asperities, which could have been related to progressive calcite recrystallization or asperity creep.

Acknowledgments

This work was supported by the National IOR center of Norway under project No. PR-10373. The AFM measurements were performed by the JPK system funded by Bjørn Jamtveit from the European Union's Horizon 2020 Research and Innovation Programme under the ERC Advanced Grant Agreement (669972). We would like to thank Tue Hassenkam, Susan L.S. Stipp, Joanna Dziadkowiec and Aksel Hiorth for the fruitful and invaluable discussions. S.J. is grateful for the constructive comments from J. Dziadkowiec, A.M. H. Pluymakers, G. Dumazer, one anonymous reviewer and the editor to improve the quality of this work.

References

[1] A.J. Skinner, J.P. LaFemina, H.J.F. Jansen, Am. Mineral. 79 (1994) 205–214.
[2] N.H. de Leeuw, S.C. Parker, J. Phys. Chem. B 102 (1998) 2914–2922.
[3] F. Heberling, T.P. Trainor, J. Lutzenkirchen, P. Eng, M.A. Denecke, D.J. Bosbach, Colloid Interface Sci. 354 (2011) 843–857.
[4] H.A. Lowenstam, Geology 62 (1954) 284–322.
[5] E. Liteanu, C.J. Spiers, Chem. Geol. 265 (2009) 134–147.
[6] K.S. Lackner, C.H. Wendt, D.P. Butt, E.L. Joyce, D.H. Sharp, Energy 20 (1995) 1153–1170.
[7] L. Truche, G. Berger, C. Destrigneville, D. Guillaume, E. Giffaut, Geochim. Cosmochim. Acta 74 (2010) 2894–2914.
[8] M. D'Heur, Mar. Pet. Geol. 1 (1984) 211–238.
[9] R. Risnes, O. Flaageng, Oil Gas Sci. Technol. 54 (1999) 751–758.
[10] T. Heggheim, M. Madland, R. Risnes, T. Austad, J. Petrol. Sci. Eng. 46 (2005) 171–184.
[11] R. Risnes, Phys. Chem. Earth (A) 26 (2001) 53–57.
[12] R. Risnes, H. Haghighi, R.I. Korsnes, O. Natvik, Tectonophysics 370 (2003) 213–226.
[13] R. Hellmann, P. Renders, J. Gratier, R. Guiguet, Water-Rock Interact. (2002) 129–152.
[14] A. Hiorth, L.M. Cathles, M.V. Madland, Transp. Porous Media 85 (2010) 1–21.
[15] M. Megawati, A. Hiorth, M.V. Madland, Rock Mech. Rock Eng. 46 (2012) 1073–1090.
[16] M.V. Madland, A. Hiorth, E. Omdal, M. Megawati, T. Hildebrand-Habel, R.I. Korsnes, S. Evje, L.M. Cathles, Transp. Porous Media 87 (2011) 679–702.
[17] A. Nermoen, R.I. Korsnes, A. Hiorth, M.V. Madland, J. Geophys. Res. 120 (2015) 2935–2960.
[18] R. Risnes, M. Madland, M. Hole, N. Kwabiah, J. Petrol. Sci. Eng. 48 (2005) 21–36.
[19] G. Newman, Soc. Petrol. Eng. 35 (1983) 976–980.
[20] R. Hellmann, J. Gratier, P. Renders, Deformation of chalk by pressure solution, 1996.
[21] P. Delage, C. Schroeder, Y. Cui, Subsidence and capillary effects in chalks, 2008.
[22] E. Liteanu, C.J. Spiers, Chem. Geol. 265 (2009) 134–147.
[23] A. Røyne, J. Bisschop, D.K. Dysthe, J. Geophys. Res. 116 (2011) B04204.
[24] A. Røyne, K.N. Dalby, T. Hassenkam, Geophys. Res. Lett. 42 (2015) 4786–4794.
[25] B. Derjaguin, L. Landau, Prog. Surf. Sci. 43 (1941) 1–4.
[26] E. Verwey, J.T.G. Overbeek, Elsevier, Amsterdam 1948.
[27] J. Overbeek, E.J.W. Verwey, Theory of the Stability of Lyophobic Colloids, Elsevier, 1948.
[28] J.N. Israelachvili, third ed., Intermolecular and Surface Forces, vol. 1, Elsevier, 2011.
[29] Y. Diao, R.M. Espinosa-Marzal, Proc. Natl. Acad. Sci. USA 113 (2016) 12047–12052.
[30] J.N. Israelachvili, R.M. Pashley, Nature 306 (1983) 249–250.
[31] Z. Zachariah, R.M. Espinosa-Marzal, N.D. Spencer, M.P. Heuberger, Phys. Chem. Chem. Phys. 18 (2016) 24417–24427.
[32] J. Chun, C.J. Mundy, G.K. Schenter, J. Phys. Chem. B 119 (2015) 5873–5881.

[33] M. Ricci, P. Spijker, F. Stellacci, J.F. Molinari, K. Voitchovsky, Langmuir 29 (2013) 2207–2216.
[34] L. Guldbrand, B. Jönsson, H. Wennerström, P. Linse, J. Chem. Phys. 80 (1984) 2221–2228.
[35] B. Joensson, H. Wennerstroem, A. Nonat, B. Cabane, Langmuir 20 (2004) 6702–6709.
[36] S.H.J. Donaldson, A. Royne, K. Kristiansen, M.V. Rapp, S. Das, M.A. Gebbie, D.W. Lee, P. Stock, M. Valtiner, J. Israelachvili, Langmuir 31 (2015) 2051–2064.
[37] S. Pourchet, I. Pochard, F. Brunel, D. Perrey, Cem. Concr. Res. 52 (2013) 22–30.
[38] F. Rostom, A. Royne, D.K. Dysthe, F. Renard, Tectonophysics 583 (2013) 68–75.
[39] M. Kohns, M. Schappals, M. Horsch, H. Hasse, J. Chem. Eng. Data 61 (2016) 4068–4076.
[40] M.J. Blandamer, J.B. Engberts, P.T. Gleeson, J.C. Reis, Chem. Soc. Rev. 34 (2005) 440–458.
[41] H.J. Butt, K. Graf, M. Kappl, Physics and Chemistry of Interfaces, Wiley, 2003.
[42] E. Ruiz-Agudo, M. Kowacz, C.V. Putnis, A. Putnis, Geochim. Cosmochim. Acta 74 (2010) 1256–1267.
[43] T. Foxall, G.C. Peterson, H.M. Rendall, A.L.J. Smith, Chem. Soc. Faraday Trans. 1 75 (1979) 1034–1039.
[44] S.L.S. Stipp, Geochim. Cosmochim. Acta 63 (1999) 3121–3131.
[45] U. Ulusoy, C. Hiçyilmaz, M. Yekeler, Chem. Eng. Process. 43 (2004) 1047–1053.
[46] U. Ulusoy, M. Yekeler, Chem. Eng. Process. 44 (2005) 555–563.
[47] S.-Y. Chen, Y. Kaufman, K. Kristiansen, D. Seo, A.M. Schrader, M.B. Alotaibi, H.A. Dobbs, N.A. Cadirov, J.R. Boles, S.C. Ayirala, J.N. Israelachvili, A.A. Yousef, Energy Fuels 31 (2017) 8925–8941.
[48] E. Thormann, Curr. Opin. Colloid Interface Sci. 27 (2017) 18–24.
[49] D.F. Parsons, R.B. Walsh, V.S.J. Craig, Chem. Phys. 140 (2014) 164701.
[50] M. Valtiner, X. Banquy, K. Kristiansen, G.W. Greene, J.N. Israelachvili, Langmuir 28 (2012) 13080–13093.
[51] E.M. Hoek, G.K.J. Agarwal, Colloid Interface Sci. 298 (2006) 50–58.
[52] J.F.L. Duval, F.A.M. Leermakers, H.P.V. Leeuwen, Langmuir 20 (2004) 5052–5065. PMID: 15984268.
[53] S. Bhattacharjee, C.H. Ko, M. Elimelech, Langmuir 14 (1998) 3365–3375.
[54] L. Suresh, J.Y. Walz, Colloids Interface Sci. 183 (1996) 199–213.
[55] Z. Adamczyk, P. Weroński, Adv. Colloid Interface Sci. 83 (1999) 137–226.
[56] B.N.J. Persson, Surf. Sci. Rep. 61 (2006) 201–227.
[57] B.N. Persson, M. Scaraggi, J Chem Phys 141 (2014) 124701.
[58] N. Eom, D.F. Parsons, V.S.J. Craig, J. Phys. Chem. B 121 (2017) 6442–6453.
[59] J.A. Brant, A.E. Childress, Environ. Eng. Sci. 19 (2004) 413–427.
[60] S. Stipp, W. Gutmannsbauer, T. Lehmann, Am. Mineral. 81 (1996) 1–8.
[61] S.L.S. Stipp, J. Konnerup-Madsen, K. Franzreb, A. Kulik, H.J. Mathieu, Nature 396 (1998) 356–359.
[62] J. Dziadkowiec, S. Javadi, J.E. Bratvold, O. Nilsen, A. Royne, Langmuir (2018).
[63] Y. Levenson, S. Emmanuel, Geochem. Perspect. Lett. (2017) 133–141.
[64] X. Liu, W. Yan, E.H. Stenby, E. Thormann, Energy Fuels 30 (2016) 3986–3993.
[65] S.J. Fathi, T. Austad, S. Strand, Water-Based Enhanced Oil Recovery (EOR) by Smart Water in Carbonate Reservoirs, 2012.
[66] S.J. Fathi, T. Austad, S. Strand, Energy Fuels 24 (2010) 2514–2519.
[67] H.-J. Butt, B. Cappella, M. Kappl, Surf. Sci. Rep. 59 (2005) 1–152.
[68] M. Farshchi-Tabrizi, M. Kappl, Y. Cheng, J. Gutmann, H.J. Butt, Langmuir 22 (2006) 2171–2184.
[69] J.L. Hutter, J. Bechhoefer, Rev. Sci. Instrum. 64 (1993) 1868–1873.
[70] D.L. Parkhurst, User's guide to Phreeqc – A computer program for speciation, reaction-path, advective-transport, and inverse geochemical calculations, Report, 1995.
[71] S.L.S. Stipp, C.M. Eggleston, B.S. Nielsen, Geochim. Coesmochim. Acta 58 (1994) 3023–3033.
[72] M. Wolthers, L. Charlet, P.V. Cappellen, Am. J. Sci. (2008).
[73] A.M. Smith, A.A. Lee, S. Perkin, J. Phys. Chem. Lett. 7 (2016) 2157–2163.
[74] M. Valtiner, K. Kristiansen, G.W. Greene, J.N. Israelachvili, Adv. Mater. 23 (2011) 2294–2299.
[75] R.M. Pashley, J.N. Israelachvili, Colloid Interface Sci. 97 (1984) 446–455. https://www.sciencedirect.com/science/article/pii/0021979784903163.
[76] S.M. Mutisya, A. Kirch, J.M. de Almeida, V.M. Sánchez, C.R. Miranda, J. Phys. Chem. C 121 (2017) 6674–6684.
[77] D. Di Tommaso, E. Ruiz-Agudo, N.H. de Leeuw, A. Putnis, C.V. Putnis, Phys. Chem. Chem. Phys. 16 (2014) 7772–7785.
[78] M.P. Heuberger, Z. Zachariah, N.D. Spencer, R.M. Espinosa-Marzal, Phys. Chem. Chem. Phys. 19 (2017) 13462–13468.
[79] S. Marčelja, Curr. Opin. Colloid Interface Sci. 16 (2011) 579–583.
[80] R.M. Espinosa-Marzal, T. Drobek, T. Balmer, M.P. Heuberger, PCCP 14 (2012) 6085–6093.
[81] K.N.G. Fuller, D. Tabor F.R.S, Proc. Roy. Soc. Lond. A. Math. Phys. Sci. 345 (1975) 327–342, https://doi.org/10.1098/rspa.1975.0138.
[82] P. Prokopovich, S. Perni, Langmuir 26 (2010) 17028–17036.
[83] J.A. Greenwood, J.B.P. Williamson, Proc. Roy. Soc. Lond. Ser. A Math. Phys. Sci. 295 (1966) 300–319.
[84] X. Huang, S. Bhattacharjee, E.M. Hoek, Langmuir 26 (2010) 2528–2537.
[85] F.P. Bowden, R.E. Cooper, Nature (1962) 1091–1092.
[86] N. Alcantar, J. Israelachvili, J. Boles, Geochim. Cosmochim. Acta 67 (2003) 1289–1304.
[87] D. Croizé, F. Renard, K. Bjørlykke, D.K. Dysthe, J. Geophys. Res. (2010) 115.
[88] F. Renard, S. Beauprêtre, C. Voisin, D. Zigone, T. Candela, D.K. Dysthe, J.-P. Gratier, Earth Planet. Sci. Lett. (2012) 20–34.

Manuscript 2

Surface Forces Apparatus Measurements of Interactions between Rough and Reactive Calcite Surfaces

Joanna Dziadkowiec, Shaghayegh Javadi, Jon E. Bratvold,
Ola Nilsen, and Anja Røyne
Langmuir, **2018**, 34(25), pp 7248-7263

Manuscript 3

Direct observation of AFM calcite probe: Implication for calcite roughness evolution measurement

Shaghayegh Javadi and Anja Røyne
In preparation, (2018)

Author contribution: Shaghayegh Javadi designed and performed the experiments, analyzed and interpreted the data and wrote the manuscript. Anja Røyne supervised the project; contributed to the design of the experiments and advised on experimental methods, data analysis and interpretation, and manuscript writing.

Direct observation of AFM calcite probe: Implication for calcite roughness evolution measurement

S. Javadi[a,c,b,*], A. Røyne[b]

[a]*The National IOR center of Norway, University of Stavanger, Norway.*
[b]*Department of Physics, University of Oslo, Norway.*
[c]*Petroleum Engineering Department, University of Stavanger, Norway*

Abstract

At nano-scale, surface roughness has a significant effect on the measured forces between two calcite surfaces in aqueous solutions [1, 2], because the contact surface area decreases and generates repulsive forces due to elastic deformation of highest asperities [3, 4]. In addition, nm-scale calcite recrystallization in aqueous solutions may increase the surface roughness and therefore give rise to repulsive forces between opposing surfaces [2]. However, the link between recrystallization and surface forces is still not well understood. In this paper, we combine the AFM force measurements (with colloidal probe) with an AFM inverse imaging technique for *in situ* characterization of the calcite probes. This allows us to measure the interaction forces between calcite surfaces, and simultaneously characterize one of the contacting calcite surfaces. We expect that recrystallization of the calcite surface might affect forces between the surfaces, and that different ions (in particular Mg^{2+}) can affect the recrystallization behavior. We, thus, performed experiments using freshly cleaved calcite surfaces in a fluid cell containing $MgSO_4$, $MgCl_2$ or NaCl solutions, to both investigate the surface forces between two calcite surfaces and image the changing calcite probe topography. The experiments in NaCl solutions are performed as control experiments to understand the effect of NaCl on the topography evolution of the calcite surfaces. Although our preliminary results are not sufficient to draw a clear conclusion about the specific ion-effects on calcite recrystallization at the present time, we show that the presented technique is a powerful tool to study the coupling between the calcite surface roughness evolution and surface forces. This could also have implications for crack healing and the mechanical strength of calcitic rocks.

1. Introduction

Nm-scale interfacial forces between fluid and calcite play a major role in controlling the mechanical strength and deformation of calcitic rocks through dissolution, recrystallization and the development of intergranular fractures influenced by fluid chemistry [1, 2, 5, 6]. A substantial loss of strength in calcite has been found to occur in the presence of water molecules, a phenomenon that is referred to *water weakening*, with a strong dependence on the chemical composition of the fluid [7–9].

When a crystal or a solid rock is in contact with so-called "adsorption-active" media, the surface energy and subsequently the mechanical threshold for fracture formation decreases, by transporting the reactants to regions of disrupted bond on the surface [10, 11]. This can affect creep deformation [12] and subcritical (discontinuous) crack growth or brittle deformation due to stress [13], which are known to be the reason for strength loss of calcitic rocks. Other mechanisms that have been suggested to describe the calcite water weakening are the interaction forces at the fracture tip and grain boundaries, which are usually repulsive in low concentration aqueous solutions due to hydration forces between two hydrophilic calcite surfaces as well as the electrical double layer (EDL) repulsion [6, 8, 14, 15].

Interactions between calcite surfaces in calcitic rocks and fluids are generally controlled by the fluid chemistry and stress concentration through e.g., pressure solution creep [16, 17], subcritical crack propagation [15, 18], dissolution and precipitation [1, 2, 19]. Chemical dissolution and recrystallization can change the roughness of calcite surfaces [2, 20–23], which in turn affects the interaction forces between surfaces. Both ionic strength and ion type of the saturating aqueous solutions have a strong effect on subcritical crack propagation and calcite strength, as shown by Bergsaker *et al.* [18]. They observed that higher NaCl concentration strengthened the calcite and prevented crack growth, whereas solutions of Na_2SO_4 caused the opposite effect. Interestingly, solutions containing $MgCl_2$ and $MgSO_4$ did not induce the enhanced subcritical cracking, but promoted crack healing, a mechanism that is still poorly understood.

Calcite cleavage surfaces are characterized by steps and kinks (terraces) that are usually the most active growth and dissolution sites on calcite. Using AFM, Ruiz-Agudo *et al.* [24] have shown that a higher concentration of Mg^{2+} (>> 50 mM) increases the dissolution rate of calcite by increasing the density and depth of the etch pits generated on calcite surfaces. Lin and Singer [25] showed that Mg^{2+} has an inhibitory effect on

*Corresponding author
Email address: shaghayegh.javadi@fys.uio.no (S. Javadi)

calcite growth, and that the ratio of Mg^{2+}/Ca^{2+}, not only the Mg^{2+}-concentration alone, controls the calcite growth mechanism. Nielsen *et al.* [26] showed that Mg^{2+} inhibits the calcite crystal growth by blocking the propagation of the kinks. They found that the growth of calcite in presence of magnesium depends on the activity level of Ca^{2+} cations. Several studies have shown that Mg^{2+} influences the thermodynamic stability of calcite [27–30], something which is believed to be due to lattice disorder [31] and strain [32] because of the ionic size difference between Ca^{2+} (r = 1.14 Å) and Mg^{2+} (r = 0.86 Å) [33].

Knowing that Mg^{2+} drives nano-scale changes in topography of calcite surfaces, we expect to observe morphological changes on the surface, when scanning the calcite probe in our experiments with AFM in high concentration Mg^{2+}-salt solutions (IS = 1.2 M). We then investigate possible effects of changes in surface topography on the forces acting between calcite surfaces. The calcite crack healing near Mg^{2+} that was observed by Bergsaker *et al.* [18], could be due to surface morphological changes that could have been a driving force to form a solid bond and increase the adhesion between surfaces separated by nano-scale cracks. We use AFM colloidal probe technique for *in situ* fabrication of a calcite probe for force measurements in a small liquid cell (method adapted from our previous work [1]). In addition, we study the possible variation in surface topography as a function of time and chemical composition of fluid using "inverse imaging", a method that was first introduced by Montelius and Tegenfeldt [34], for imaging and characterizing an *in situ* deposited silver probe. Several people have reported using this technique for biological applications, e.g. [35], but to the best of our knowledge, this method has not been used for characterization of calcite surfaces.

2. Experimental details

2.1. Methods

2.1.1. AFM force measurement

We use a JPK NanoWizard®4 Bioscience AFM. During the force measurements, the AFM is set to the force spectroscopy mode at a constant approach and retract velocity of 150 nm/s. We apply a maximum normal load of 20 nN and holding the surfaces in contact at this load for 1 s during each force measurement. An *in situ* fabricated calcite probe (following the method as presented in our previous work [1]) moves up and down, vertically, above a freshly cleaved calcite crystal (see Figure 1a) while the interaction force is recorded as a force-distance curve (FR). The sequence of a typical experiment is shown in Figure 2. Force-distance data are processed using the JPK data processing software and further analyzed using Matlab.

2.1.2. Inverse Imaging

We use the inverse imaging technique to image the topography of the calcite probe. We use a self-curing rubber (Reprorubber) to fix a cantilever (RTESP-300, 300 kHz, 40 N/m), tip pointing upward, on the glass bottomed of our fluid cell. The cantilever chip is placed next to a cleaved calcite crystal (see Figure 1b). We first scan the probe in air to make a clear overview of the probe. Imaging in fluid starts after the first FR

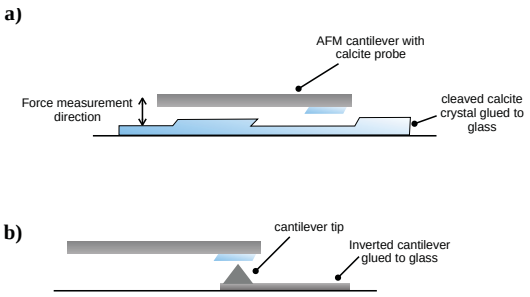

Figure 1: Illustration of the experimental procedure, including force measurement with a fabricated calcite probe (following the same procedure as our previous work [1]), and an inverted AFM cantilever next to the calcite crystal. This sketch is not in scale due to cantilevers' small sizes. This setup is placed in a cylindrical shaped fluid cell with 3 ml fluid capacity and 20 mm inner diameter.

measurements in liquid by moving the cantilever to the exact same position as initially imaged in air. See Figure 2 for the measurement procedure.

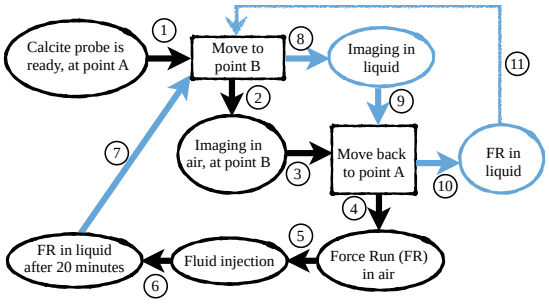

Figure 2: Typical experimental day in the lab. Point A refers to the initial position where the calcite fragment was picked and glued to the cantilever. Point B refers to the position of the inverted cantilever for imaging. Blue color indicates measurements in liquid. The force measurements (FR) are performed in 3 sets of 200 curves. The probe is moved to point B and imaged between each set, and then moved back to point A for force runs. We wait 20 minutes between imaging and force runs for the system to stabilize.

2.2. Materials

We use Iceland spar calcite in $\approx 3 \times 3$ mm to glue to a glass microscope slide with a UV-curing adhesive (Casco Glaslim). The calcite crystal is freshly cleaved before the experiment. Cleaving the calcite leaves small fragments on the surface, and a suitable fragment is chosen and glued to the tipless cantilever to be used as calcite probe. This method along with fluid cell development is identical to what is described in our previous work [1]. We loosely seal the fluid cell with a silicon rubber flap to prevent fluid evaporation. A cantilever (RTESP-300, 300 kHz, 40 N/m) is fixed to the same glass slide adjacent to the cleaved calcite for the inverse imaging purposes. We continuously monitor the temperature inside the AFM enclosure and found to vary between 25° and 30°C.

All solutions are saturated with $CaCO_3$ powder (MERCK). We use anhydrous $MgSO_4$ (MERCK, 98%), $MgCl_2$ hexahy-

drate (MERCK, 99.0-101.0%) and NaCl (VWR, 100.2%) in pre-saturated $CaCO_3$ solutions in deionized water (type II). We isolate the effect of ion type by using a constant ionic strength (IS) of 1.2 M.

3. Results and discussion

For our measured force-distance curves (FR), we observe pure repulsive interactions, regardless of the type of electrolyte solution. We find that these repulsive forces can fit into an exponential function, whose fitting parameter can adequately describe the surface topography changes as a function of time. Since calcite surface is charged in electrolyte solutions, we always expect that electrostatic double layer forces (EDL) have contributions in repulsive forces. However, we discuss that EDL contributions might be overlapped by the repulsive forces due to the highest asperities being in contact or by hydration forces. Hydration forces are a function of distance (separations below the Debye length) and can be monotonically repulsive between hydrophilic atomically rough surfaces [36, 37].

Our results include the decay length λ, found as a fitting parameter for Equation 1 to the FRs on approach, and the representative AFM deflection images of the calcite probes in each electrolyte solutions. Table 1 shows the list of all measurements in which no adhesion was measured between two calcite surfaces.

Exp. (#)	$CaCO_3$ saturated with	Measured force	IS (mol/l)
1	$MgCl_2$ (0.4 M)	repulsion	1.2
2	$MgCl_2$ (0.4 M)	repulsion	1.2
3	$MgSO_4$ (0.3 M)	repulsion	1.2
4	$MgSO_4$ (0.3 M)	repulsion	1.2
5	NaCl (1.2 M)	repulsion	1.2
6	NaCl (1.2 M)	repulsion	1.2

Table 1: List of experiments and observations

3.1. Roughness evolution from force measurements

For rough surfaces, the magnitude and onset of repulsive forces depend on the degree of surface roughness [38–41]. We, therefore, fit the approach data to an exponential function of the form,

$$F(D) = F_0 exp(-D/\lambda) \quad (1)$$

where F is the measured force, D is surface separation ($D = 0$ is chosen at the position where the surface separation shows negligible change with increasing the applied force), and λ is the decay length. Two representative FRs, upon approach, are shown in Figure 3: forces on approach are in all cases repulsive, with no significant jumps-in.

As shown by Eom *et al.* [3], for rough surfaces, contacting asperities generate exponentially decaying repulsive forces on approach [3], which can be potentially confused with EDL or hydration repulsive forces [3, 42]. We assume that the measured decay length λ can be used as an indirect measure of surface roughness, as discussed by Parsons *et al.* [4].

We observe a consistent trend for the decay length λ in our measurements in all used aqueous solutions, where the average value of λ decreasing with time, indicating that the contacting surfaces become less rough with time.

3.2. Experiments in $MgCl_2$

Two experiments were performed in $MgCl_2$ solutions with ionic strength (IS) of 1.2 M. Only one round of FRs were performed for the first experiment, because the calcite probe was accidentally lost. Figure 4 shows measured decay lengths for both experiments, indicating decreasing and then stabilizing surface roughness with time. On the second day, the decay length was found to be stable for each round of FR measurement, and we observed no significant change with time, indicating a stable surface during each FR measurement. However, the averaged value of λ (Figure 4 (inset)) decreases (from 2.8 to 0.46 nm) with the elapsed time, suggesting a surface with less roughness after 5.5 hours of experiment.

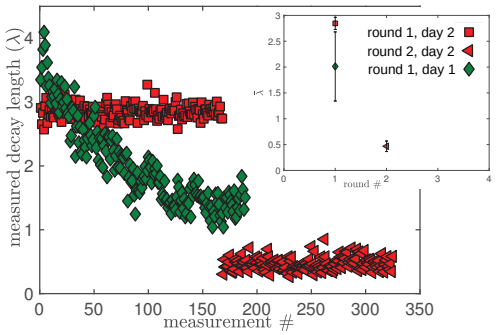

Figure 4: Fitting parameter λ in $MgCl_2$ solution with IS = 1.2 M. Indicating the surface topography variation with time for the same contact. This plot shows the measured λ for all FRs on approach for two experimental days. Only 1 round of measurements for day 1, and 2 rounds for day 2. The inset shows the averaged λ values for both days of measurements, that decreases with time for day 2. The measurement unit for λ and $\bar{\lambda}$ is nm.

Inverse AFM images of the calcite probe in $MgCl_2$ were obtained first in air, and then between each sequence of FRs at scan sizes 10×10 and 20×20 μm^2. Figure 5 shows chosen images for day 1 (with the best resolution among all scanned images) only at 20×20 μm^2. The first image in Figure 5 shows our attempt to scan the whole particle in air before liquid injection. These images show a stable surface in $MgCl_2$ solutions however, we expect that higher resolution images could have revealed topography variation that can be estimated by measured λ for day 1, as shown by Figure 4.

3.3. Experiments in $MgSO_4$

We performed two experiments in $MgSO_4$ (IS = 1.2 M), with two rounds of FRs on day 1 and three rounds of FRs on day 2. We observe a consistent decrease of λ with time for both days.

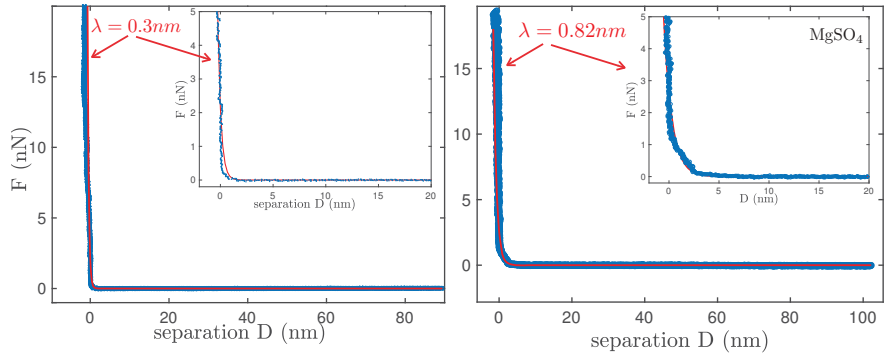

Figure 3: Representative force-distance curves on approach with an exponential fit, used to quantify the contacting surface roughness on loading, in $MgCl_2$ (left) and $MgSO_4$ (right) with IS = 1.2 M. λ is the fitting coefficient and representing the local roughness of contacting surfaces. Both insets show the closest point to the contact, with shifted hardwall to zero. The red line shows the fitting curve.

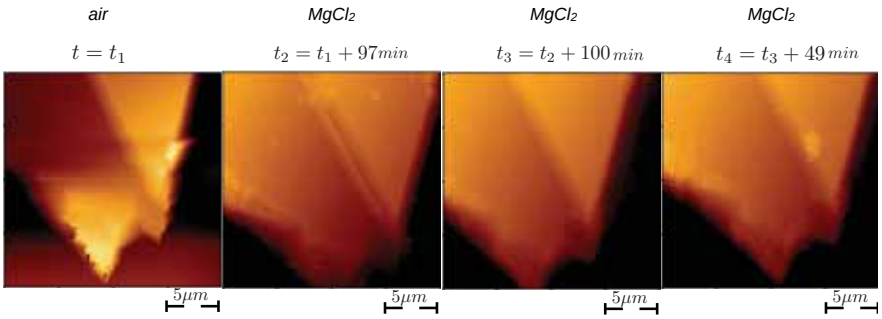

Figure 5: Representative AFM deflection images ($20\times20\ \mu m^2$) of a calcite probe in air and $MgCl_2$ between sequences of force runs.

The average values of λ, $\bar{\lambda}$, are between 0.31 and 2.4 nm, similar to what was found in the experiments with $MgCl_2$.

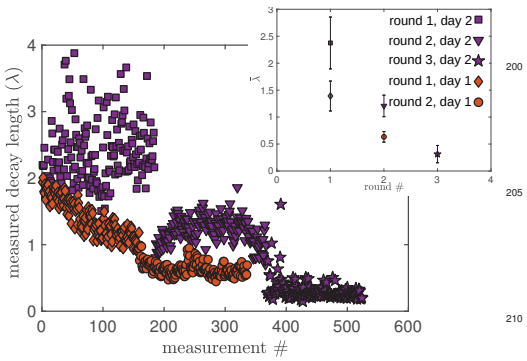

Figure 6: Fitting parameter λ (nm) in $MgSO_4$ solution (IS = 1.2 M). Measured λ for all FRs on approach for two experimental days. Two rounds of measurements for day 1, and 3 rounds for day 2. The inset shows the averaged λ values for both days of measurements, that decreases for both days.

We observe no significant change on the surface topography in $MgSO_4$ solutions within 6.5 hours of measurements. Ruiz-Agudo *et al.* [24] observed increased density of etch pit on calcite $\{10\bar{1}4\}$ surfaces in concentrated $MgSO_4$ and $MgCl_2$ solutions. They measure the density and dimension of the observed etch pits and calculate the dissolution rate of calcite, that shows overall increase influenced by Mg^{2+} ions. Figure 7 shows a representative calcite probe in $MgSO_4$ solutions (day 2). At first glance, we see a generation of etch pits on the surface that could be in line with observations of Ruiz-Agudo *et al.* [24]. This is, however, cannot be the case in our experiments. Because this observation is inconsistent and limited to only one calcite among 4 imaged calcite probes (2 in $MgSO_4$, and 2 in $MgCl_2$). In addition, due to the instrumental drift, we see a lateral shift in these images that prevents etch pit depth and spreading measurements as suggested by Ruiz-Agudo *et al.* [24].

3.4. Experiments in NaCl

Measured $\bar{\lambda}$ in NaCl solutions (IS = 1.2M) is in the range of $0.24\ \text{nm} \leq \bar{\lambda} \leq 2.2\ \text{nm}$. The first day of experiments shows stable surfaces with very short ranged repulsion (Figure 8), where

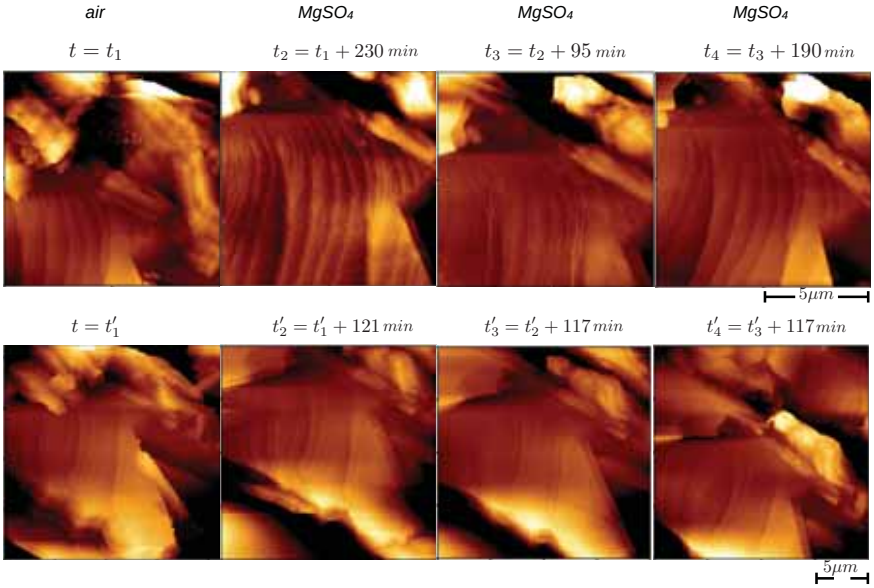

Figure 7: Representative inverse AFM images of a calcite probe in air and $MgSO_4$ between sequences of force runs. The top row shows images with 10×10 μm^2 and bottom row 20×20 μm^2 scan sizes.

the surfaces on the second day behave similarly to the surfaces in Mg-salt solutions, and λ decreases with time. This indicates that the calcite surfaces in our measurements undergo dissolution, recrystallization and/or plastic deformation of asperities in aqueous solutions [43], that changes the total contacting area known as the sum of discrete nano-scaled asperities as discussed in [1].

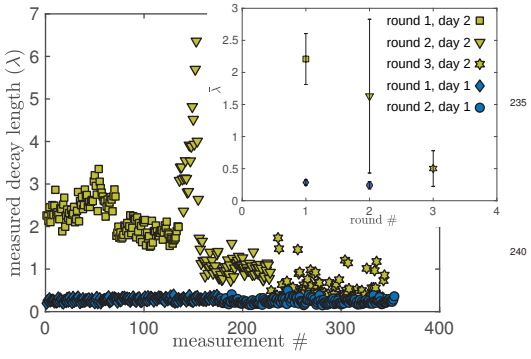

Figure 8: Fitting parameter λ (nm) in NaCl solution (IS = 1.2 M). This plot shows the measured λ for all FRs on approach for two experimental days. Two rounds of measurements for day 1, and 3 rounds for day 2. The inset represents the averaged λ values for both days of measurements, that decreases with time for both days.

We have no successive AFM images in air for these two sets of experiments. It is usual that a piece of dust or a water droplet (due to capillary condensation) attaches to the calcite probe that prevents contact between the tip and calcite probe. This can explain the failure in good resolution images in air, which was solved for one day of experiments, by injecting the NaCl solution in the fluid cell. This data is presented by Figure 9. Naively, one would see pit deepening and stretching on the calcite probe by looking at both scan sizes (10×10 μm^2 and 20×20 μm^2), in Figure 9. This is, however, not the case. We observe a significant shift, laterally, in both scan sizes comparing the rightmost panels with the first ones. This is because of the inevitable instrumental drift.

4. Outcome

Although λ-measurements display topography variation (smoothing) on all surfaces, the resolution of AFM images is too poor to verify this result. This could be because of, 1) inevitable instrumental drift; 2) the imaging cantilever might be tilted with respect to the bottom surface of the fluid cell, which avoids uniaxial loading and consequently poor image resolution; and/or 3) the imaging cantilever tip is too long. A shorter tip could have been better to use for these experiments, due to roughness of the calcite probe surfaces.

The measured repulsive forces on approach may mostly be attributed to the calcite surface roughness, which is being reduced with time. This might be due to the dissolution of the highest contacting asperities and inadequate contact areas. We have previously performed a series of similar AFM experiments in NaCl solutions, in which we altered the concentration of the solutions with regard to NaCl, with 1.2 M as the maximum value [1]. We observed an increase in strength of calcite by

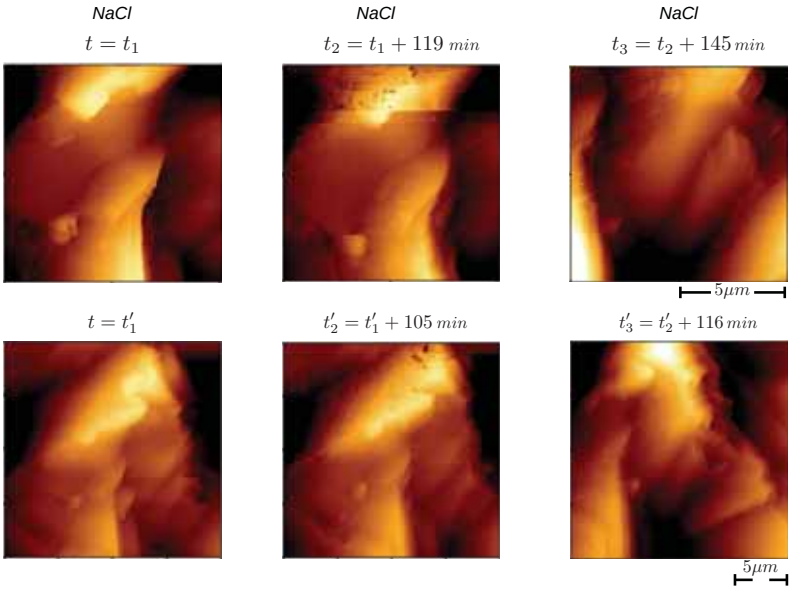

Figure 9: Representative AFM deflection images of a calcite probe in NaCl solutions (IS = 1.2 M) between sequences of force runs. The top row shows images with 10×10 μm^2 and bottom row 20×20 μm^2 scan sizes.

increasing the salt concentration, which was attributed to ion-ion correlation and chemical roughness. The current results are in contrary with our previous study, which suggests that differences in the experimental methods could influence the final results. Moving the calcite probe back and forth between imaging and force measurements could enhance the drift possibility (in addition to instrumental drift), and landed the probe each time on an approximate (but not exact) same position. Since surface forces are not only function of ionic concentration but also surface topography, disturbing the surface species could result into repulsive forces.

We suggest that an extended number of experiments are required, with minor changes in the method, such as 1) using a shorter tip for the imaging cantilever, 2) using a glue with less viscosity than the self-curing rubber used in these experiments, although one must be careful with the reactivity of the glue with calcite surfaces. A homogeneous glue film must be possible to make to avoid tilting the imaging cantilever, 3) reducing the number of times to move the calcite probe back and forth, this might reduce the lateral drift and results into better resolution images.

5. Acknowledgments

This work was supported by the National IOR center of Norway under project no. PR-10373. The AFM measurements were performed by the JPK system funded by Bjørn Jamtveit from the European Union's Horizon 2020 Research and Innovation Programme under the ERC Advanced Grant Agreement (669972). S. Javadi would like to express her gratitude to Joanna Dziadkowiec for her helpful comments to improve the quality of manuscript.

References

[1] Javadi, S.; Røyne, A. *Journal of Colloid and Interface Science* **2018**, *532*, 605–613.
[2] Dziadkowiec, J.; Javadi, S.; Bratvold, J. E.; Nilsen, O.; Royne, A. *Langmuir* **2018**, *34*, 7248–7263.
[3] Eom, N.; Parsons, D. F.; Craig, V. S. J. *Journal of Physical Chemistry B* **2017**, *121*, 6442–6453.
[4] Parsons, D. F.; Walsh, R. B.; Craig, V. S. *Journal of Chemical Physics* **2014**, *140*.
[5] Risnes, R.; Flaageng, O. *Oil and Gas Science and Technology* **1999**, *54*, 751–758.
[6] Røyne, A.; Dalby, K. N.; Hassenkam, T. *Geophysical Research Letters* **2015**, *42*, 4786–4794.
[7] Risnes, R.; Haghighi, H.; Korsnes, R. I.; Natvik, O. *Tectonophysics* **2003**, *370*, 213–226.
[8] Risnes, R.; Madland, M.; Hole, M.; Kwabiah, N. *Journal of Petroleum Science and Engineering* **2005**, *48*, 21–36.
[9] Heggheim, T.; Madland, M. V.; Risnes, R.; Austad, T. *Journal of Petroleum Science and Engineering* **2005**, *46*, 171–184.
[10] Shchukin, E. D.; Bessonov, A. I.; Kontorovich, S. I.; Polukarova, Z. M.; Sokolova, L. N.; Amelina, E. A.; Burenkova, L. N.; Romanovsky, B. V. *Colloids and Surfaces A: Physicochemical and Engineering Aspects* **2006**, *282-283*, 287–297.
[11] Rehbinder, P. A.; Lichtman, V. Effect of surface active media on strain and rupture in solids. 1954.
[12] Brantut, N.; Heap, M. J.; Meredith, P. G.; Baud, P. *Journal of Structural Geology* **2013**, *52*, 17–43.
[13] Atkinson, B. K. *Journal of Geophysical Research: Solid Earth* **1984**, *89*, 4077–4114.
[14] Megawati, M.; Hiorth, A.; Madland, M. V. *Rock Mechanics and Rock Engineering* **2012**, *46*, 1073–1090.

[15] Røyne, A.; Bisschop, J.; Dysthe, D. K. *Journal of Geophysical Research* **2011**, *116*.
[16] Hellmann, R.; Renders, P.; Gratier, J.; Guiguet, R. *Water-Rock Interactions* **2002**, 129–152.
[17] Croizé, D.; Renard, F.; Bjørlykke, K.; Dysthe, D. K. *Journal of Geophysical Research* **2010**, *115*.
[18] Bergsaker, A. S.; Røyne, A.; Ougier-Simonin, A.; Aubry, J.; Renard, F. *Journal of Geophysical Research: Solid Earth* **2016**, *121*, 1631–1651.
[19] Ciantia, M. O.; Castellanza, R.; Crosta, G. B.; Hueckel, T. *Engineering Geology* **2015**, *184*, 1–18.
[20] Bisschop, J.; Dysthe, D. K.; Putnis, C. V.; Jamtveit, B. *Geochimica et Cosmochimica Acta* **2006**, *70*, 1728–1738.
[21] Chiarello, R. P.; Wogelius, R. A.; Sturchio, N. C. *Geochimica et Coesmochimica Acta* **1993**, *57*, 4103–4110.
[22] Stipp, S. L. S. *Geochimica et Cosmochimica Acta* **1999**, *63*, 3121–3131.
[23] Bohr, J.; Wogelius, R. A.; Morris, P. M.; Stipp, S. L. S. *Geochimica et Cosmochimica Acta* **2010**, *74*, 5985–5999.
[24] Ruiz-Agudo, E.; Putnis, C. V.; Jiménez-López, C.; Rodriguez-Navarro, C. *Geochimica et Cosmochimica Acta* **2009**, *73*, 3201–3217.
[25] Lin, Y.; Singer, P. C. *Journal of Crystal Growth* **2009**, *312*, 136–140.
[26] Nielsen, L. C.; Yoreo, J. J. D.; DePaolo, D. J. *Geochimica et Cosmochimica Acta* **2013**, *115*, 100–114.
[27] Davis, K. J.; Dove, P. M.; Yoreo, J. J. D. *Science* **2000**, *290*, 1134–1137.
[28] Davis, K. J.; Dove, P. M.; Wasylenki, L. E.; Yoreo, J. J. D. *American Mineralogist* **2004**, *89*, 714–720.
[29] Kulik, D. A. *Chemical Geology* **2006**, *225*, 189–212.
[30] Hong, M.; Xu, J.; Teng, H. H. *Geochimica et Cosmochimica Acta* **2016**, *172*, 55–64.
[31] Mucci, A.; Morse, J. W. *Geochimica et Coesmochimica Acta* **1983**, *47*, 217–233.
[32] Paquette, J.; Reeder, R. J. *Geology* **1990**, *18*, 1244–1247.
[33] Shannon, R. D. *Acta Crystallographica: Section A* **1976**, *A*, 751–767.
[34] Montelius, L.; Tegenfeldt, J. O. *Applied Physics Letters* **1993**, *62*, 2628–2630.
[35] Stewart, M. P.; Hodel, A. W.; Spielhofer, A.; Cattin, C. J.; Muller, D. J.; Helenius, J. *Methods* **2013**, *60*, 186–94.
[36] Donaldson, J., S. H.; Røyne, A.; Kristiansen, K.; Rapp, M. V.; Das, S.; Gebbie, M. A.; Lee, D. W.; Stock, P.; Valtiner, M.; Israelachvili, J. *Langmuir* **2015**, *31*, 2051–2064.
[37] Israelachvili, J. N. *Intermolecular and Surface forces*, 3rd ed.; Elsevier, 2011; Vol. 1.
[38] Valtiner, M.; Banquy, X.; Kristiansen, K.; Greene, G. W.; Israelachvili, J. N. *Langmuir* **2012**, *28*, 13080–13093.
[39] Teng, F.; Zeng, H.; Liu, Q. *The Journal of Physical Chemistry C* **2011**, *115*, 17485–17494.
[40] Benz, M.; Rosenberg, K. J.; Kramer, E. J.; Israelachvili, J. N. *The Journal of Physical Chemistry B* **2006**, *110*, 11884–11893.
[41] Zappone, B.; Rosenberg, K. J.; Israelachvili, J. *Tribology Letters* **2007**, *26*, 191.
[42] Brant, J. A.; Childress, A. E. *Environmental Engineering Science* **2004**, *19*, 413–427.
[43] Stipp, S. L. S.; Eggleston, C. M.; Nielsen, B. S. *Geochimica et Coesmochimica Acta* **1994**, *58*, 3023–3033.